Electronic Supplementary Material (ESI) for Organic & Biomolecular Chemistry.

Supplementary Information

Controlling Helicene Pitch by Molecular Tethering

Abhijeet Agrawal, Israa Shiouki, Yinon Deree, Benny Bogoslavsky and Ori Gidron*

Institute of Chemistry, The Hebrew University of Jerusalem, Edmond J. Safra Campus, Jerusalem, Israel.

Contents

Supplementary Methods

S1 General

Commercially available reagents and chemicals were used without further purification unless otherwise stated. Phenylboronic acid was received from Angene Chemical. The initial precursor compound 1 was synthesized according to the methodology given for the synthesis of compound 3 in the SI of a previous report[1].

Flash chromatography (FC) was performed using CombiFlash SiO_2 columns. Chiral HPLC separations were performed with a Chiralpak® IG semi-preparative column and CHIRALPAK® IB-N (250 × 4.6 mm / 5μm) preparative columns, with hexane/dichloromethane as eluent.

^{1}H and ^{13}C NMR spectra were recorded in solution on Bruker-AVIII 400 MHz and 500 MHz spectrometers using tetramethylsilane (TMS) as the external standard. The spectra were recordedusing chloroform-d as the solvent. Chemical shifts are expressed in δ units.

UV-vis absorption spectra were recorded with an Agilent Cary-5000 spectrophotometer. The spectra were measured using a quartz cuvette (1 cm) at 25 °C. The absorption wavelengths are reported in nm with the extinction coefficient ε ($M^{-1}cm^{-1}$) given in brackets.

Steady state fluorescence measurements were performed on a HORIBA JOBIN YVON Fluoromax-4 spectrofluorometer with the excitation/emission geometry at a right angle. Fluorescence quantum yields (Θ_f) were determined using HORIBA-Ø integrating sphere. The lifetimes of the excited species were measured using an NL-C2 Pulsed Diode Controller NanoLED light source with time-correlated single proton counting (TSCPC) Controller DeltaHub (HORIBA), referenced against colloidal Ludox solution (50 wt. % solution in water) obtained from Aldrich. Electronic circular dichroism (ECD) spectra were recorded on aMOS-500 spectrophotometer from BioLogic Science Instruments.

High resolution mass spectra were measured on: Quadrupole Time-of-Flight (QTOF) Mass Spectrometry SCIEX X500R QTOF.

S2 Synthesis

S2.1 Synthesis of untethered S-shaped double [4] helicene (**DH-C0**)

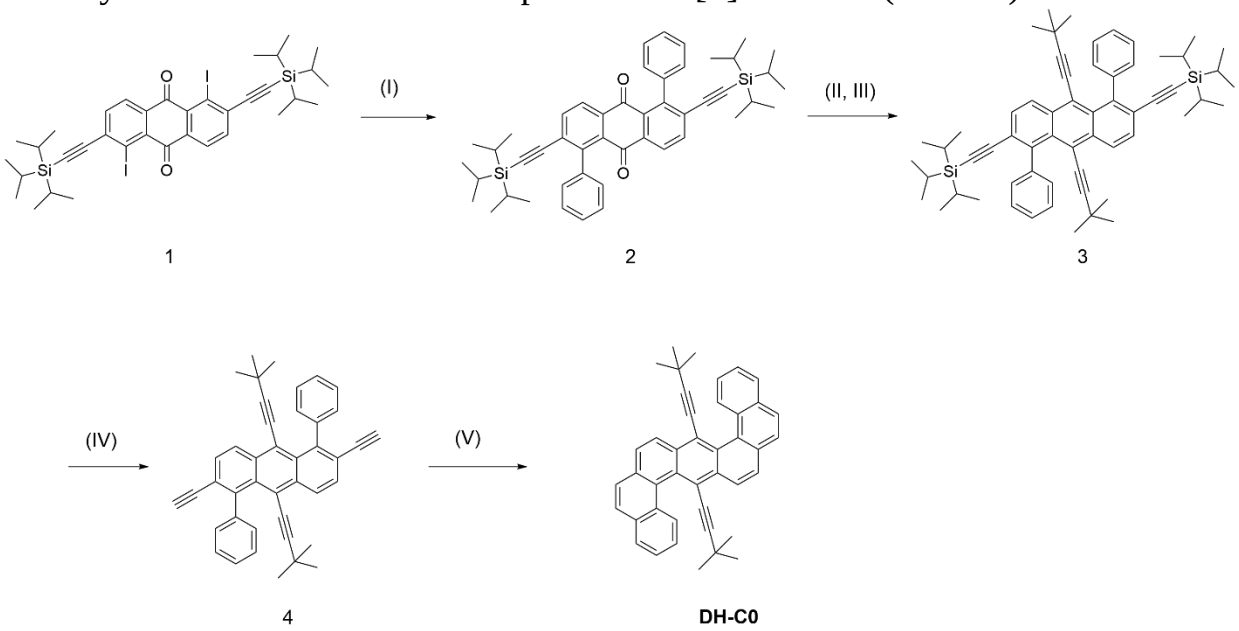

Scheme 1. Synthesis of **DH-C0**. (I) $Pd(PPh_3)_4$,dioxane/water (4:1), 94 °C, 3 d; (II) 3,3-Dimethyl-1-butyne, n-BuLi, THF, −5 °C→RT, 10 h; (III) $SnCl_2$, THF, 4 h; (IV) N,N,N,N-tetra n-butylammonium fluoride, THF, 0 °C→RT, 0.5 h; (V) $PtCl_2$, toluene, 90 °C 12h. Bu, butyl; Ph, phenyl; THF, tetrahydrofuran.

*Synthesis of **2***

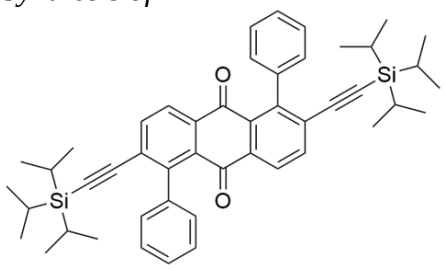

A two-necked round-bottomed (RB) flask fitted with a condenser was evacuated and refilled with Ar three times. 1,4-Dioxane (80 mL) and water (20 mL) were added and the mixture was purged with Ar for 20 min before adding **1** (5 g, 6.09 mmol), phenylboronic acid (2.23 g, 18.28mmol), Na_2CO_3 (1.94 g, 18.28 mmol) and $Pd(PPh_3)_4$ (353 mg, 0.304 mmol) at once. The reaction mixture was then maintained at 94 °C for 3 days. Then, 1, 4-dioxane was evaporated off and the resulting mixture was extracted with chloroform (3 x 90 mL). The combined organic layers are dried over $MgSO_4$ and concentrated to obtain a brown-yellow crude. Purification of the crudeby silica gel column chromatography using DCM/hexane (2:3) resulted in an orange solid. Washing the solid with hexane (50 mL) afforded **2** as a golden-yellow solid (2.70 g, yield = 62%).

^{1}H NMR (400 MHz, $CDCl_3$) δ 8.11 (d, *J* = 8.1 Hz, 2H), 7.85 (d, *J* = 8.1 Hz, 2H), 7.47 – 7.37 (m, 6H), 7.24 – 7.21 (m, 4H), 0.92 (s, 36H).

^{13}C NMR (101 MHz, $CDCl_3$) δ 183.10, 145.94, 140.45, 137.69, 135.01, 131.43, 130.89, 128.46, 128.34, 127.58, 127.40, 104.64, 101.28, 77.68, 77.56, 77.36, 77.04, 18.82, 11.39.

HR-ESI-MS m/z (%): 721.3885 (100, $[M+H]^+$) calcd. for $C_{48}H_{57}O_2Si_2^+$: 721.38916

*Synthesis of **3***

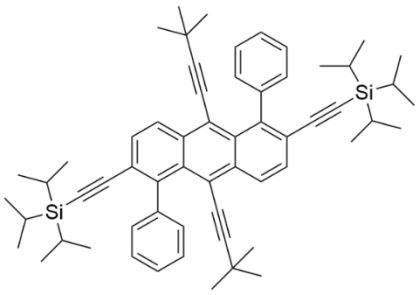

Step 1: An oven-dried two-necked RB flask was charged with anhydrous tetrahydrofuran and maintained at -5 °C for 10 min and then 3,3-dimethyl-1-butyne (2.28 g, 27.73 mmol) was added to it. To the chilled solution, n-BuLi (1.6 M in hexanes, 17.33 mL) was added slowly to maintain the temperature and the reaction mixture was kept at the same temperature for one hour to complete lithiation. The lithium-alkynide salt was quenched by dropwise addition of a solution of **2** (2 gm, 2.77 mmol) in 20 mL of anhydrous tetrahydrofuran, and fading of the golden-yellow color of **2** was observed. The resulting reaction mixture was kept at -5 °C for 0.5 h before allowing it rise to RT, at which temperature it was then stirred for an additional hour. Then, the reaction mixture was quenched with water and the solvents were evaporated off in a rotavapor, producing an off-white solid. The solid was washed with water and hexane and dried under vacuum to afford a whitesolid (1.8 g) that was immediately used in the next step without further purification and characterization.

Step 2: The white solid produced at the end of Step 1 was reacted with $SnCl_2{\cdot}5H_2O$ for 4 h in THF under Ar to accomplish full conversion as monitored by thin layer chromatography and by the appearance of a bright yellow color and a bright green emission under a 365 nm lamp. The THF was distilled off and the resulting orange crude product was purified by silica gel column and eluted with DCM/hexane (5:95) to afford a bright yellow solid **3** (1.25 g, 53% of two steps).

^{1}H NMR (400 MHz, $CDCl_3$) δ 8.53 (dd, *J* = 9.1, 0.8 Hz, 2H), 7.56 (dd, *J* = 9.1, 0.9 Hz, 2H), 7.44 – 7.39 (m, 4H), 7.37 (q, *J* = 2.9 Hz, 6H), 1.08 (d, *J* = 0.8 Hz, 18H), 0.99 (d, *J* = 1.9 Hz, 36H).

^{13}C NMR (400 MHz, $CDCl_3$) δ 143.64, 141.89, 135.21, 132.69, 131.45, 131.28, 130.46, 130.10, 128.04, 127.96, 127.55, 127.23, 123.56, 119.75, 117.56, 107.63, 97.02, 78.59, 77.62, 77.56, 77.36, 77.10, 30.99, 30.67, 28.83, 18.96, 18.86, 11.59, 11.45.

HR-ESI-MS m/z (%): 851.53964 (100, $[M+H]^+$) calcd. for $C_{60}H_{75}Si_2^+$: 851.54018.

*Synthesis of **4***

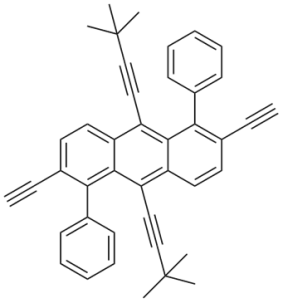

To a solution of **3** (1.2 g, 1.41 mmol) in 20 mL THF kept under Ar in a single-neck RB flask, *N*,*N*,*N*,*N*-tetrabutylammonium fluoride (TBAF) solution (1 M in THF, 1.42 mL) at 0°C was added in a dropwise manner. Then, the reaction mixture was stirred at room temperature for an additional 0.5 h. The THF was evaporated off in a rotavapor and the resulting semisolid crude was directly subjected to silica gel column chromatography using DCM/hexane (1:4) to obtain a bright yellowsolid **4** (0.560 g, yield = 74%;) with green emission under a 365 nm lamp.

^{1}H NMR (500 MHz, $CDCl_3$) δ 8.55 (d, *J* = 9.1 Hz, 2H), 7.58 (d, *J* = 9.1 Hz, 2H), 7.44 (d, *J* = 0.9 Hz, 10H), 3.05 (s, 2H), 1.09 (s, 18H).

^{13}C NMR (400 MHz, $CDCl_3$) δ 144.28, 141.59, 135.34, 131.40, 130.48, 129.75, 127.93, 127.81, 127.46, 127.00, 125.97, 122.28, 119.95, 117.95, 84.18, 82.68, 78.43, 77.61, 77.56, 77.36, 77.10, 30.97, 28.85.

HR-ESI-MS m/z (%): 539.27368 (100, $[M+H]^+$) calcd. for $C_{42}H_{35}^+$: 539.27333.

Synthesis of **DH-C0**

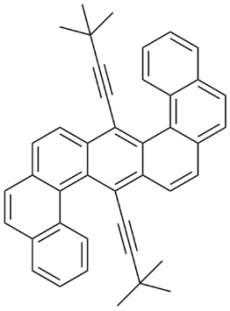

A solution of alkyne **4** (300 mg, 0.556 mmol) and $PtCl_2$ (15 mg, 0.055 mmol) in toluene (10 mL) was stirred for 24 h at 90 °C under Ar until complete conversion of the substrate. The solvent was then evaporated, and the residue was purified by flash chromatography (silica gel, hexanes) to give **DH-C0** as an orange solid (110 mg, 37%):

^{1}H NMR (400 MHz, $CDCl_3$) δ 8.64 (d, *J* = 8.8 Hz, 2H), 8.57 – 8.52 (m, 2H), 8.08 – 8.04 (m, 2H), 8.03 – 7.99 (m, 2H), 7.95 – 7.90 (m, 4H), 7.61 – 7.53 (m, 4H), 0.95 (s, 18H).

^{13}C NMR (101 MHz, $CDCl_3$) δ 132.64, 132.37, 132.04, 131.67, 130.78, 129.83, 129.02, 128.42, 127.74, 127.68, 125.93, 125.84, 125.80, 125.27, 119.31, 111.67, 79.44, 77.68, 77.36, 77.04, 30.79, 28.68.

HR-ESI-MS m/z (%): 539.27314 (100, $[M+H]^+$) calcd. for $C_{42}H_{35}^+$: 539.27333.

S2.2 Synthesis of tethered S-shaped double [4]helicene (**DH-C4, DH-C6, and DH-C8**)

Compounds **Ant-C4, Ant-C6 and Ant-C8** were synthesized according to a previous report.[1]

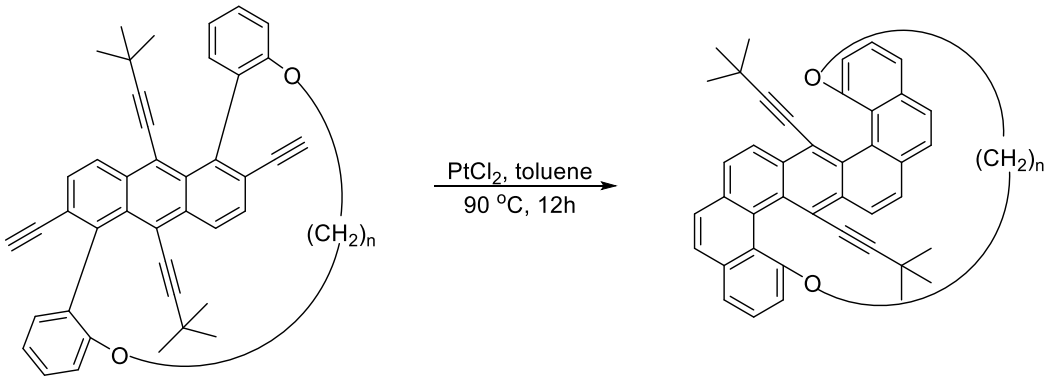

Ant-C4; n= 4
Ant-C6; n= 6
Ant-C8; n= 8

DH-C4; n= 4, 34%
DH-C6; n= 6, 23%
DH-C8; n= 8, 15%

Scheme 2. Synthesis of **DH-Cn** (n=4, 6, 8).

S2.2.1 General procedure for $PtCl_2$-mediated benzannulation of the tethered compounds

A solution of alkyne **Ant-Cn**; n=4, 6, 8 (1 equiv.) and $PtCl_2$ (10 mol%) in toluene (5 mL) was stirred for 24 h at 90 °C under Ar until complete conversion of the substrate was achieved. The solvent was then evaporated, and the residue was purified by flash chromatography (silica gel, hexanes) to give **DH-Cn**; n=4, 6, 8.

Synthesis of **DH-C4**

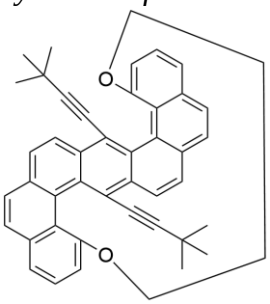

A solution of alkyne **Ant-C4** (50 mg, 0.0801 mmol) and $PtCl_2$ (3 mg, 0.008 mmol) in toluene (5 mL) was stirred for 24 h at 90 °C under Ar until complete conversion of the substrate was achieved. The solvent was then evaporated, and the residue was purified by flash chromatography (silica gel, hexane) to give **DH-C4** as a greenish yellow solid (17 mg, 34%):

^{1}H NMR (400 MHz, $CDCl_3$) δ 8.32 (d, *J* = 8.6 Hz, 2H), 7.94 (d, *J* = 8.4 Hz, 2H), 7.82 (d, *J* = 8.4 Hz, 2H), 7.72 (d, *J* = 8.7 Hz, 2H), 7.64 (dd, *J* = 8.3, 1.1 Hz, 2H), 7.52 (dd, *J* = 8.1, 7.5 Hz, 2H), 6.83 (dd, *J* = 7.6, 1.1 Hz, 2H), 3.97 (dd, *J* = 8.1, 3.8 Hz, 2H), 2.97 – 2.85 (m, 2H), 0.95 (s, 18H), 0.82 – 0.78 (m, 2H), 0.74 – 0.67 (m, 2H).

^{13}C NMR (101 MHz, $CDCl_3$) δ 157.36, 133.67, 132.17, 132.04, 128.54, 128.06, 126.71, 126.53, 125.53, 125.38, 124.78, 124.28, 120.26, 119.40, 108.46, 106.39, 77.95, 77.68, 77.36, 77.04, 69.19, 31.24, 30.06, 28.43, 26.78.

HR-ESI-MS m/z (%): 625.30982 (100, $[M+H]^+$) calcd. for $C_{46}H_{41}O_2^+$: 625.31011.

Synthesis of **DH-C6**

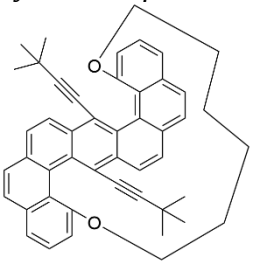

A solution of alkyne **Ant-C6** (80 mg, 0.122 mmol) and $PtCl_2$ (4 mg, 0.0122 mmol) in toluene (5 mL) was stirred for 24 h at 90 °C under Ar until complete conversion of the substrate was

achieved. The solvent was then evaporated, and the residue was purified by flash chromatography (silica gel, hexane) to give **DH-C6** as a Greenish Yellow solid (18 mg, 23%):

^{1}H NMR (400 MHz, $CDCl_3$) δ 8.59 (d, *J* = 8.7 Hz, 2H), 7.97 (d, *J* = 8.3 Hz, 2H), 7.83 (dd, *J* = 11.8, 8.5 Hz, 4H), 7.64 (d, *J* = 7.9 Hz, 2H), 7.58 (t, *J* = 7.8 Hz, 2H), 7.00 (d, *J* = 7.6 Hz, 2H), 3.90 (ddt, *J* = 14.0, 10.2, 6.3 Hz, 4H), 1.16 (d, *J* = 7.2 Hz, 2H), 0.96 (d, *J* = 0.9 Hz, 18H), 0.85 (s, 2H), 0.40 – 0.28 (m, 2H), 0.24 (t, *J* = 9.1 Hz, 2H).

^{13}C NMR (101 MHz, $CDCl_3$) δ 156.40, 134.28, 132.72, 131.18, 129.40, 128.47, 127.29, 126.54, 126.18, 126.15, 125.30, 123.76, 120.95, 120.21, 107.32, 105.98, 79.01, 77.68, 77.36, 77.04, 66.06, 31.41, 28.44, 27.94, 24.00.

HR-ESI-MS m/z (%): 653.34062 (100, $[M+H]^+$) calcd. for $C_{48}H_{45}O_2^+$: 653.34141.

Synthesis of **DH-C8**

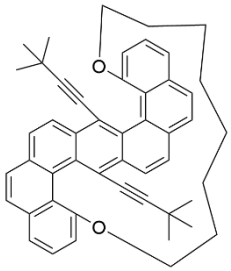

A solution of alkyne **Ant-C8** (100 mg, 0.146 mmol) and $PtCl_2$ (4 mg, 0.0146 mmol) in toluene (5 mL) was stirred for 24 h at 90 °C under Ar until complete conversion of the substrate was achieved. The solvent was then evaporated, and the residue was purified by flash chromatography (silica gel, hexane) to give **DH-C8** as a greenish yellow solid (15 mg, 15%):

^{1}H NMR (500 MHz, $CDCl_3$) δ 8.69 (d, *J* = 8.7 Hz, 2H), 7.99 (d, *J* = 8.3 Hz, 2H), 7.89 (dd, *J* = 8.5, 7.3 Hz, 4H), 7.66 (dd, *J* = 8.0, 1.2 Hz, 2H), 7.61 (t, *J* = 7.8 Hz, 2H), 7.07 (dd, *J* = 7.7, 1.3 Hz, 2H), 4.23 (td, *J* = 6.6, 3.4 Hz, 2H), 3.99 – 3.94 (m, 2H), 1.37 (d, *J* = 9.0 Hz, 2H), 1.13 – 1.07 (m, 4H), 0.97 (s, 18H), 0.90 – 0.88 (m, 4H), 0.81 (d, *J* = 6.7 Hz, 2H), 0.71 – 0.67 (m, 2H), 0.50 (d, *J* = 4.9 Hz, 2H).

^{13}C NMR (126 MHz, $CDCl_3$) δ 157.60, 134.48, 132.98, 130.27, 130.25, 128.59, 127.92, 126.67, 126.54, 126.32, 125.55, 122.68, 121.43, 120.41, 107.01, 106.47, 79.33, 77.62, 77.36, 77.11, 68.50, 32.28, 31.51, 30.06, 28.47, 27.06, 26.81, 26.12, 23.05, 14.47

HR-ESI-MS m/z (%): 681.37239 (100, $[M+H]^+$) calcd. for $C_{50}H_{49}O_2^+$: 681.37271.

S3 Chiral HPLC

Racemic **DH-C4, DH-C6 and DH-C8** were resolved using semi-preparative CHIRALPAK-IG with eluents of 20% DCM/hexane for **DH-C4**, 10% DCM/hexane for **DH-C6**, and hexane for **DH-C8**. The *M*-enantiomer was eluted first, followed by the *P*-enantiomer, with baseline separation between them.

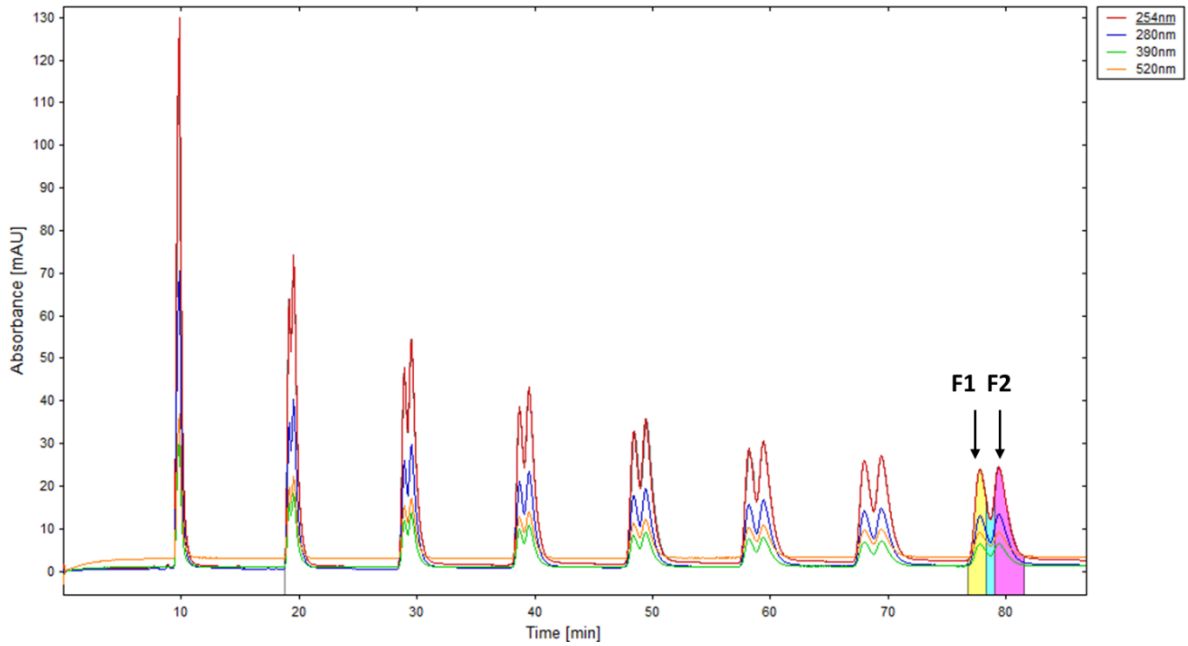

Figure S1. Chiral HPLC of racemic-**DH-C4**.

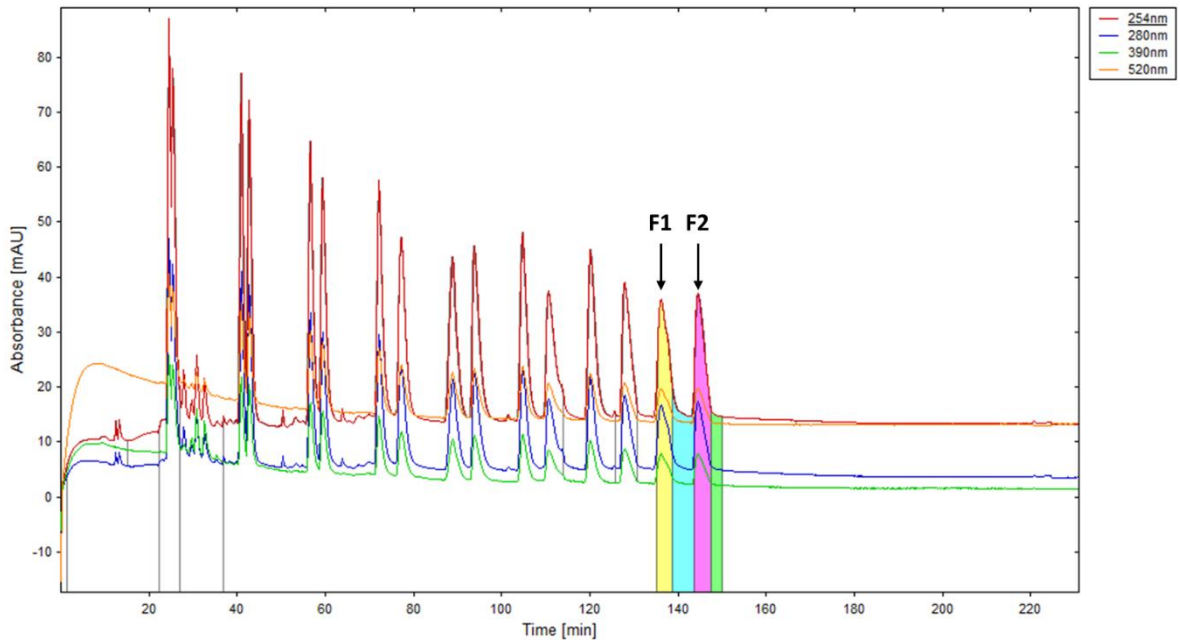

Figure S2. Chiral HPLC of racemic- **DH-C6**.

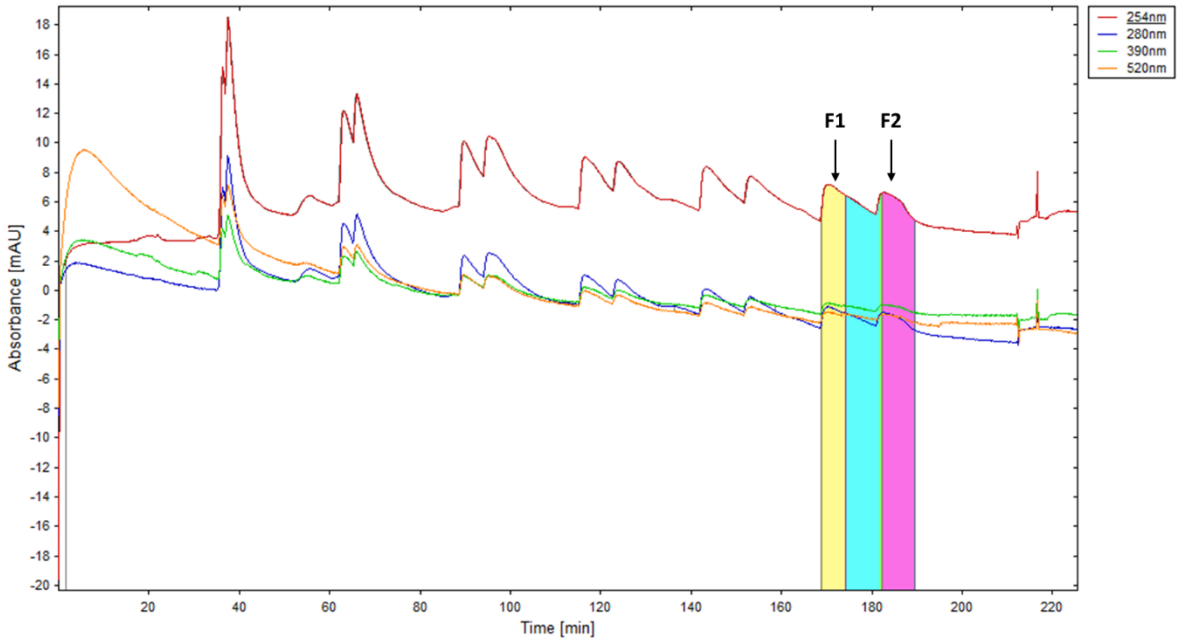

Figure S3. Chiral HPLC of racemic- **DH-C8**.

S4 Characterization

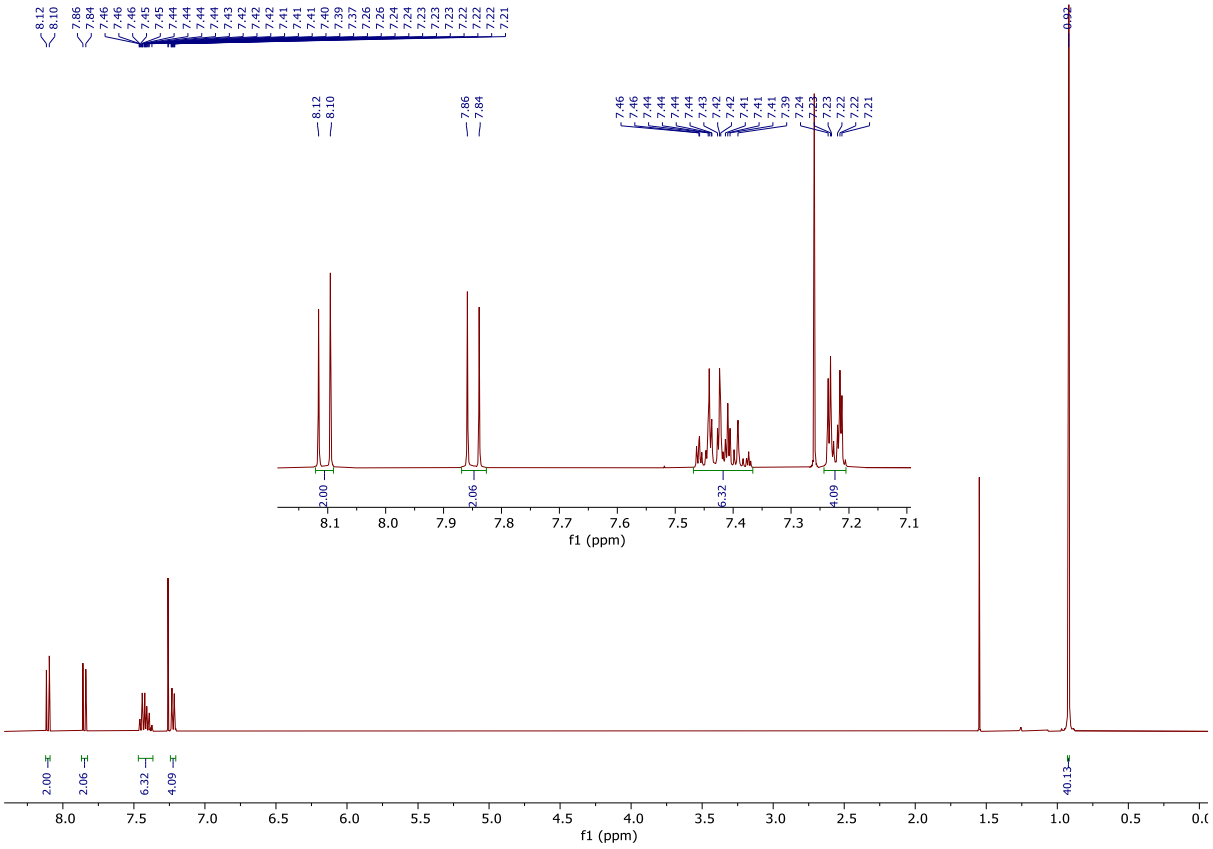

Figure S4. ^{1}H NMR (400 MHz) of **2** in $CDCl_3$, measured at 298 K.

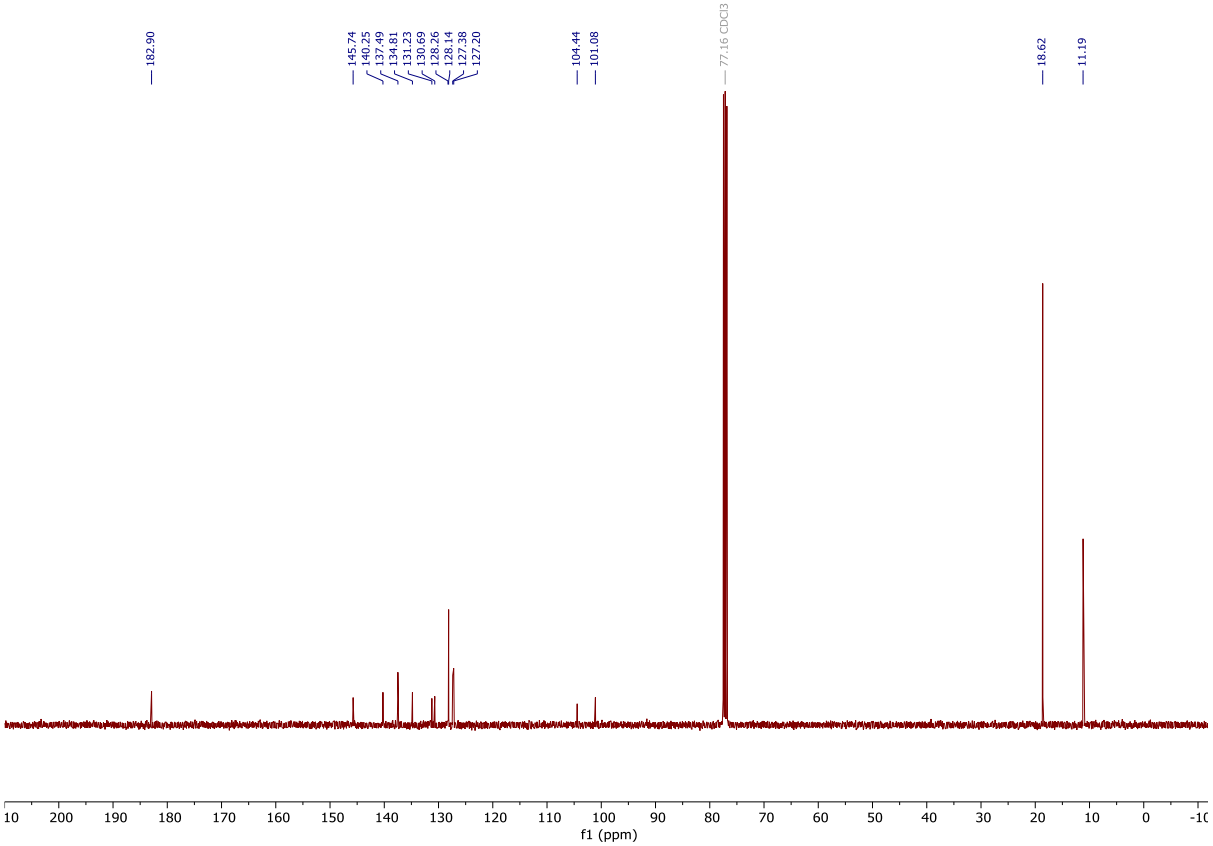

Figure S5. ^{13}C NMR (101 MHz) of **2** in $CDCl_3$, measured at 298 K.

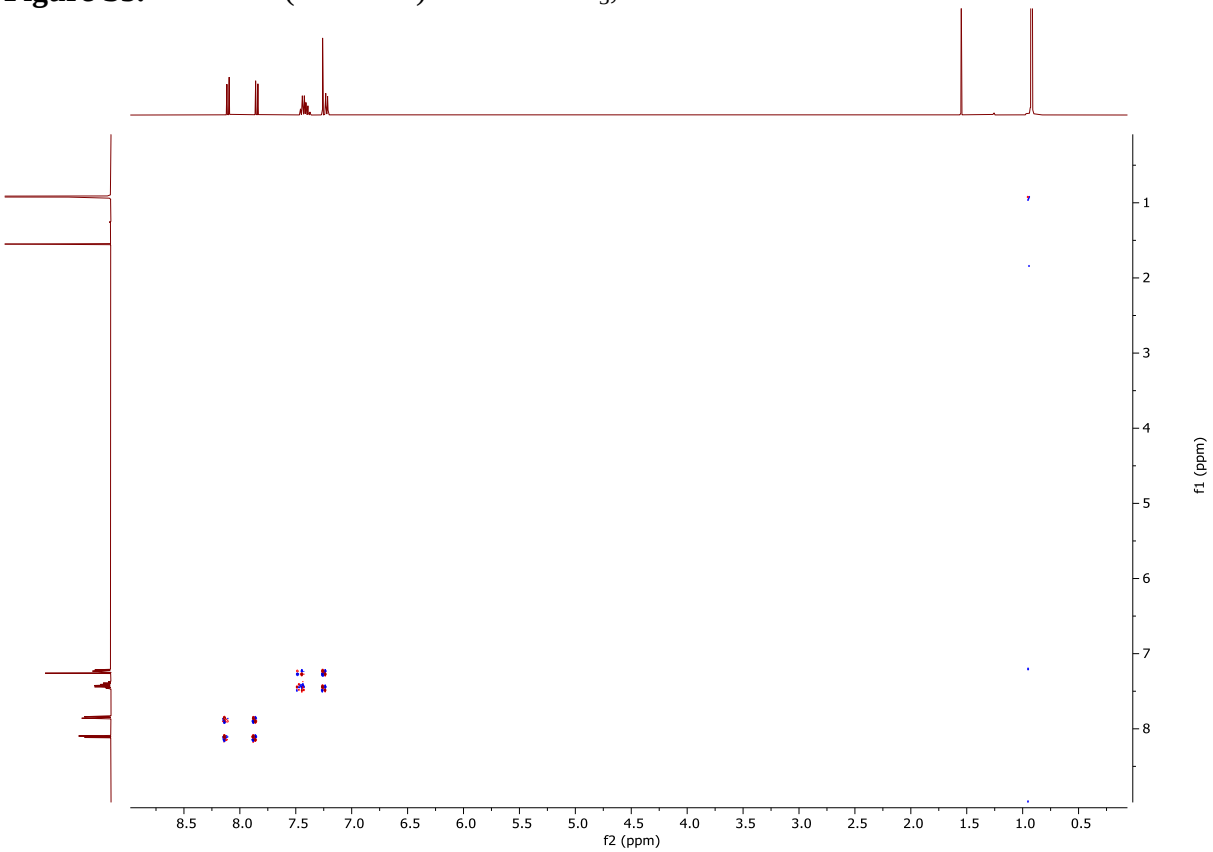

Figure S6. COSY NMR (400 MHz) of **2** in $CDCl_3$, measured at 298 K.

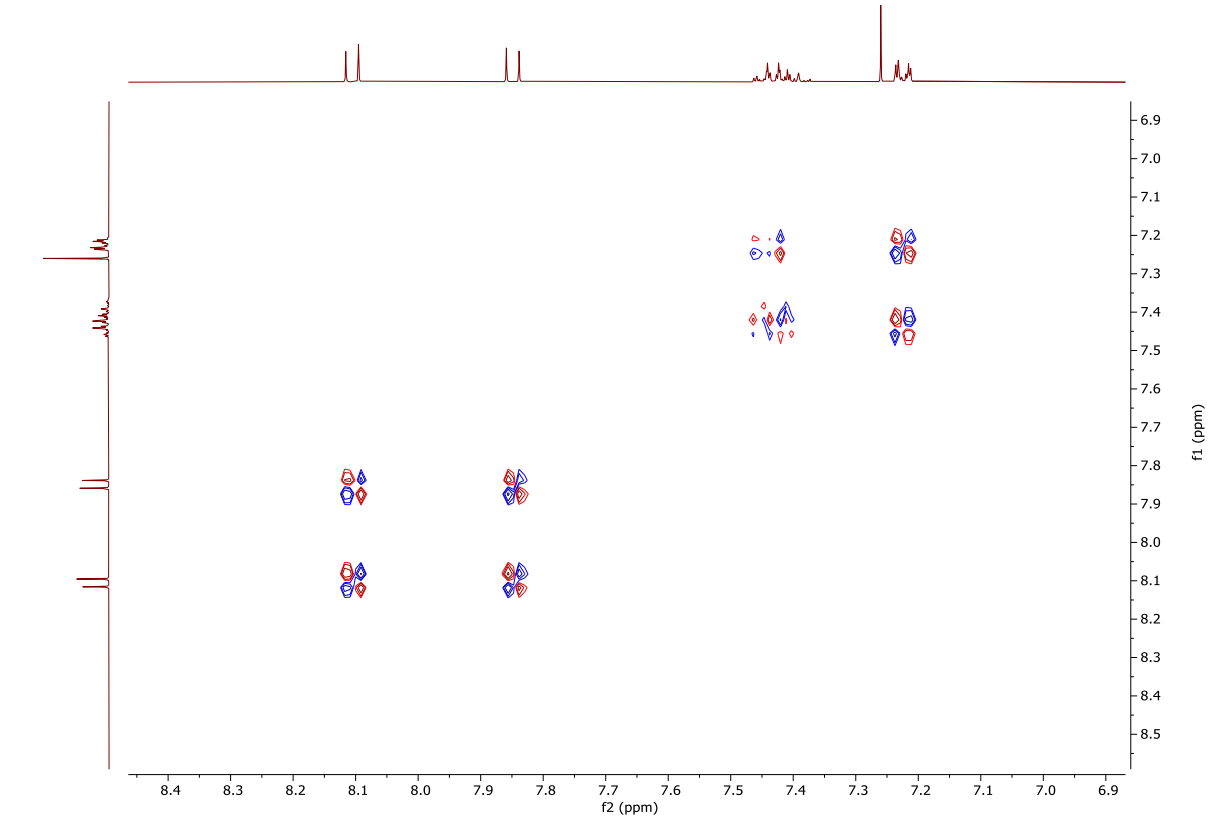

Figure S7. COSY NMR (400 MHz) of **2** in $CDCl_3$, measured at 298 K (expansion in aromatic region).

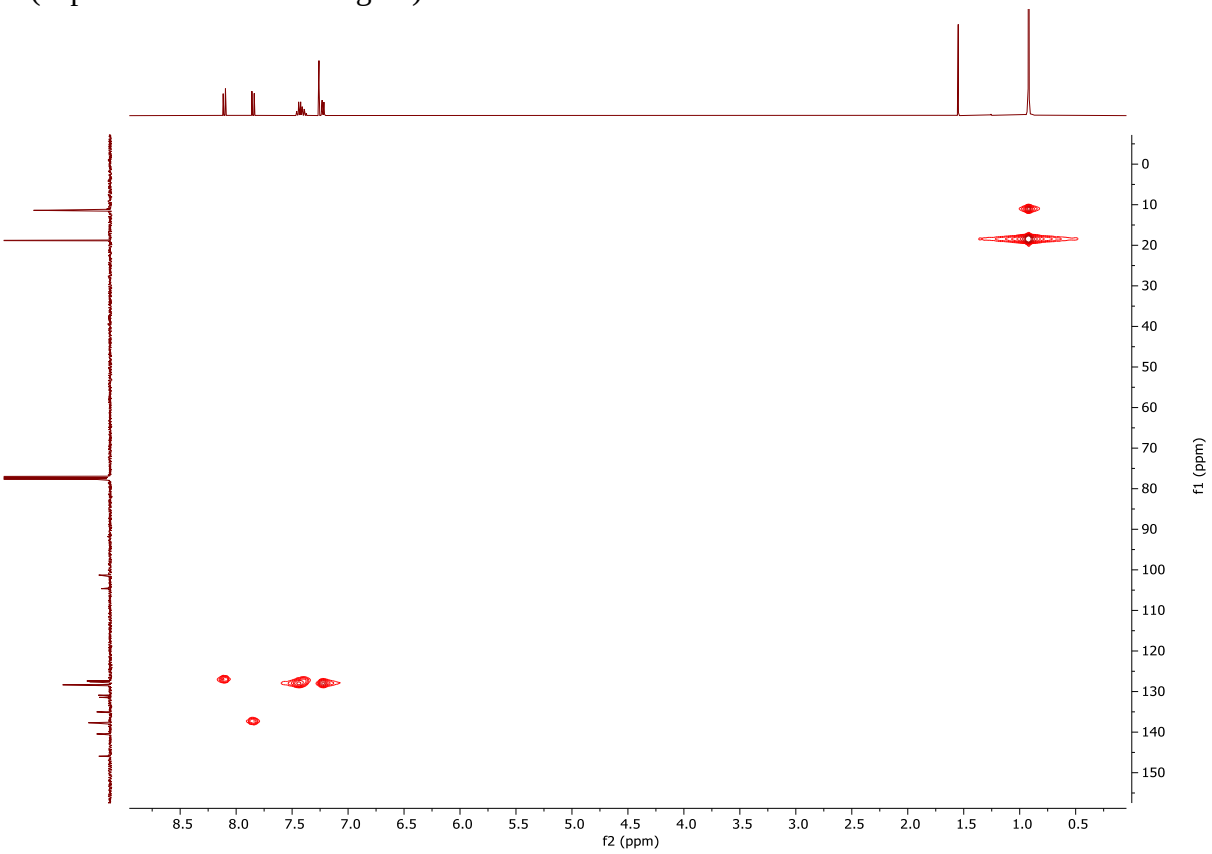

Figure S8. HSQC NMR (400 MHz) of **2** in $CDCl_3$, measured at 298 K.

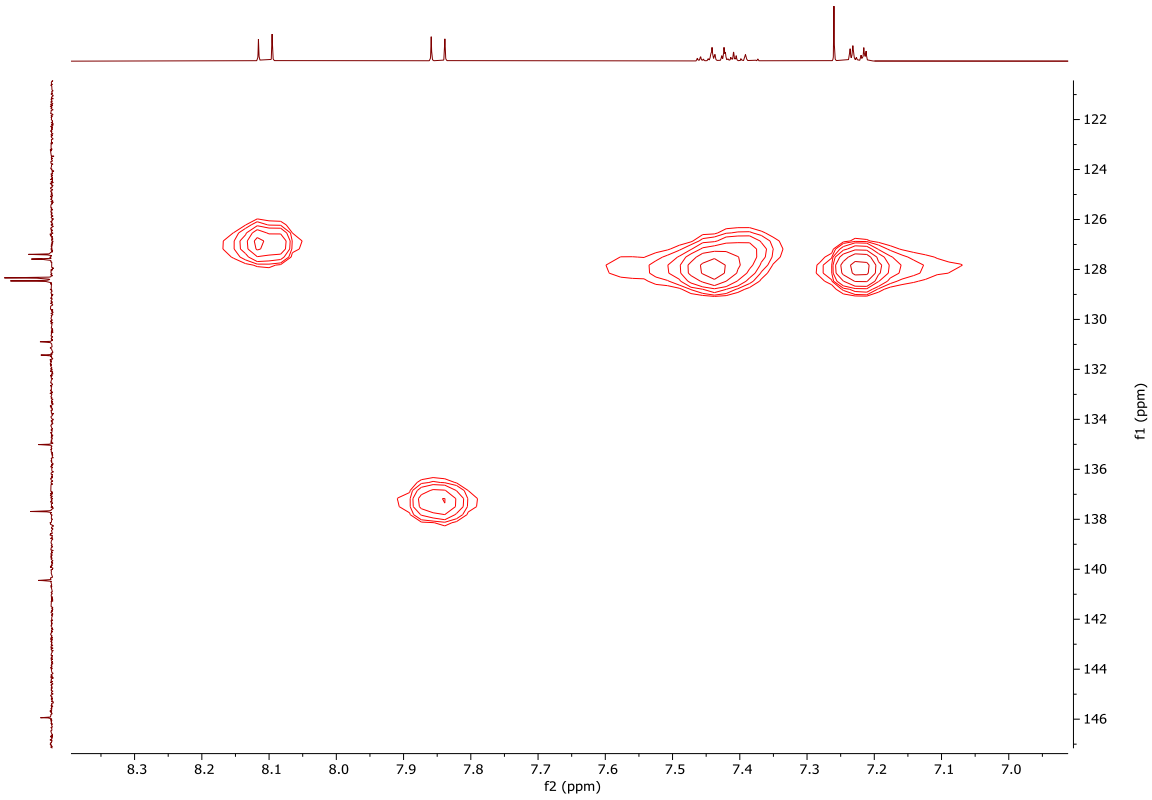

Figure S9. HSQC NMR (400 MHz) of **2** in $CDCl_3$, measured at 298 K (expansion in aromatic region).

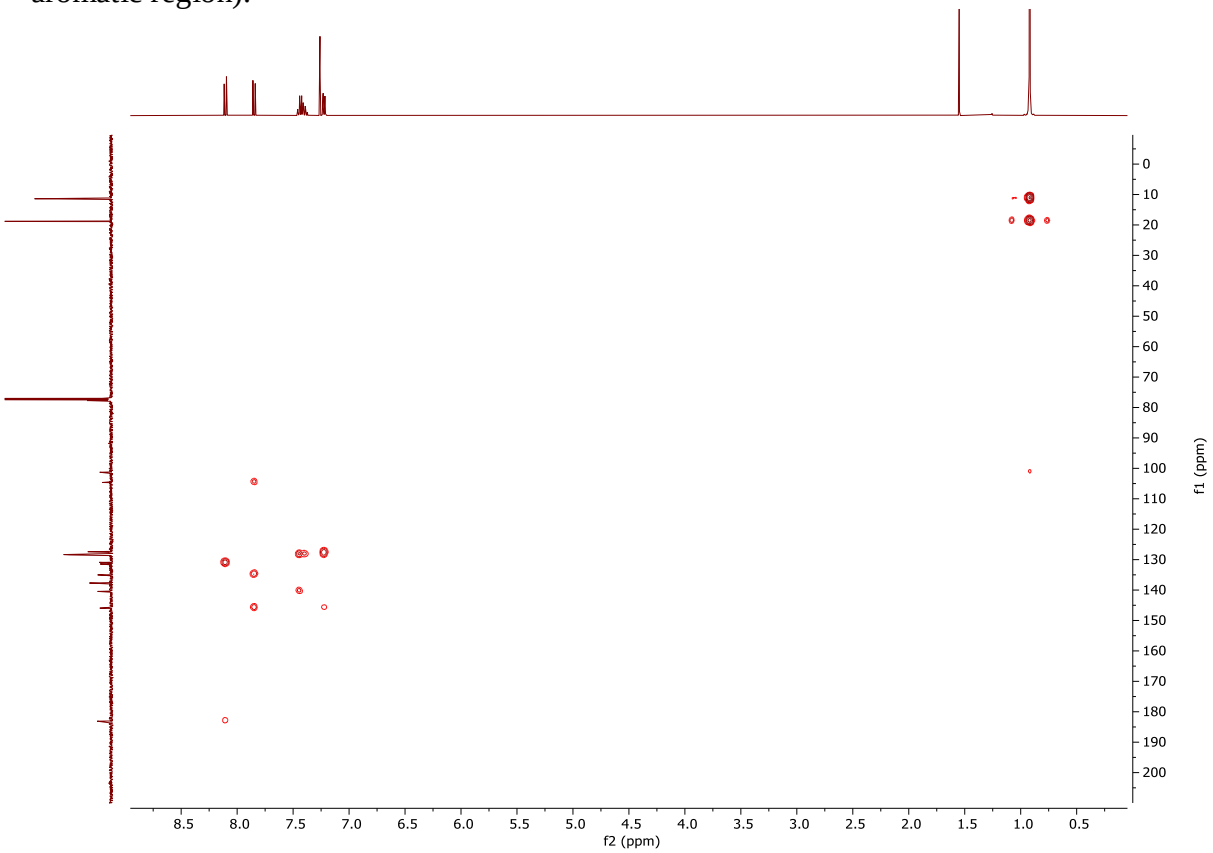

Figure S10. HMBC NMR (400 MHz) of **2** in $CDCl_3$, measured at 298 K.

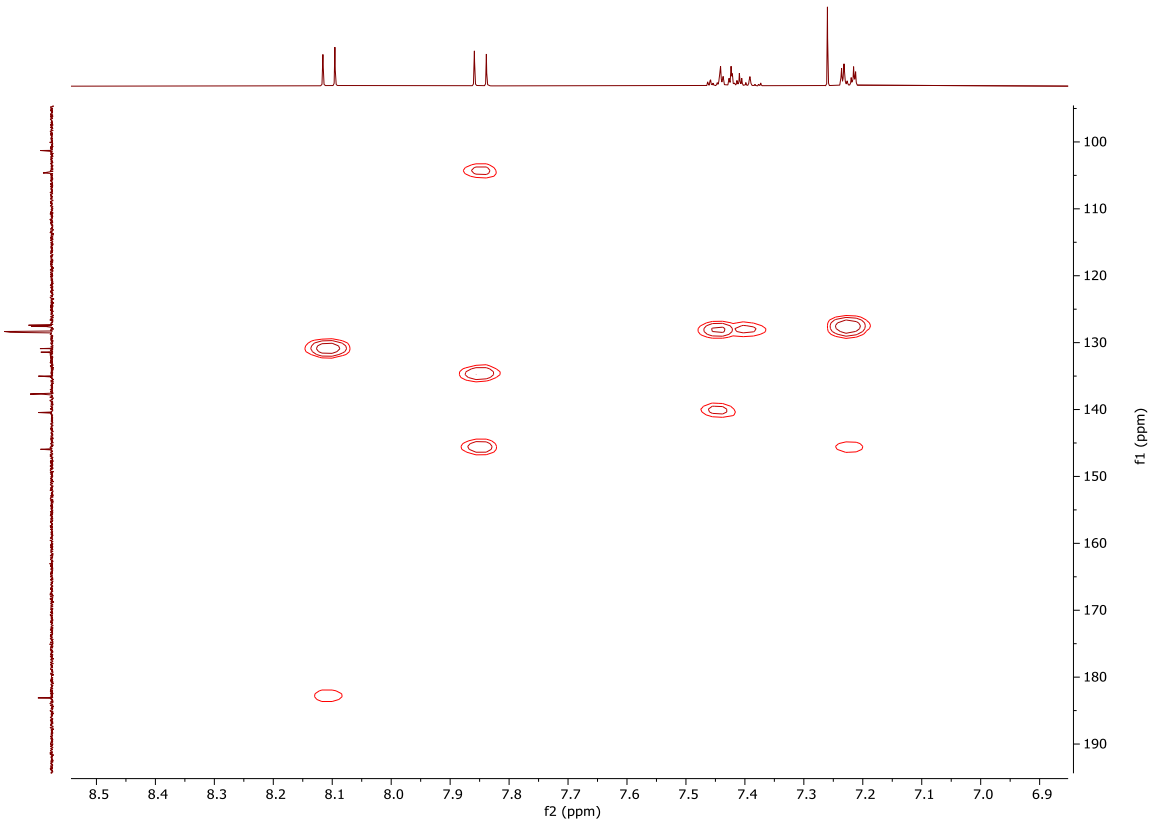

Figure S11. HMBC NMR (500 MHz) of **3** in $CDCl_3$, measured at 298 K (expansion in aromatic region).

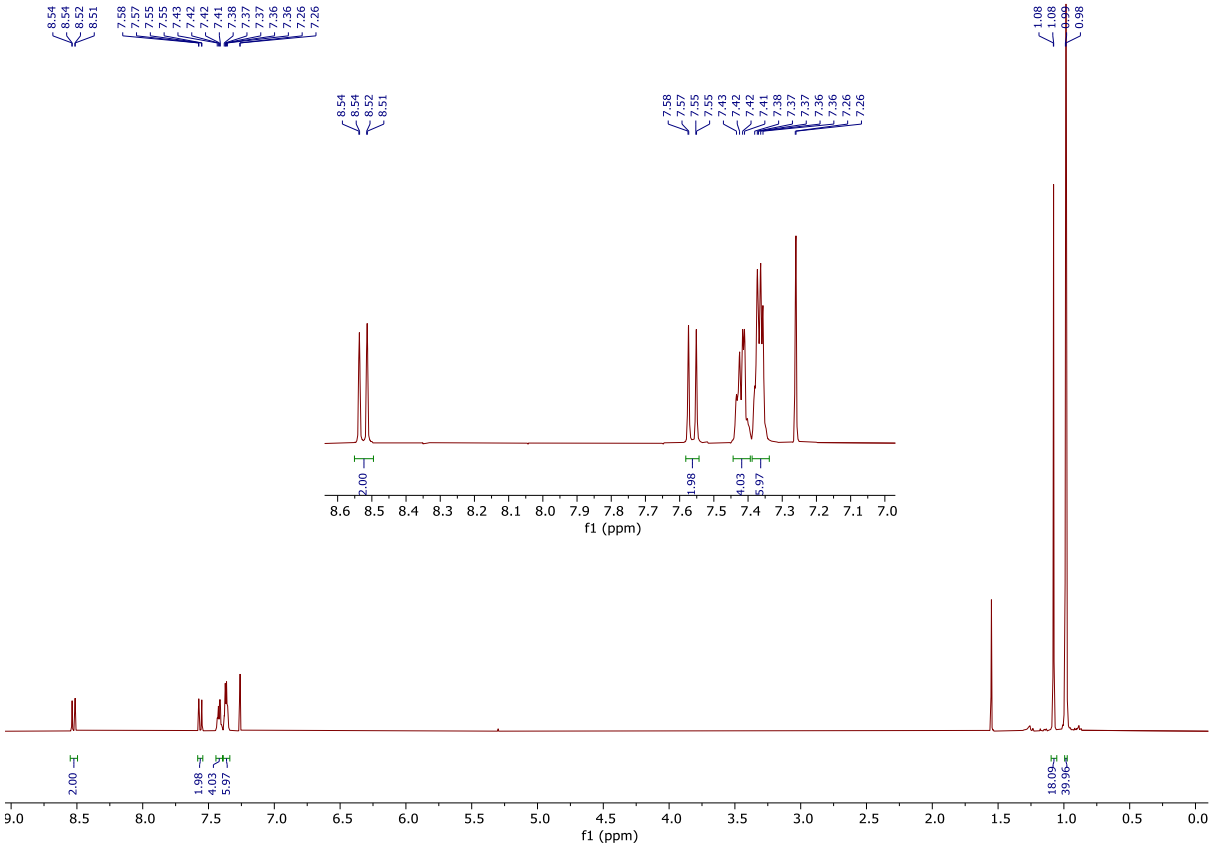

Figure S12. ^1H NMR (400 MHz) of **3** in $CDCl_3$, measured at 298 K.

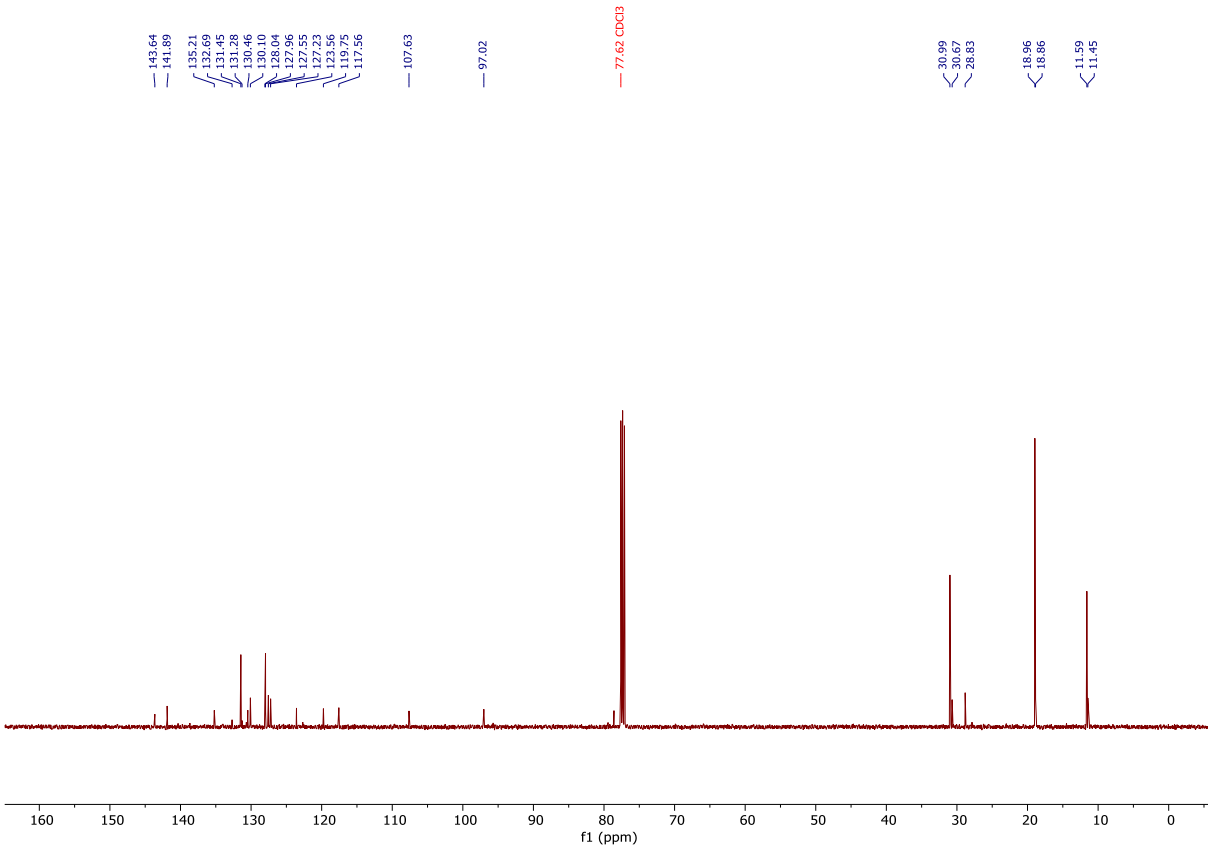

Figure S13. ^{13}C NMR (101 MHz) of **3** in $CDCl_3$, measured at 298 K.

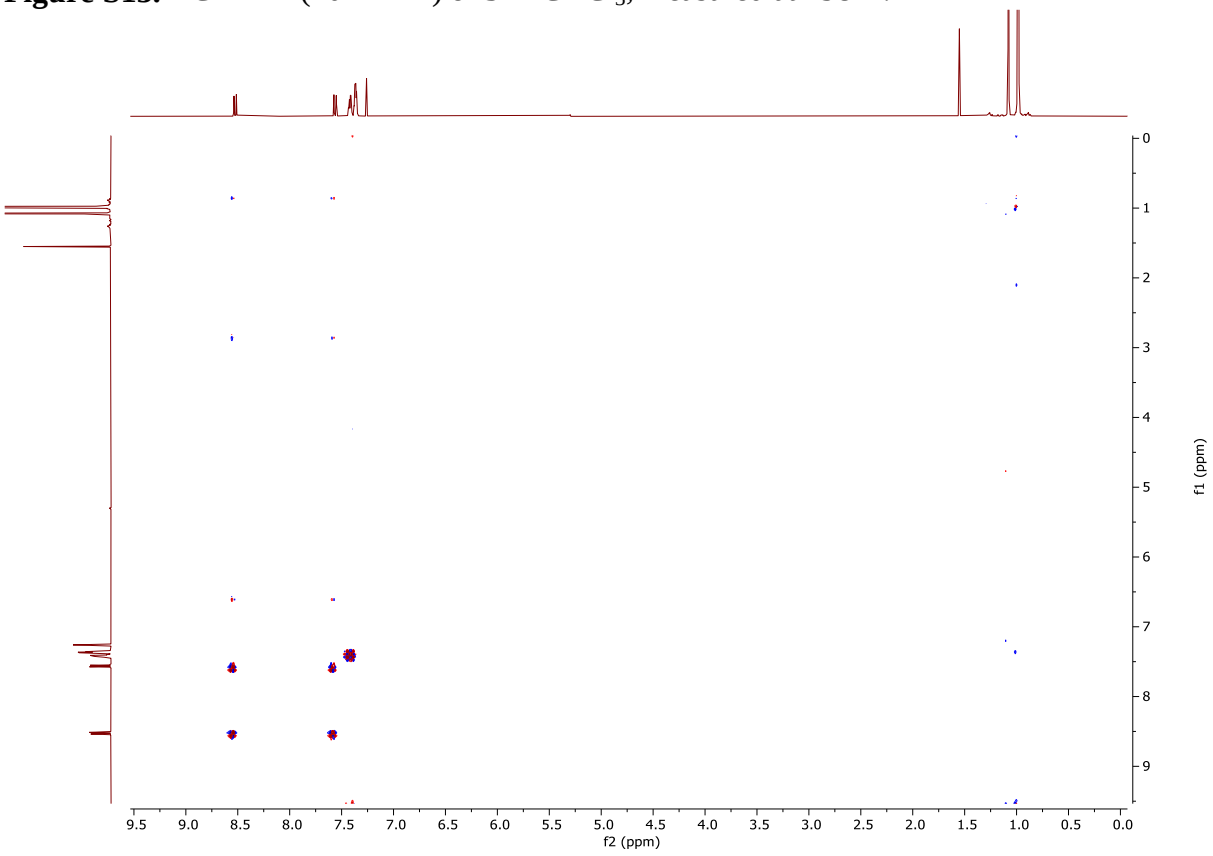

Figure S14. COSY NMR (400 MHz) of **3** in $CDCl_3$, measured at 298 K.

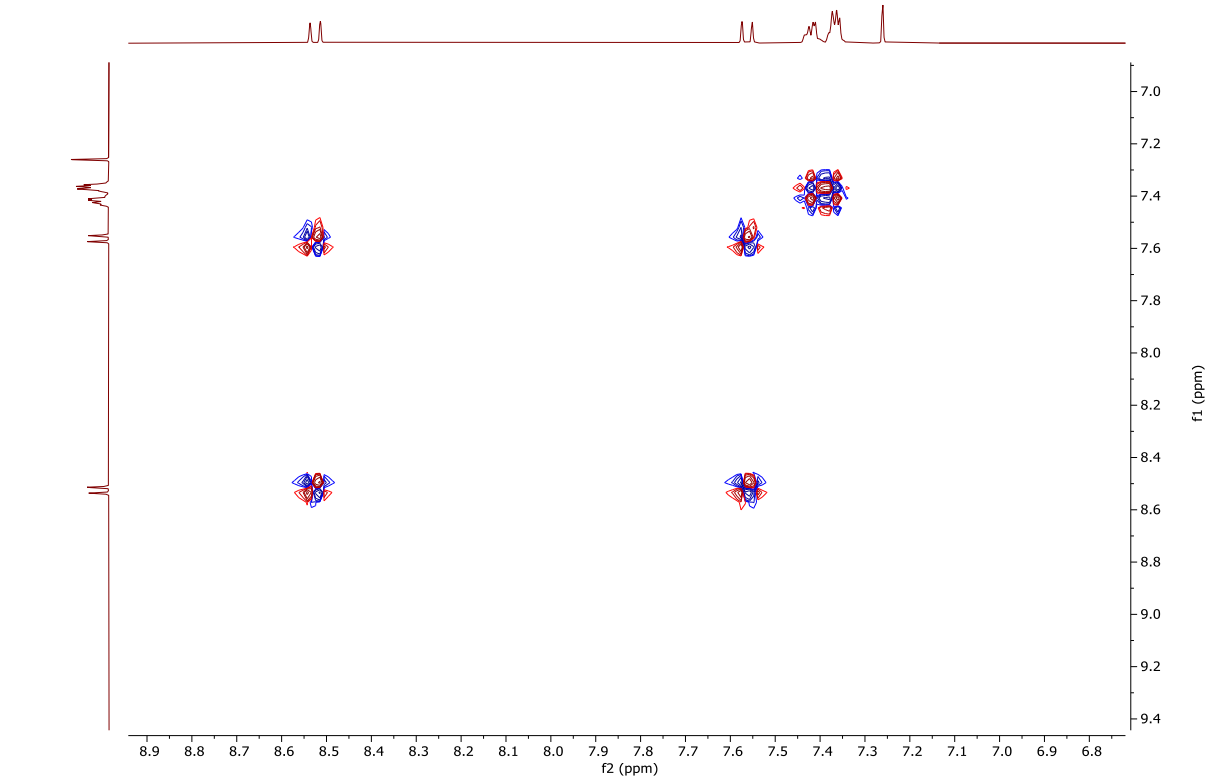

Figure S15. COSY NMR (400 MHz) of **3** in $CDCl_3$, measured at 298 K (expansion in aromatic region).

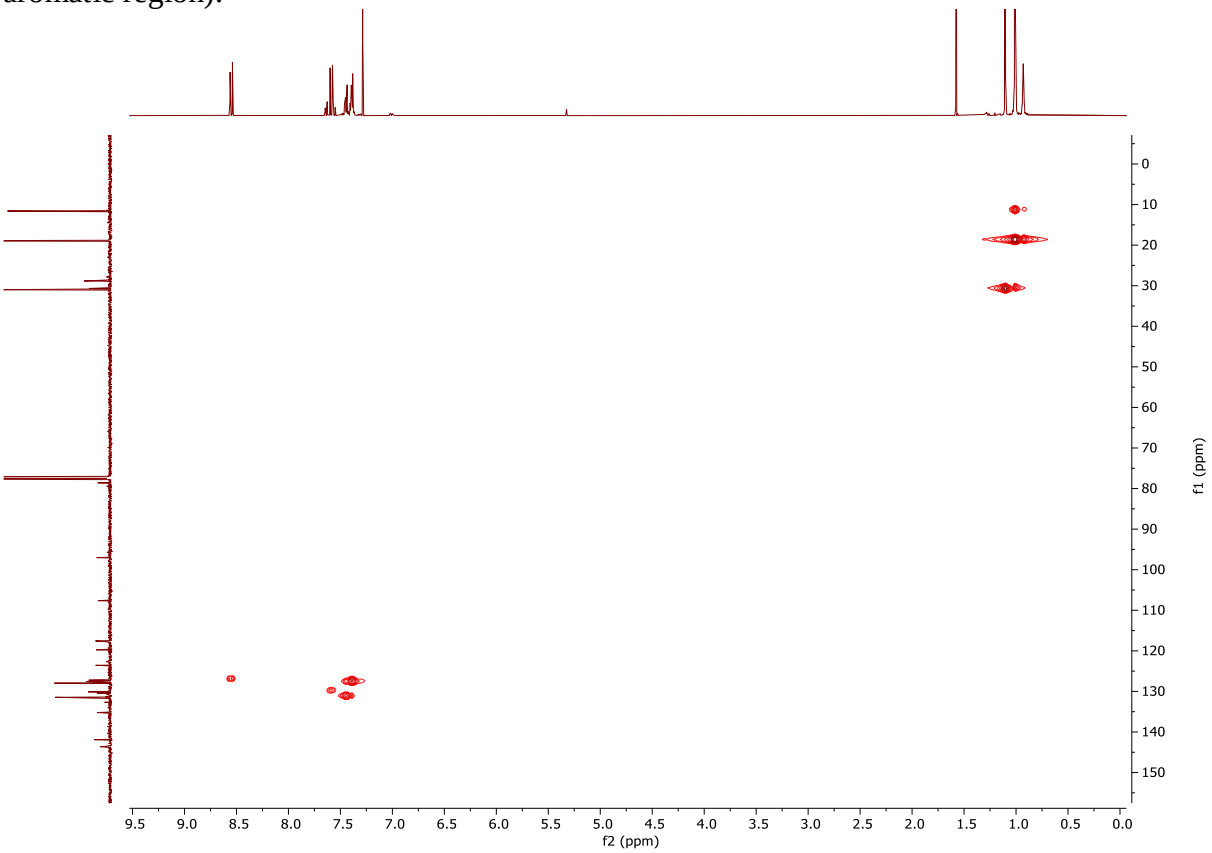

Figure S16. HSQC NMR (400 MHz) of **3** in $CDCl_3$, measured at 298 K.

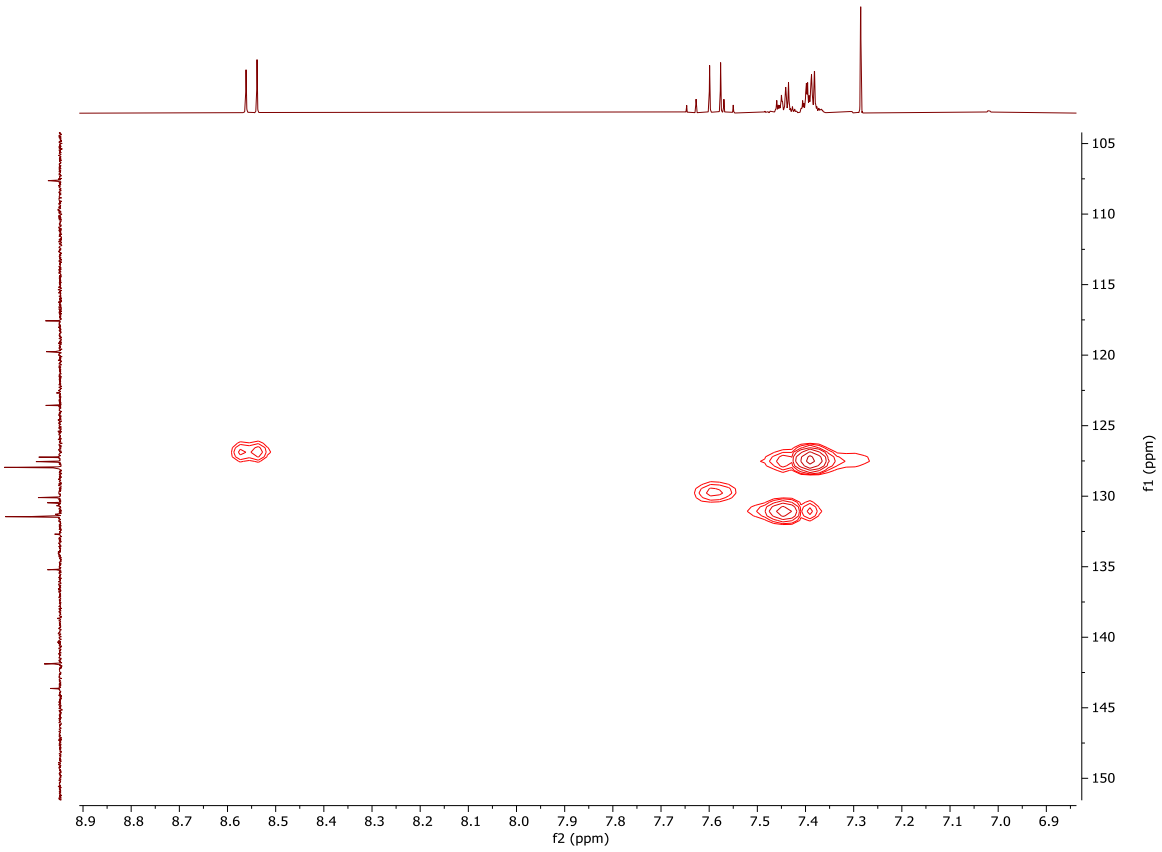

Figure S17. HSQC NMR (400 MHz) of **3** in $CDCl_3$, measured at 298 K (expansion in aromatic region).

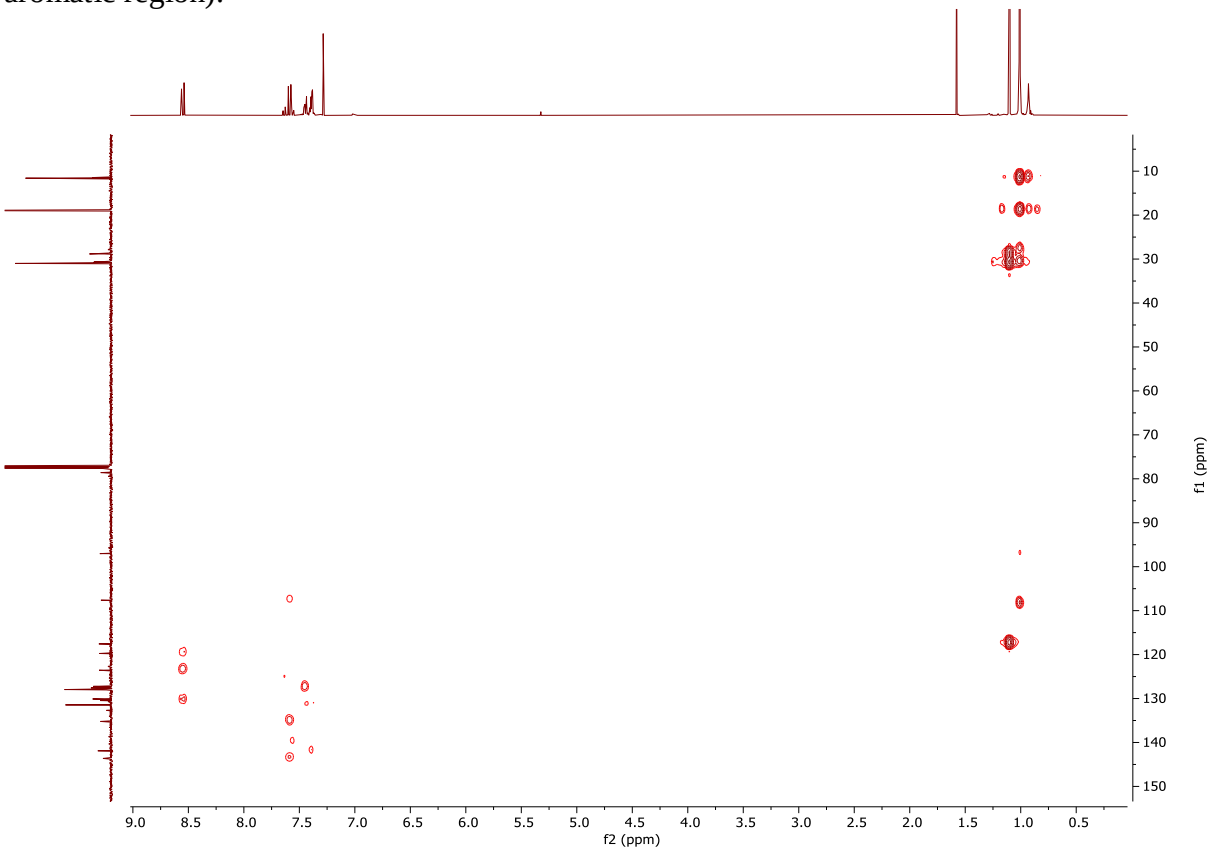

Figure S18. HMBC NMR (400 MHz) of **3** in $CDCl_3$, measured at 298 K.

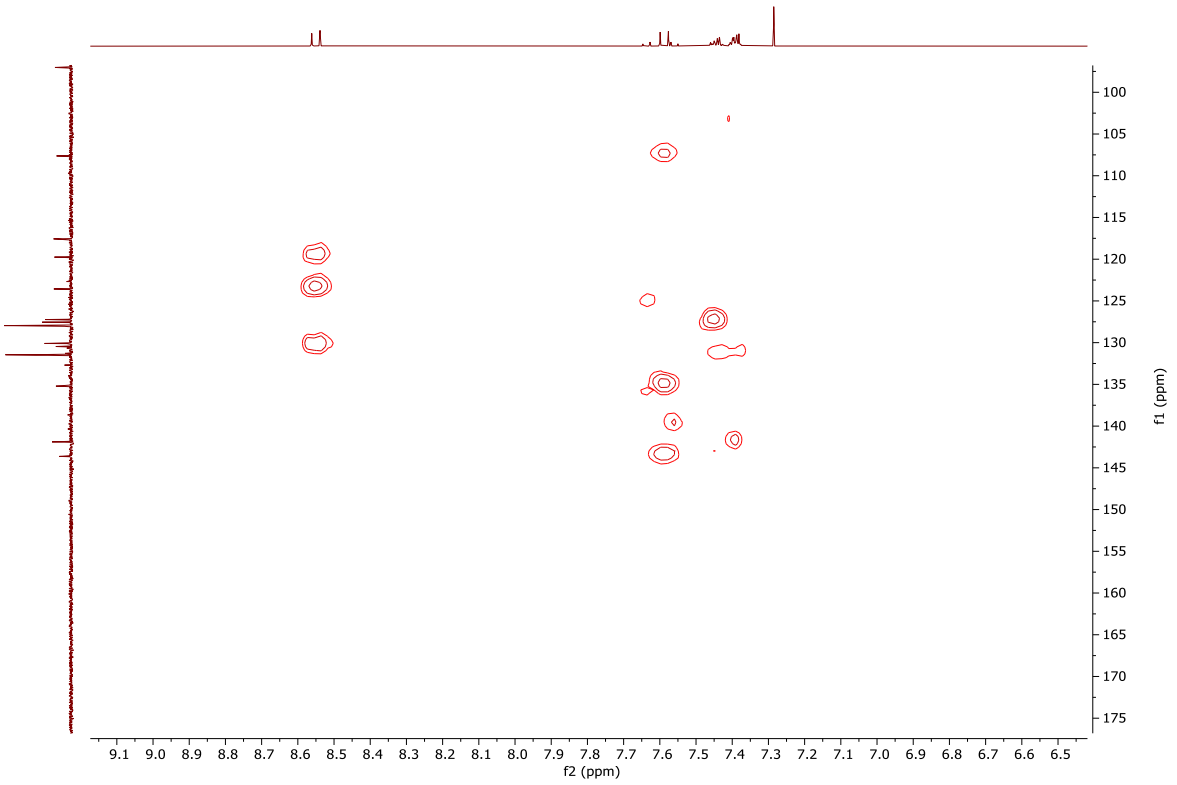

Figure S19. HMBC NMR (400 MHz) of **3** in $CDCl_3$, measured at 298 K (expansion in aromatic region).

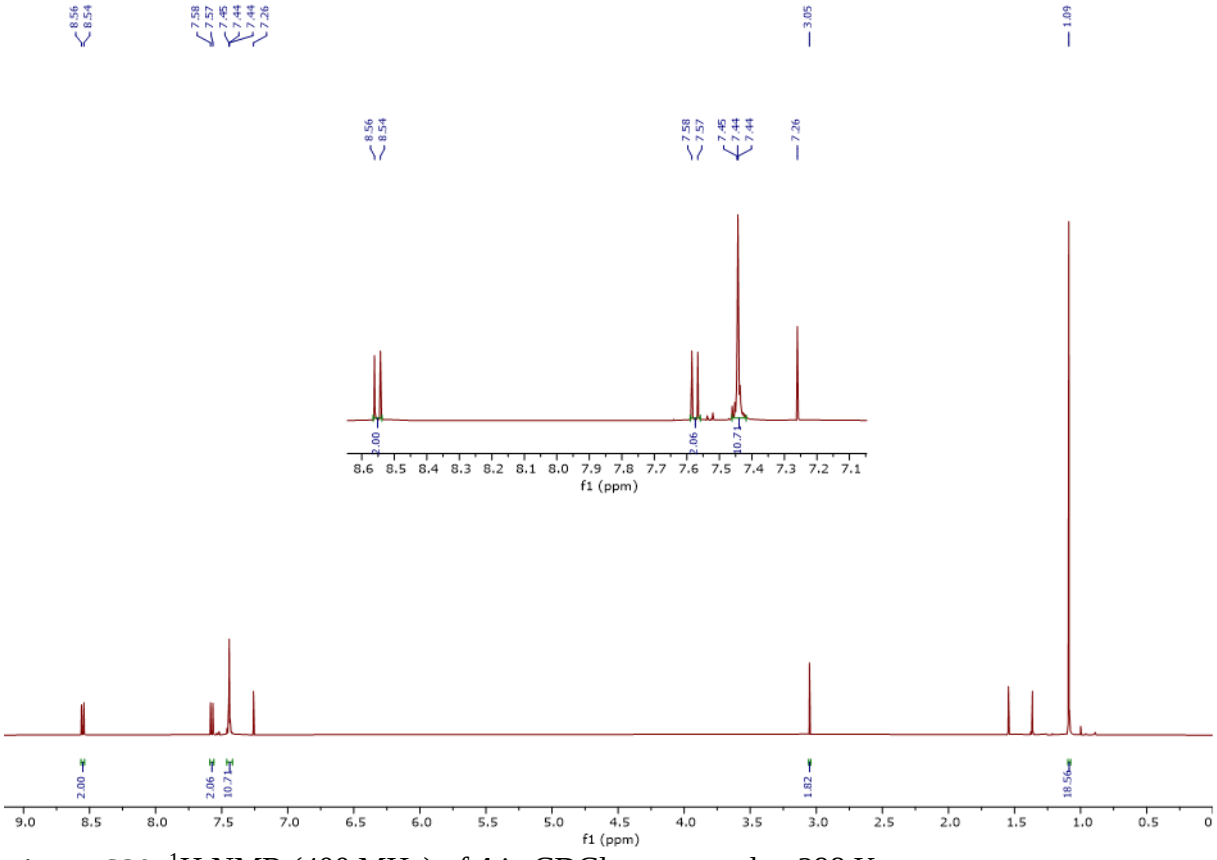

Figure S20. ^{1}H NMR (400 MHz) of **4** in $CDCl_3$, measured at 298 K.

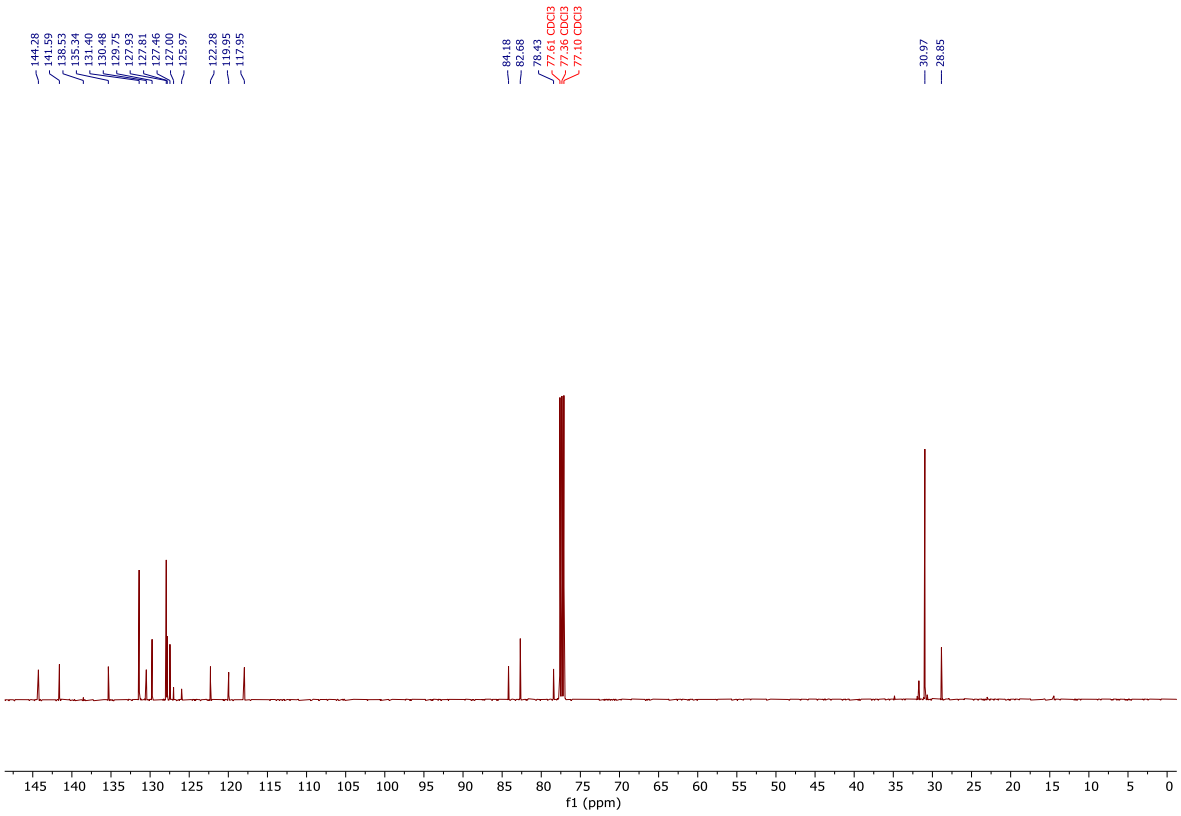

Figure S21. ^{13}C NMR (101 MHz) of **4** in $CDCl_3$, measured at 298 K.

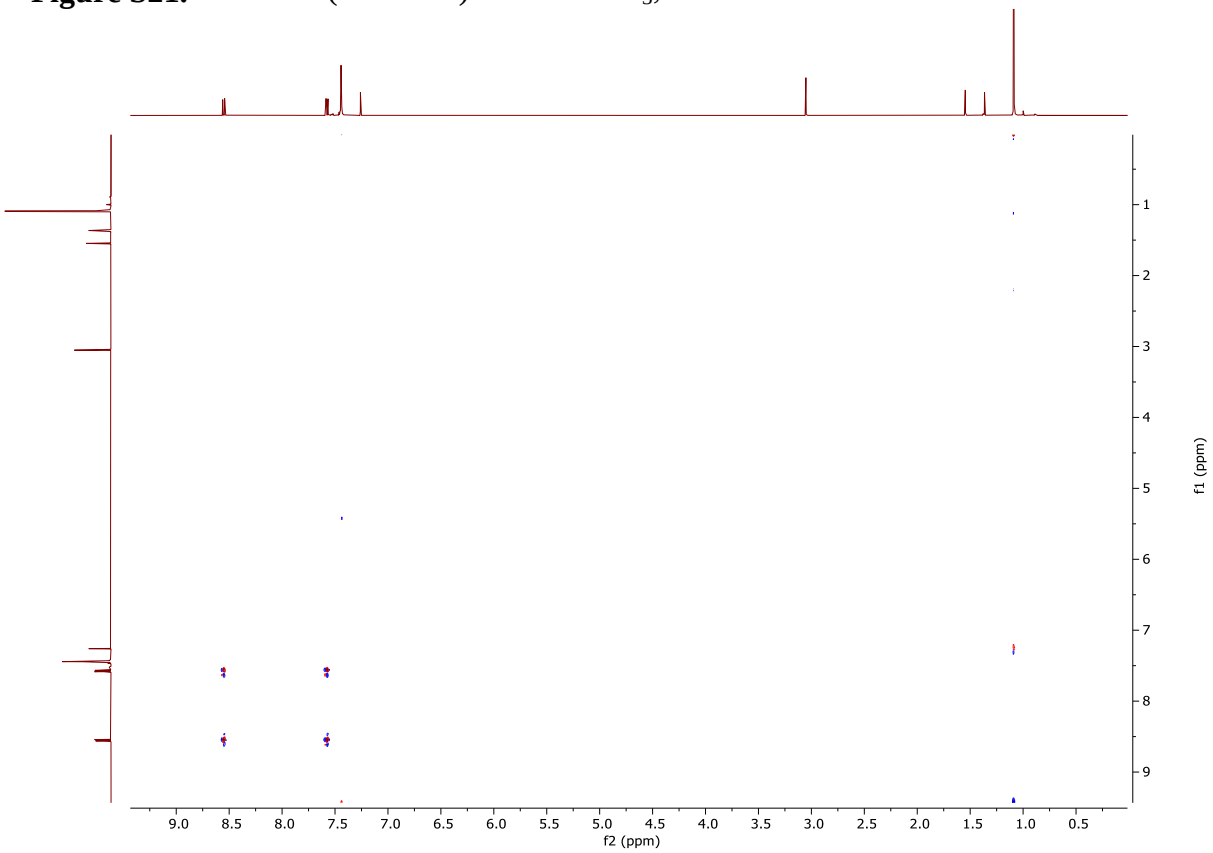

Figure S22. COSY NMR (400 MHz) of **4** in $CDCl_3$, measured at 298 K.

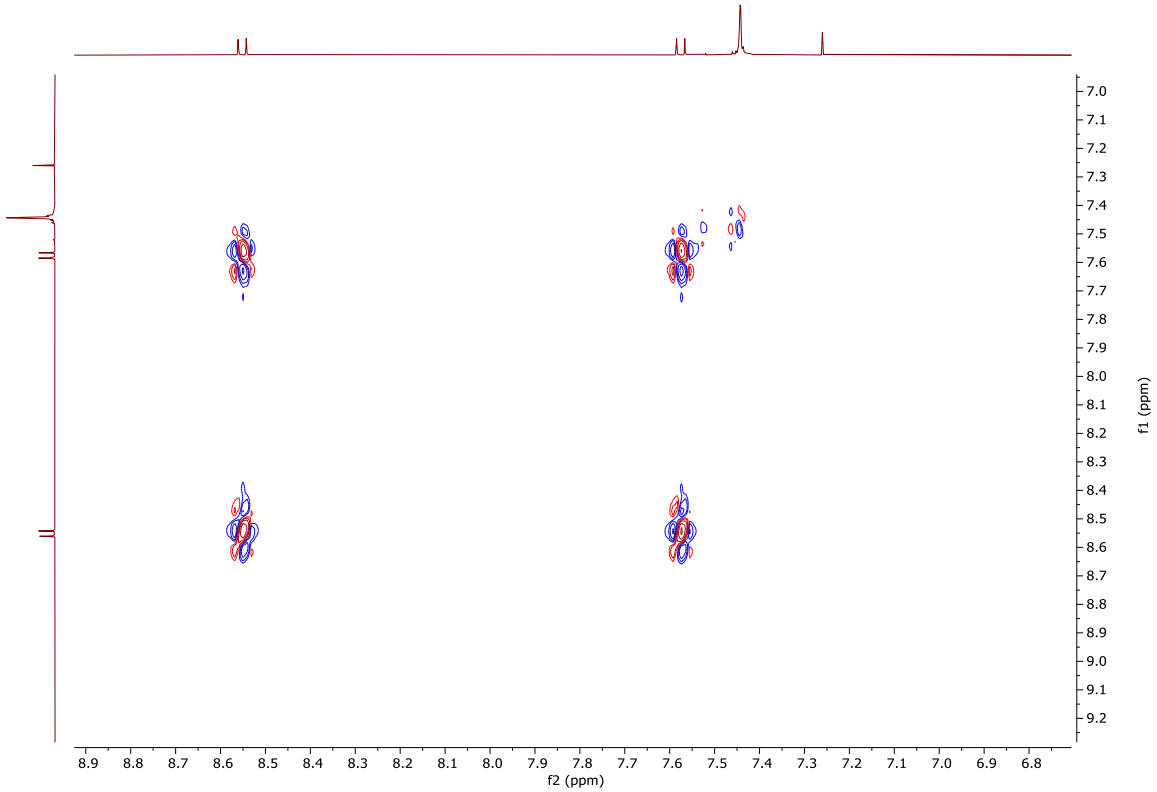

Figure S23. COSY NMR (400 MHz) of **4** in $CDCl_3$, measured at 298 K (expansion in aromatic region).

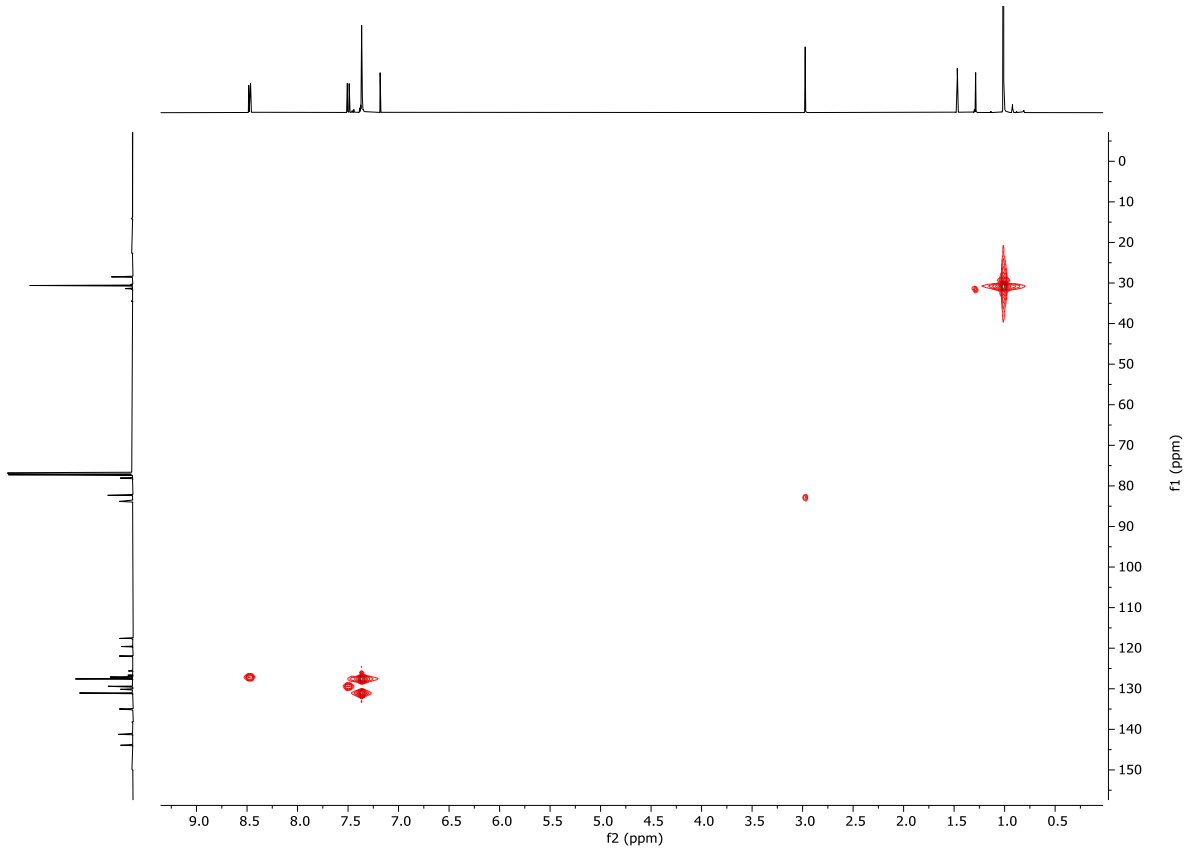

Figure S24. HSQC NMR (400 MHz) of **4** in $CDCl_3$, measured at 298 K.

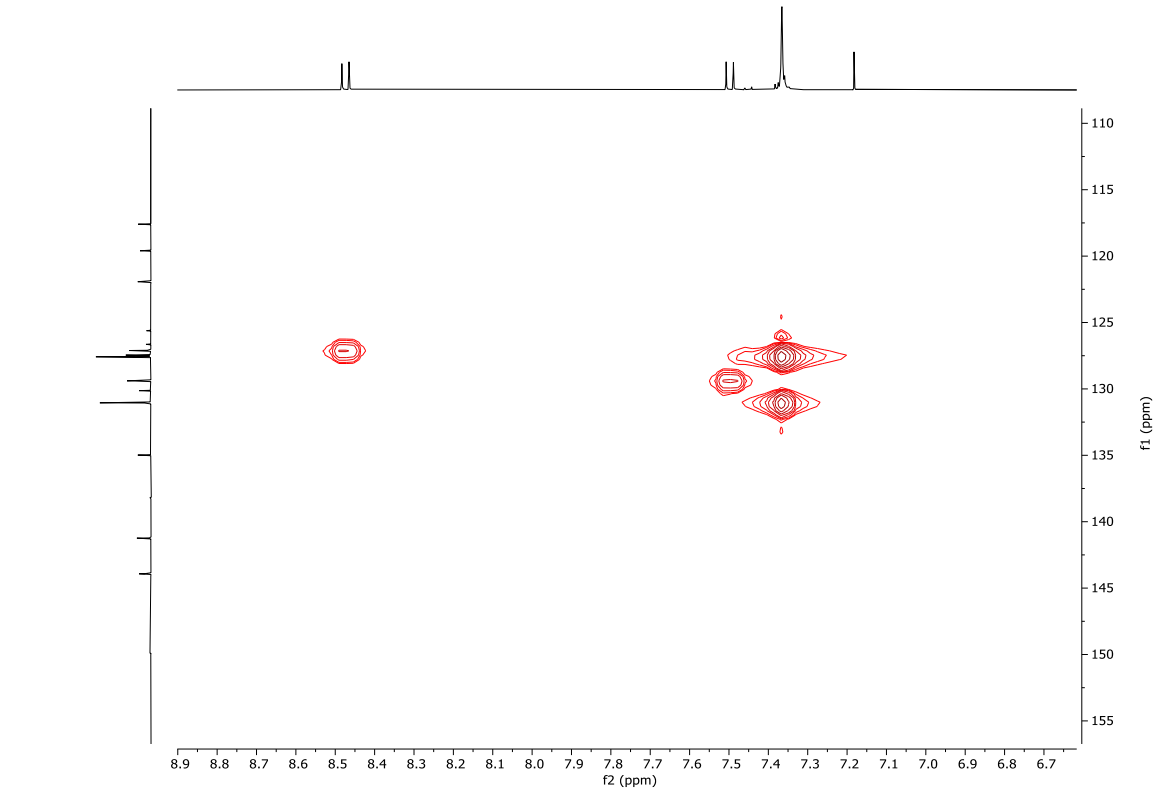

Figure S25. HSQC NMR (400 MHz) of **4** in $CDCl_3$, measured at 298 K (expansion in aromatic region).

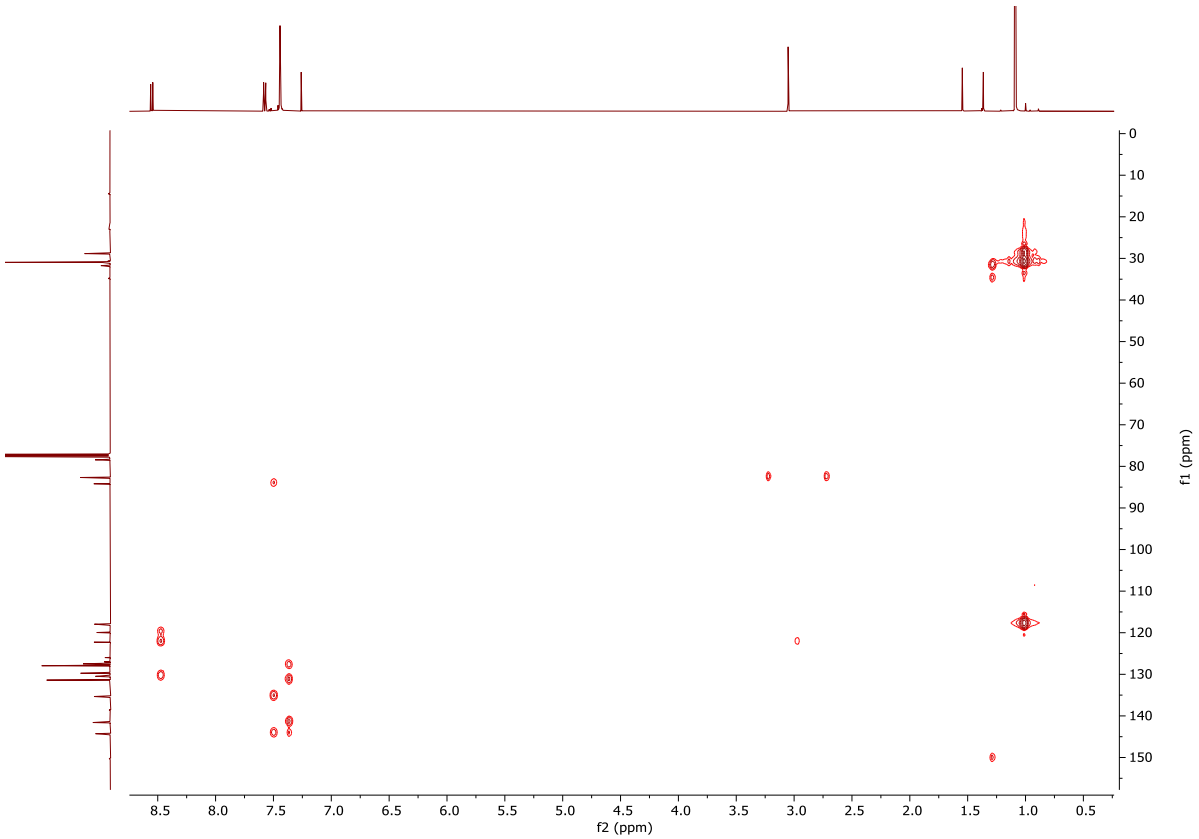

Figure S26. HMBC NMR (400 MHz) of **4** in $CDCl_3$, measured at 298 K.

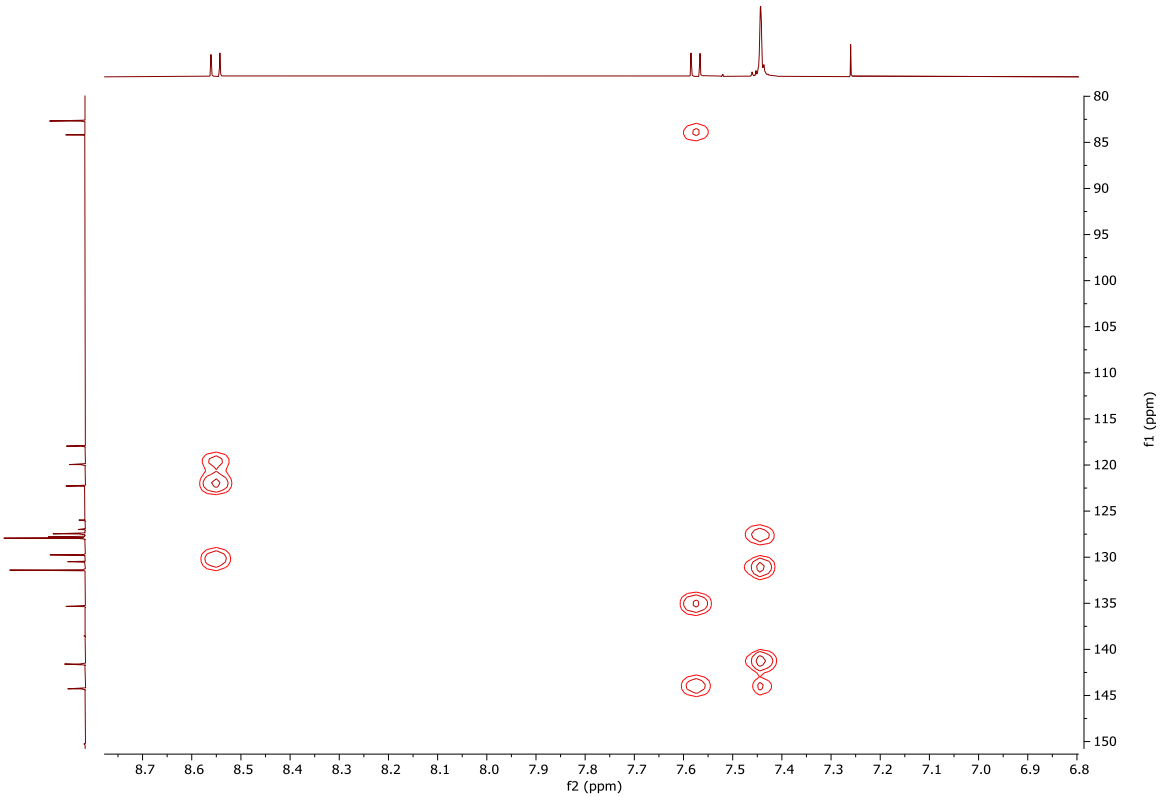

Figure S27. HMBC NMR (400 MHz) of **4** in $CDCl_3$, measured at 298 K (expansion in aromatic region).

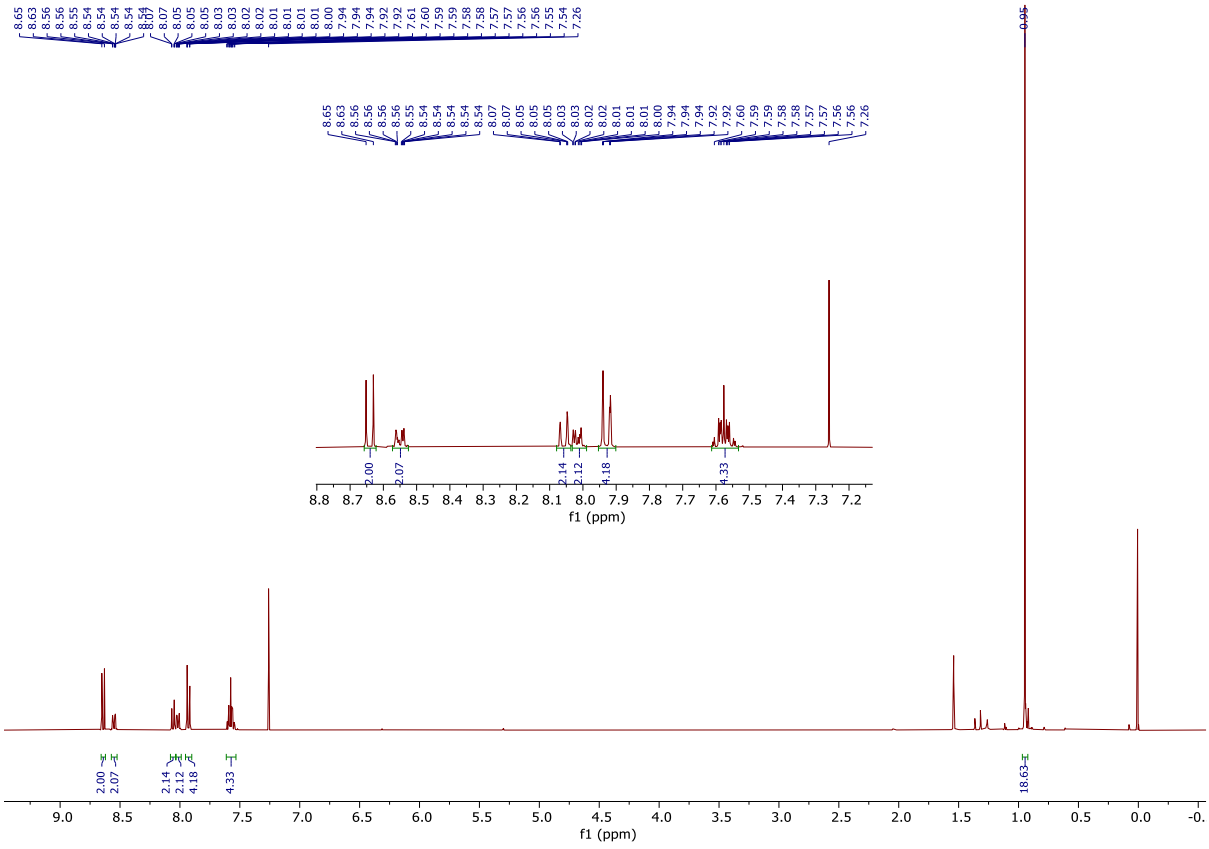

Figure S28. ^{1}H NMR (400 MHz) of **DH-C0** in $CDCl_3$, measured at 298 K.

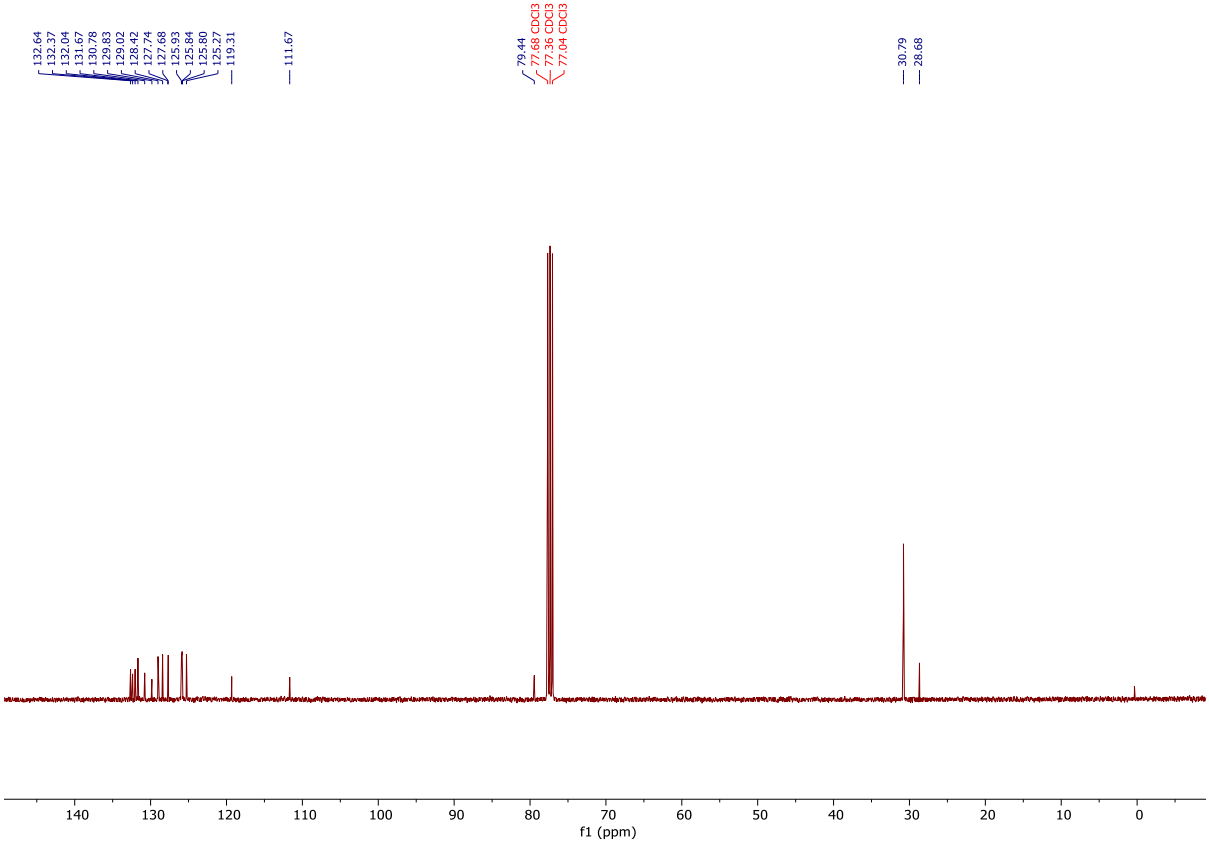

Figure S29. ^{13}C NMR (101 MHz) of **DH-C0** in $CDCl_3$, measured at 298 K.

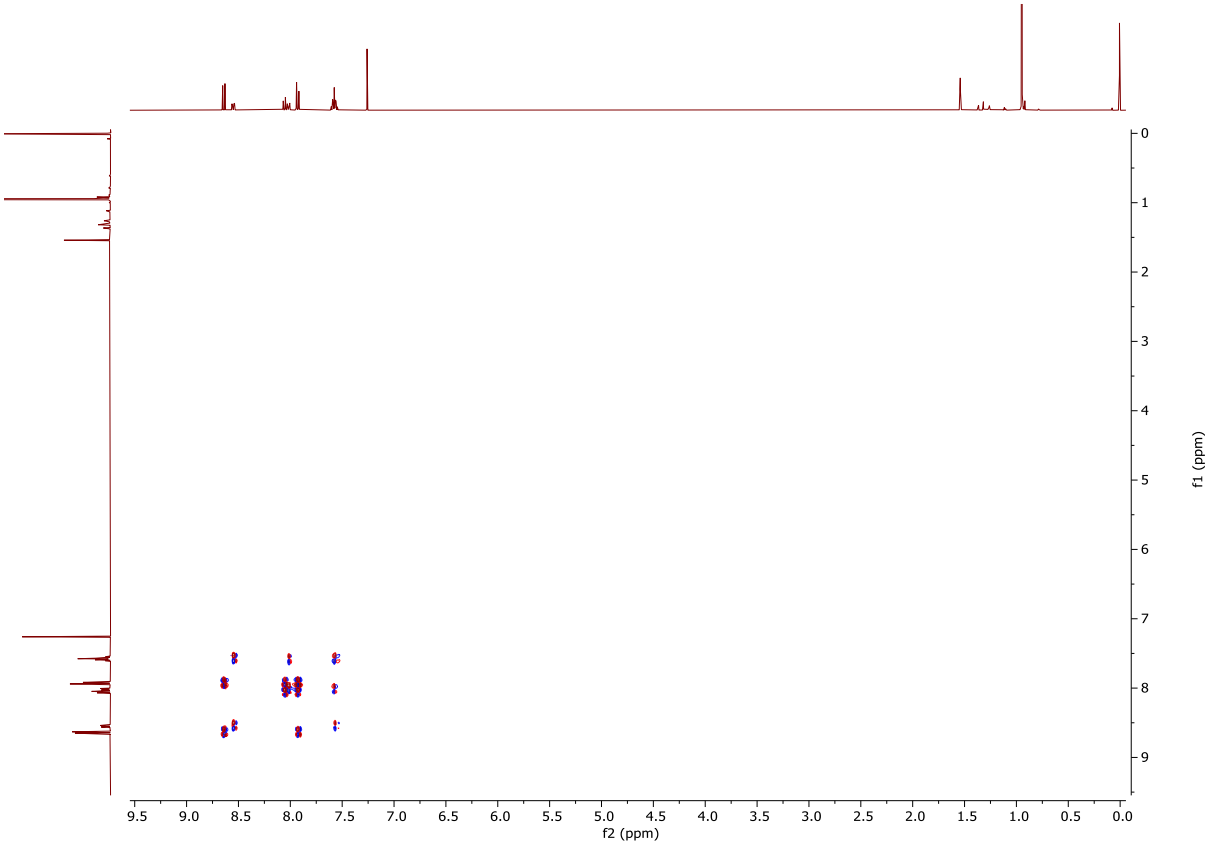

Figure S30. COSY NMR (400 MHz) of **DH-C0** in $CDCl_3$, measured at 298 K.

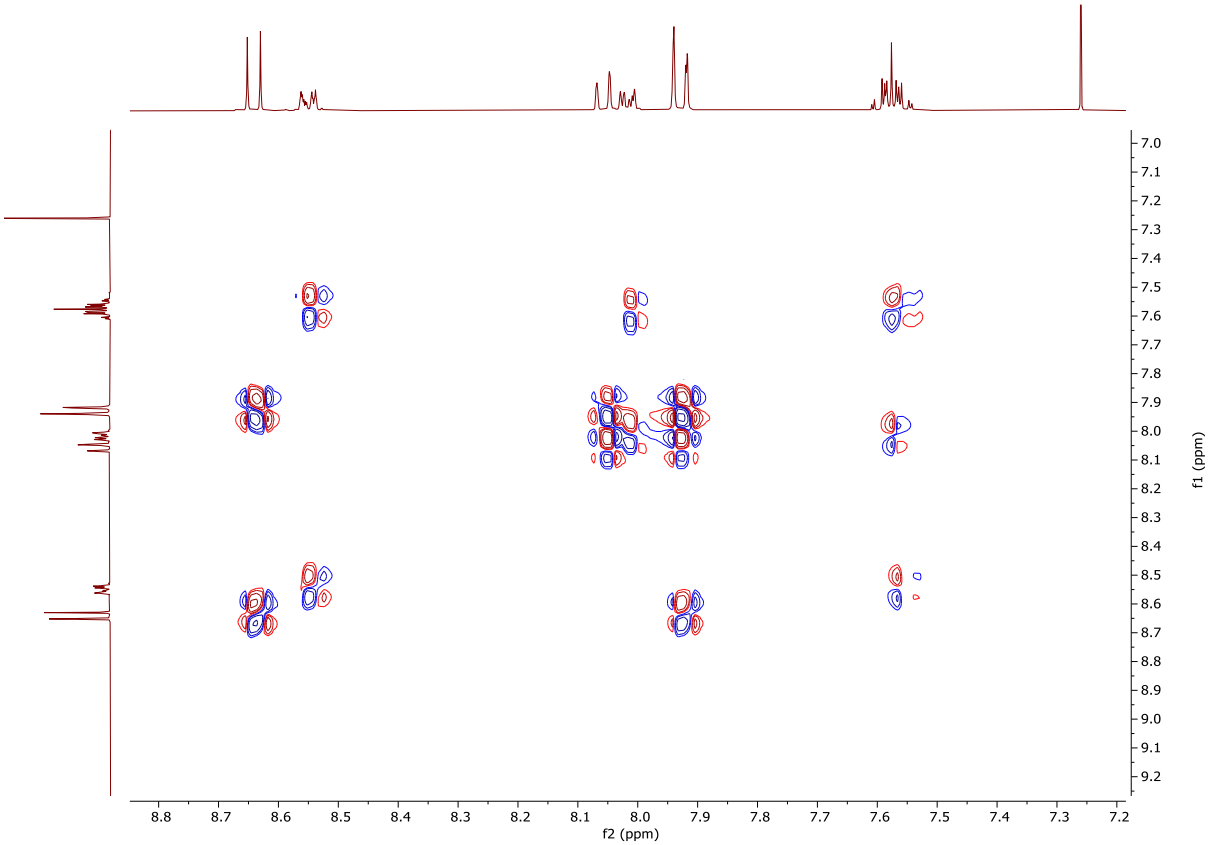

Figure S31. COSY NMR (400 MHz) of **DH-C0** in $CDCl_3$, measured at 298 K (expansion in aromatic region).

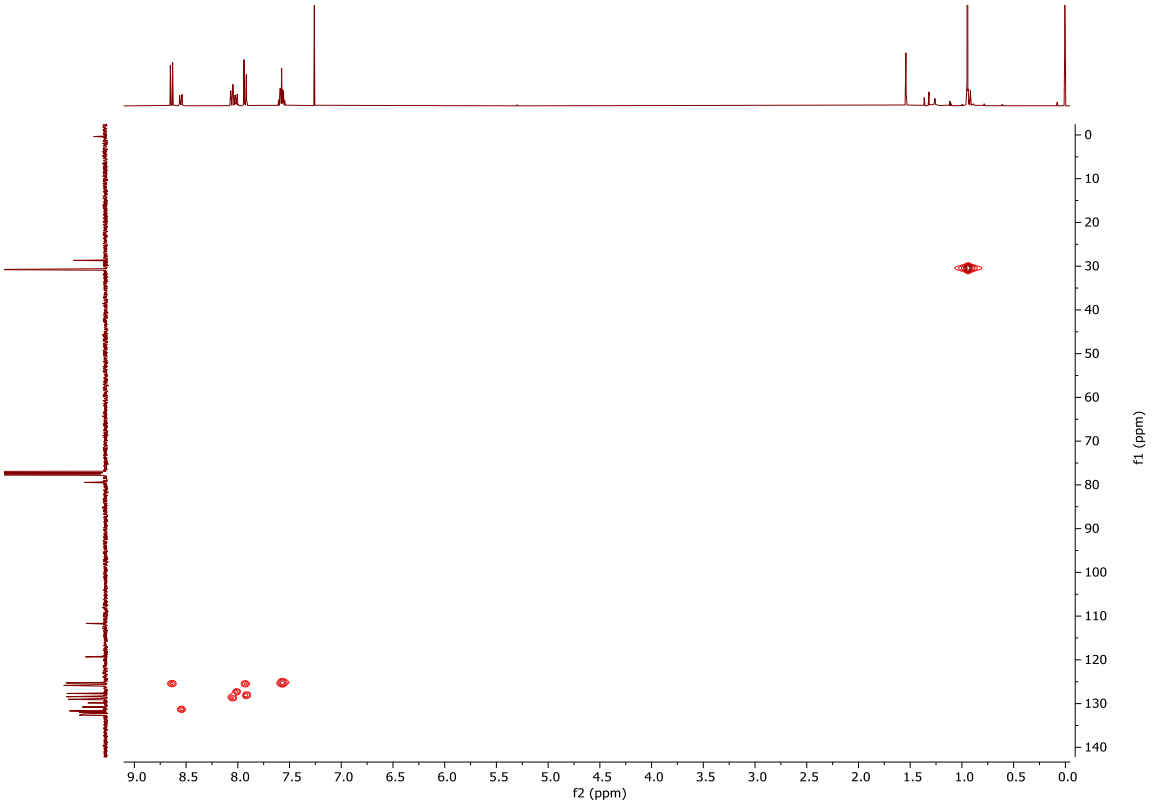

Figure S32. HSQC NMR (400 MHz) of **DH-C0** in $CDCl_3$, measured at 298 K.

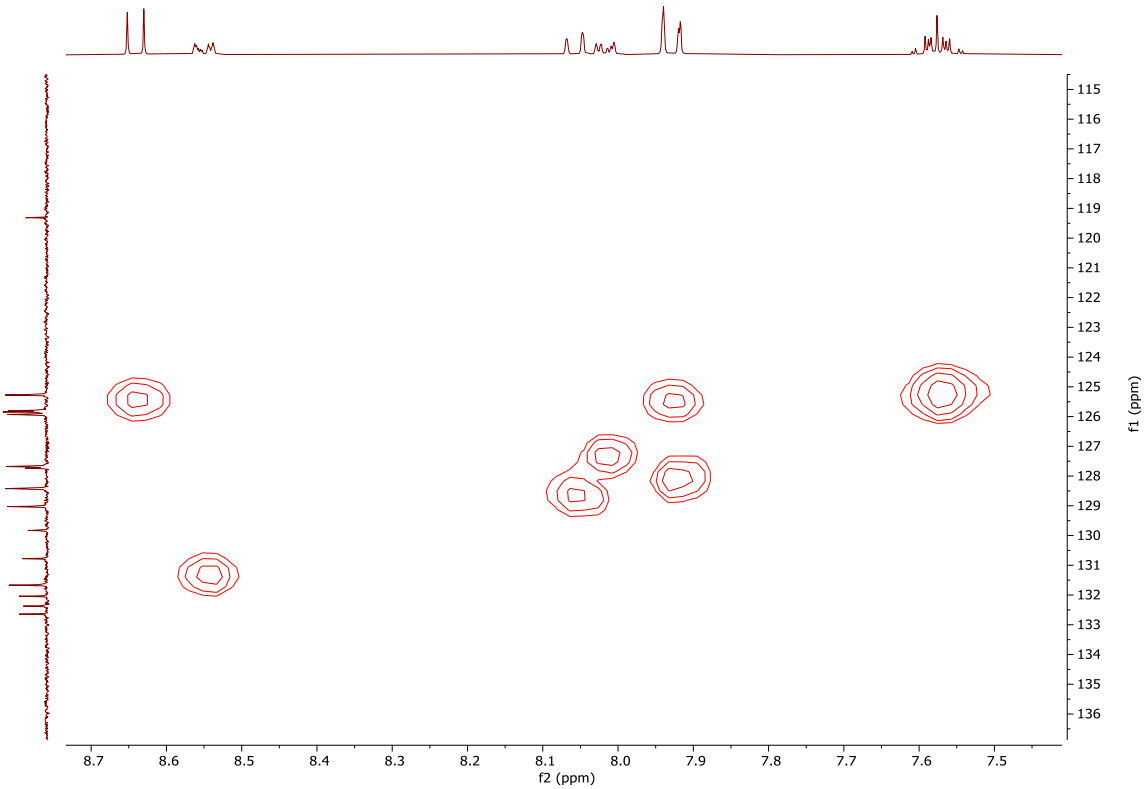

Figure S33. HSQC NMR (400 MHz) of **DH-C0** in $CDCl_3$, measured at 298 K (expansion in aromatic region).

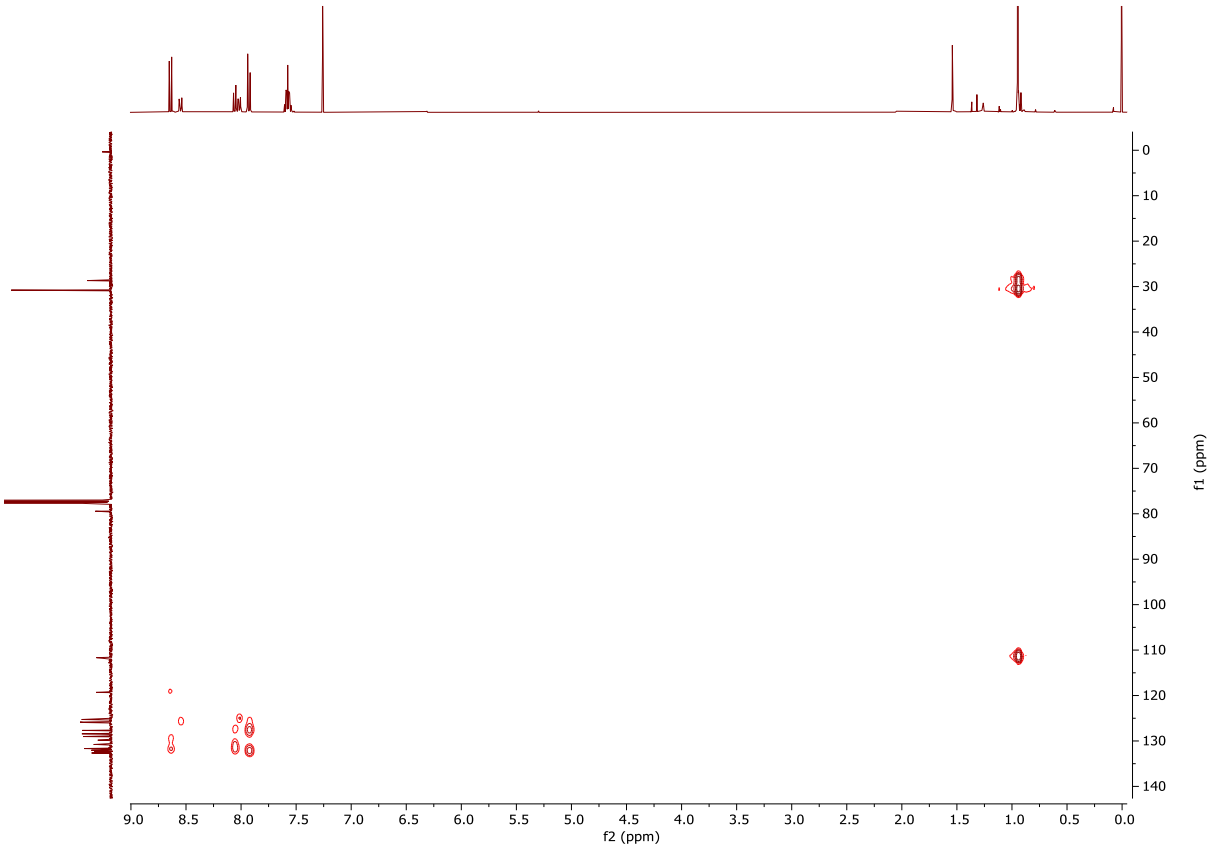

Figure S34. HMBC NMR (400 MHz) of **DH-C0** in $CDCl_3$, measured at 298 K.

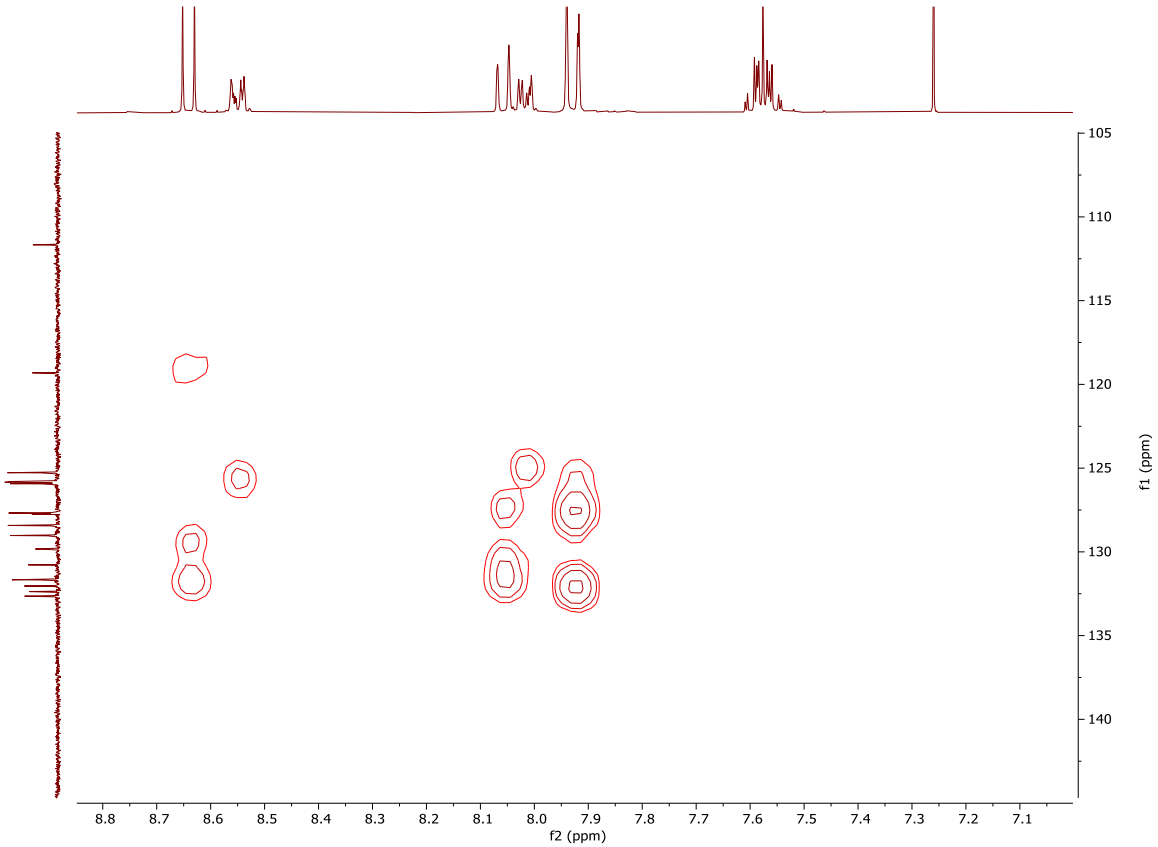

Figure S35. HMBC NMR (400 MHz) of **DH-C0** in $CDCl_3$, measured at 298 K (expansion in aromatic region).

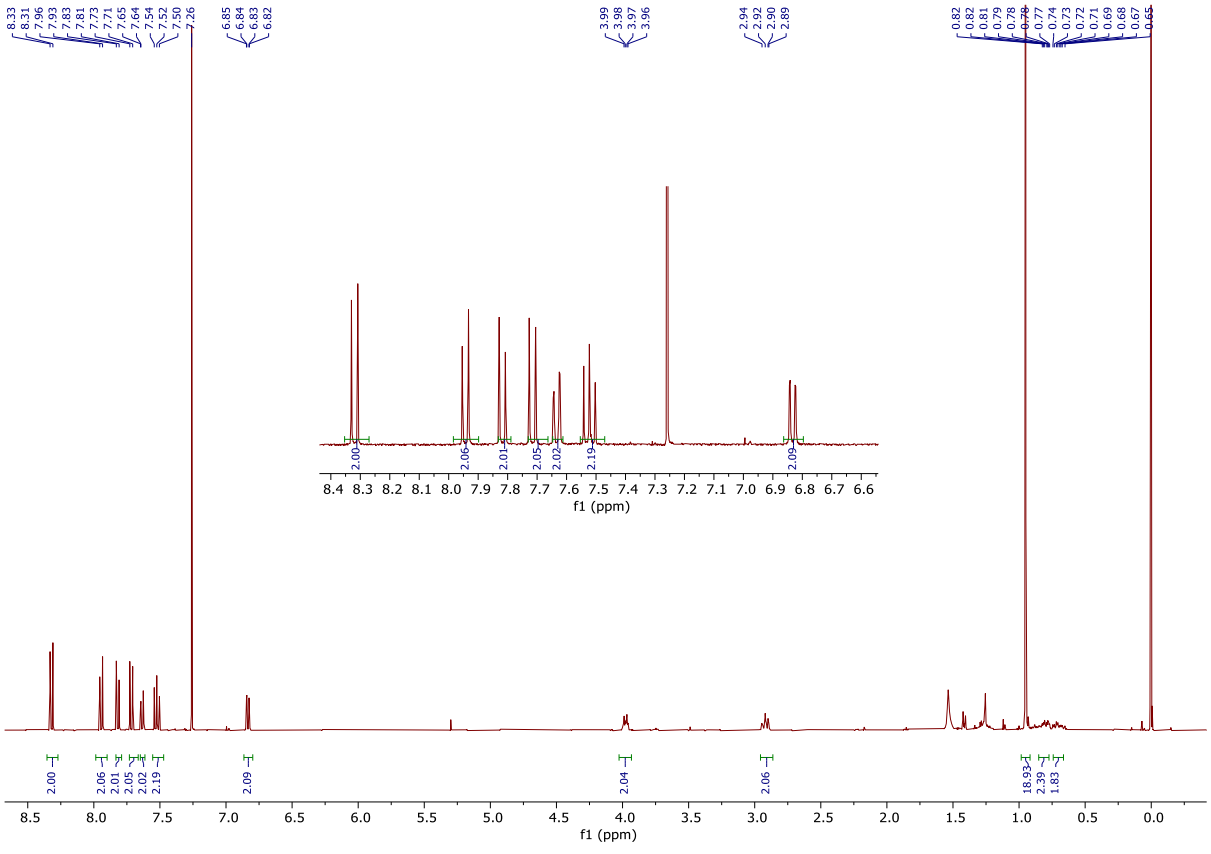

Figure S36. ^1H NMR (400 MHz) of **DH-C4** in $CDCl_3$, measured at 298 K.

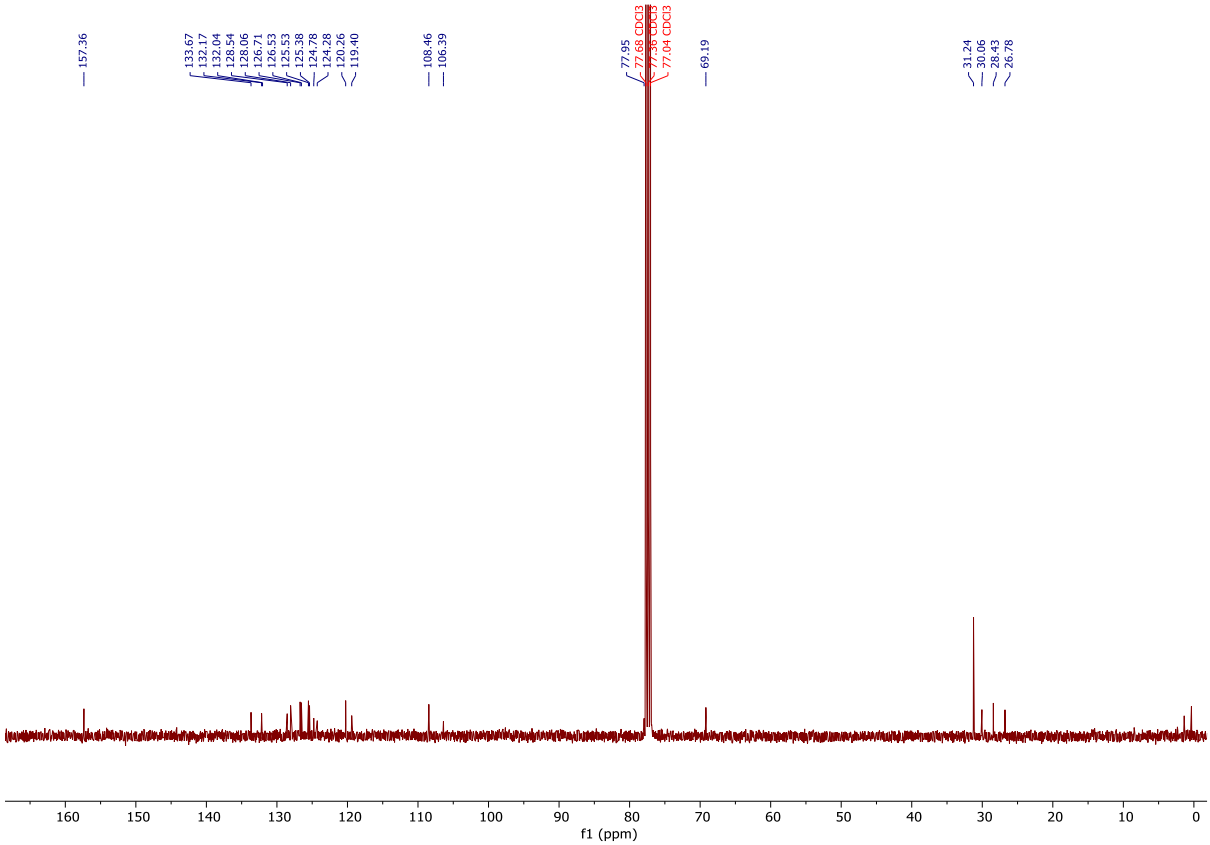

Figure S37. ^{13}C NMR (101 MHz) of **DH-C4** in $CDCl_3$, measured at 298 K.

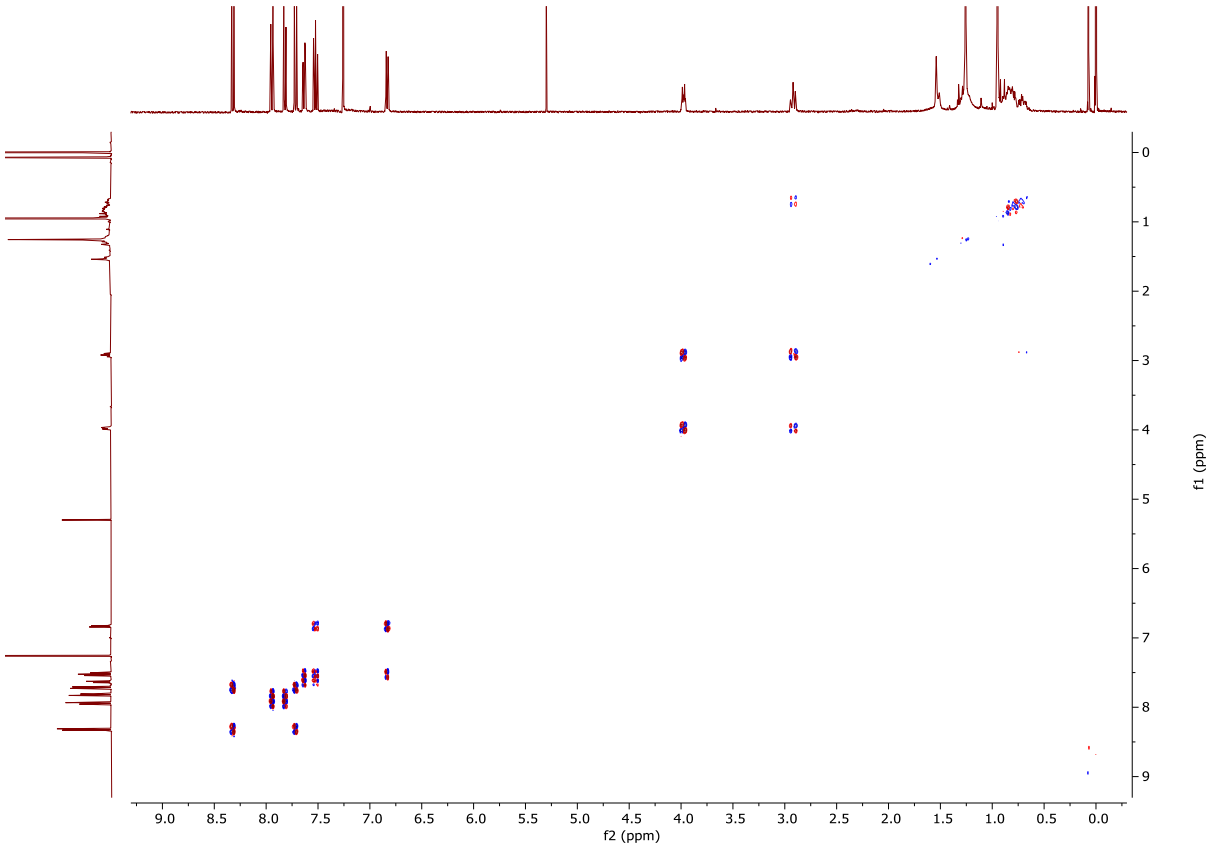

Figure S38. COSY NMR (400 MHz) of **DH-C4** in $CDCl_3$, measured at 298 K.

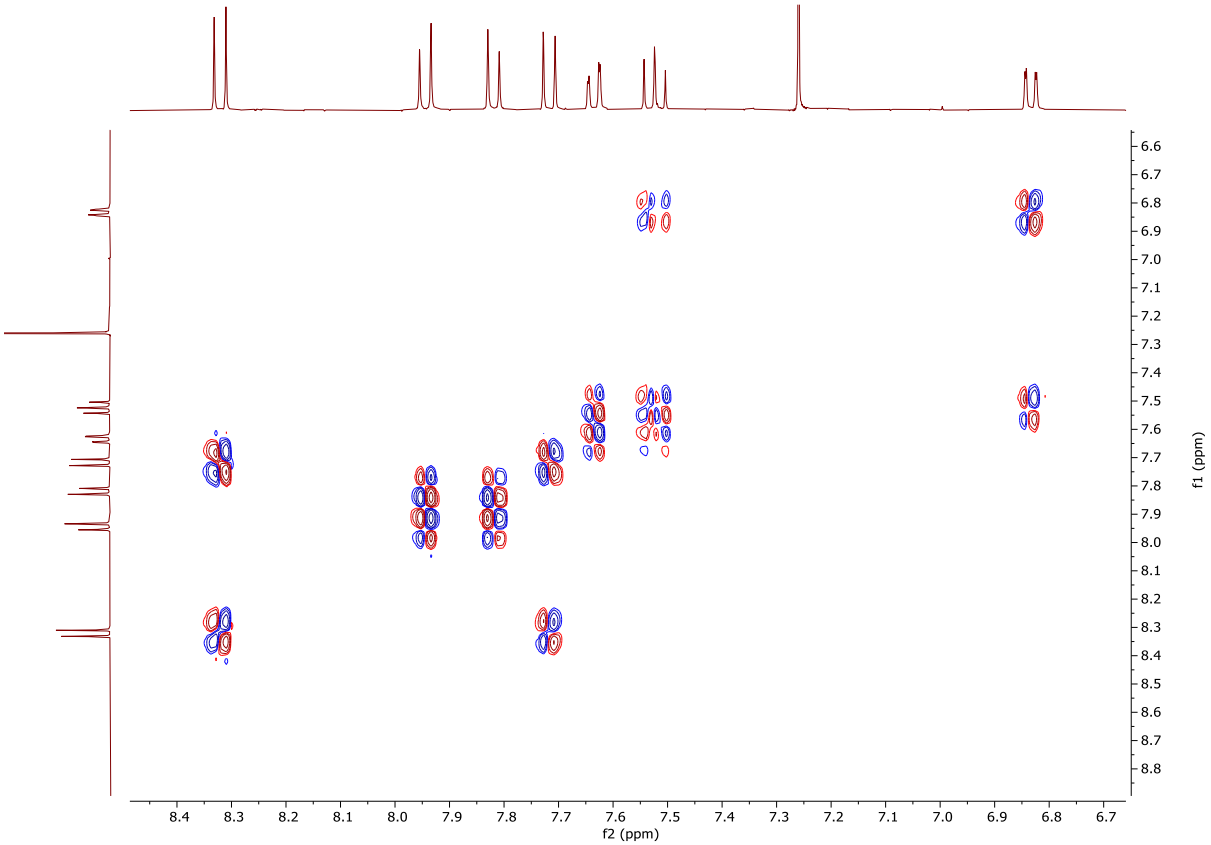

Figure S39. COSY NMR (400 MHz) of **DH-C4** in $CDCl_3$, measured at 298 K (expansion in aromatic region).

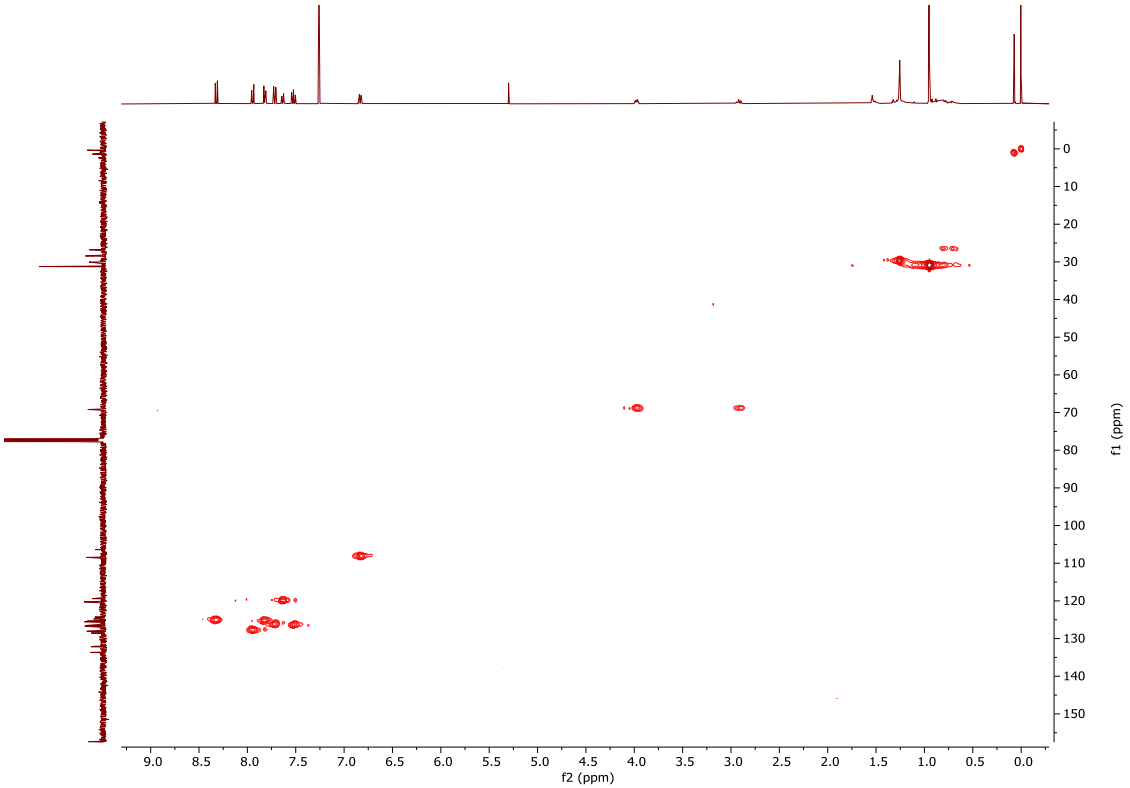

Figure S40. HSQC NMR (400 MHz) of **DH-C4** in $CDCl_3$, measured at 298 K.

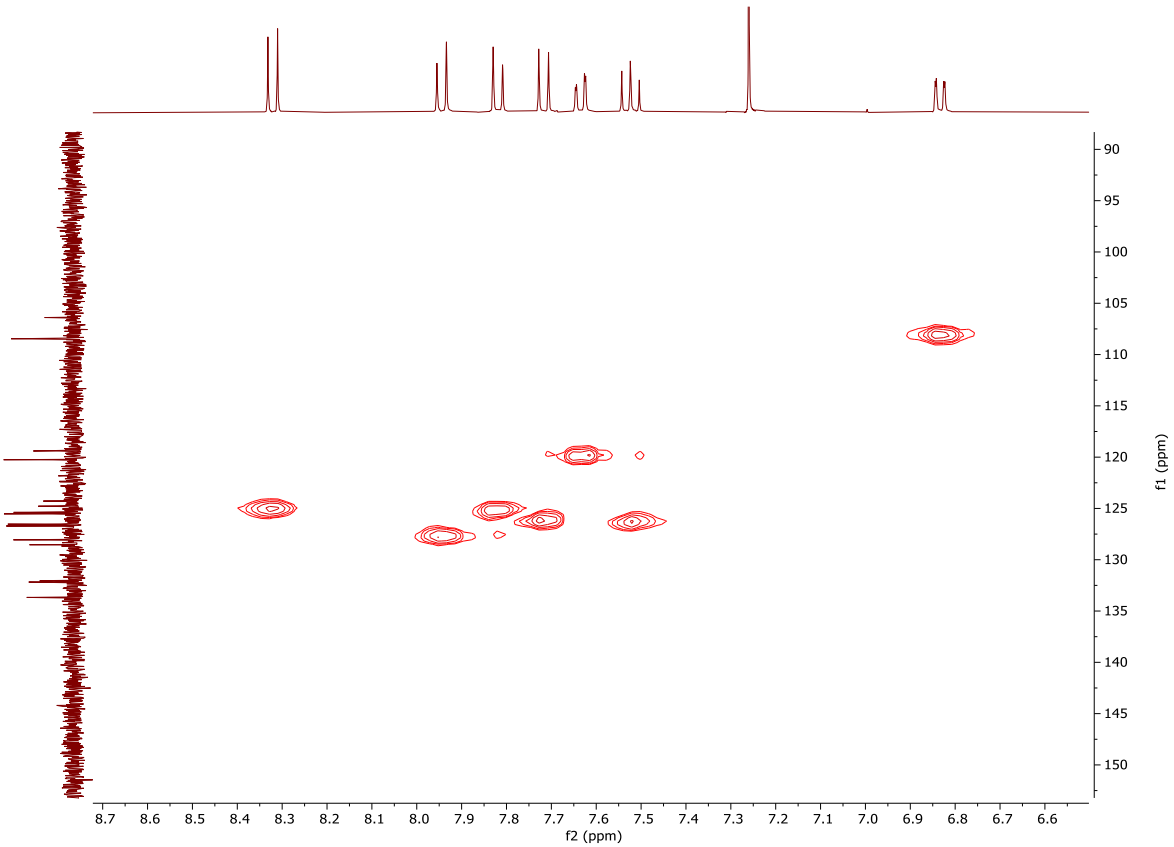

Figure S41. HSQC NMR (400 MHz) of **DH-C4** in $CDCl_3$, measured at 298 K (expansion in aromatic region).

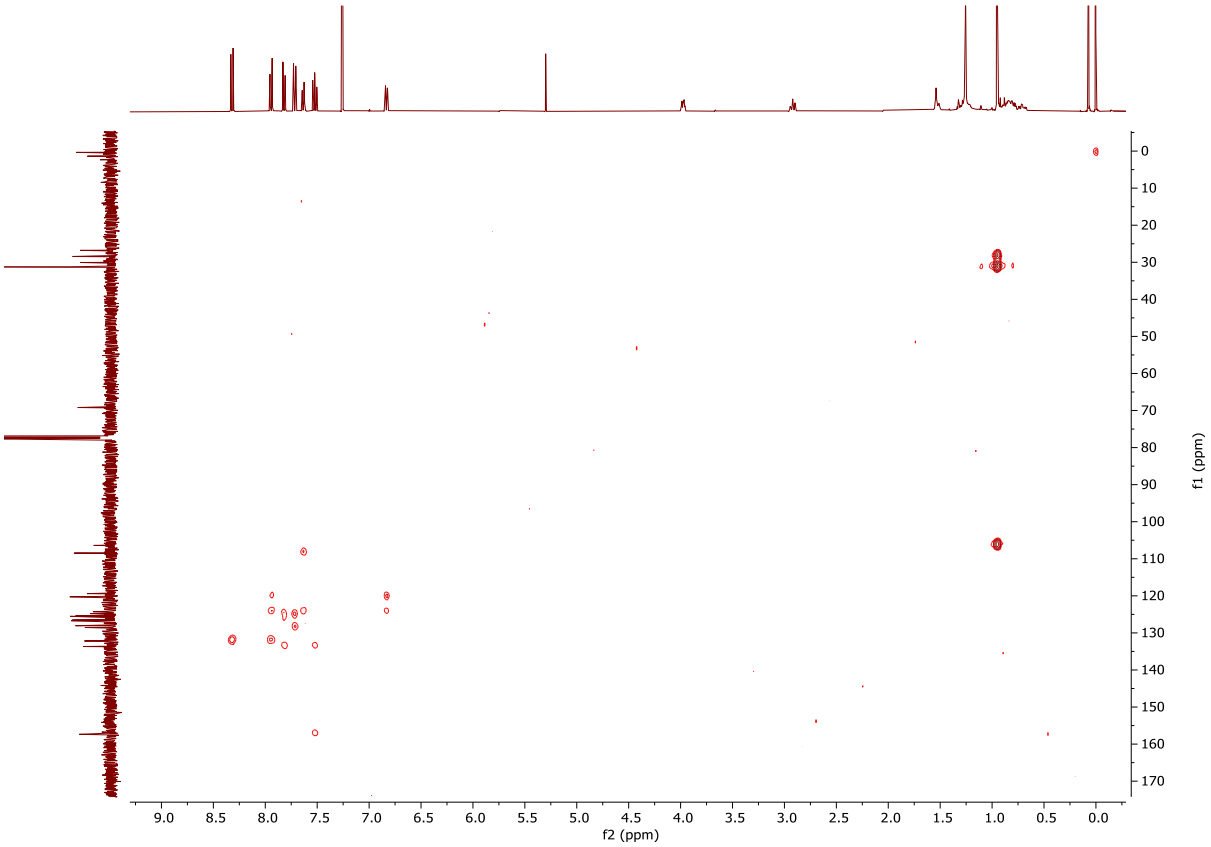

Figure S42. HMBC NMR (400 MHz) of **DH-C4** in $CDCl_3$, measured at 298 K.

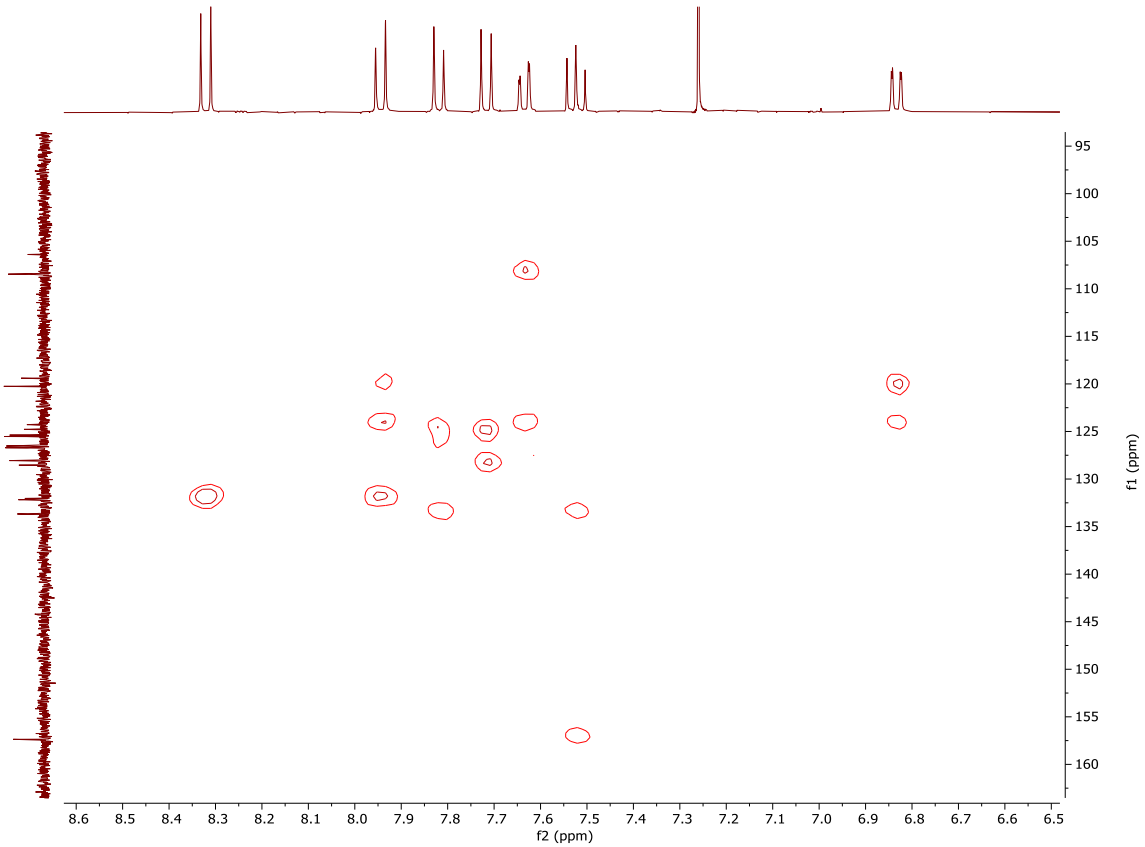

Figure S43. HMBC NMR (400 MHz) of **DH-C4** in $CDCl_3$, measured at 298 K (expansion in aromatic region).

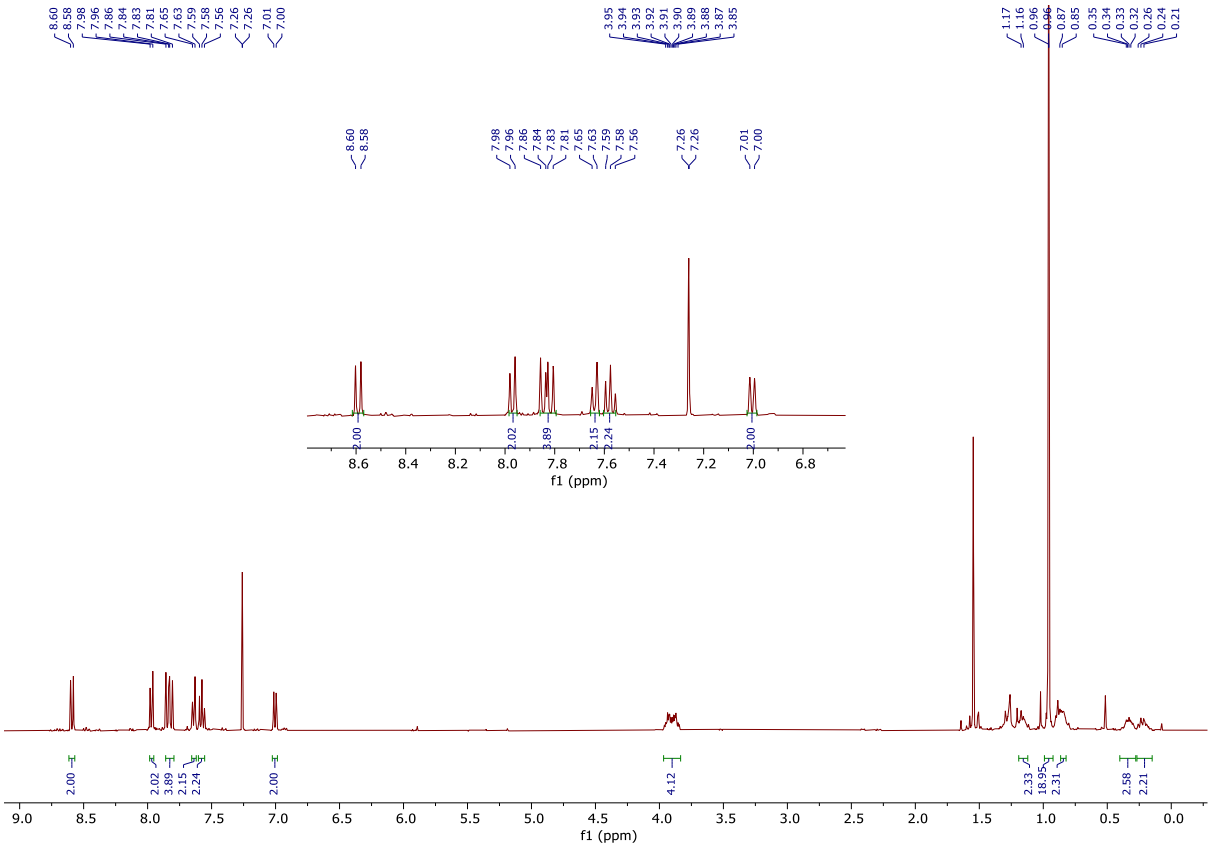

Figure S44. ^{1}H NMR (400 MHz) of **DH-C6** in $CDCl_3$, measured at 298 K.

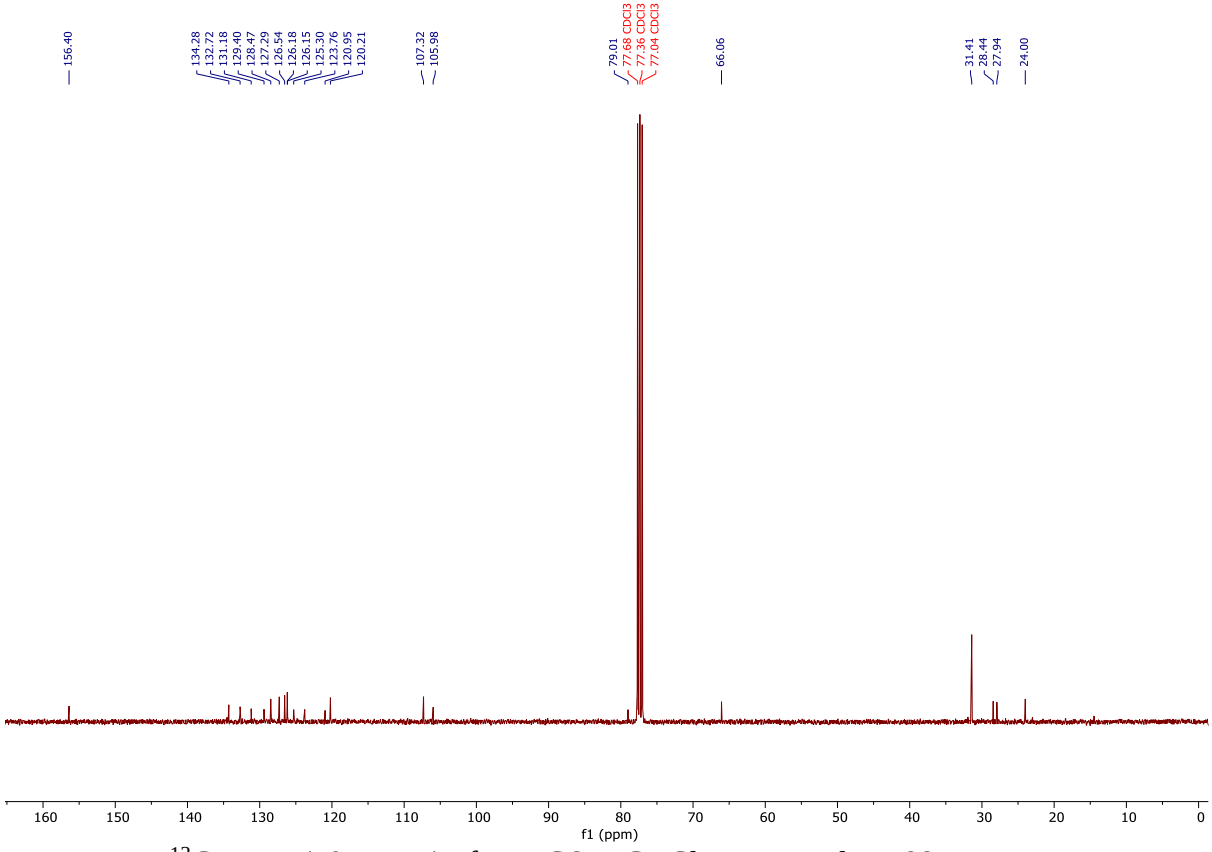

Figure S45. ^{13}C NMR (101 MHz) of **DH-C6** in $CDCl_3$, measured at 298 K.

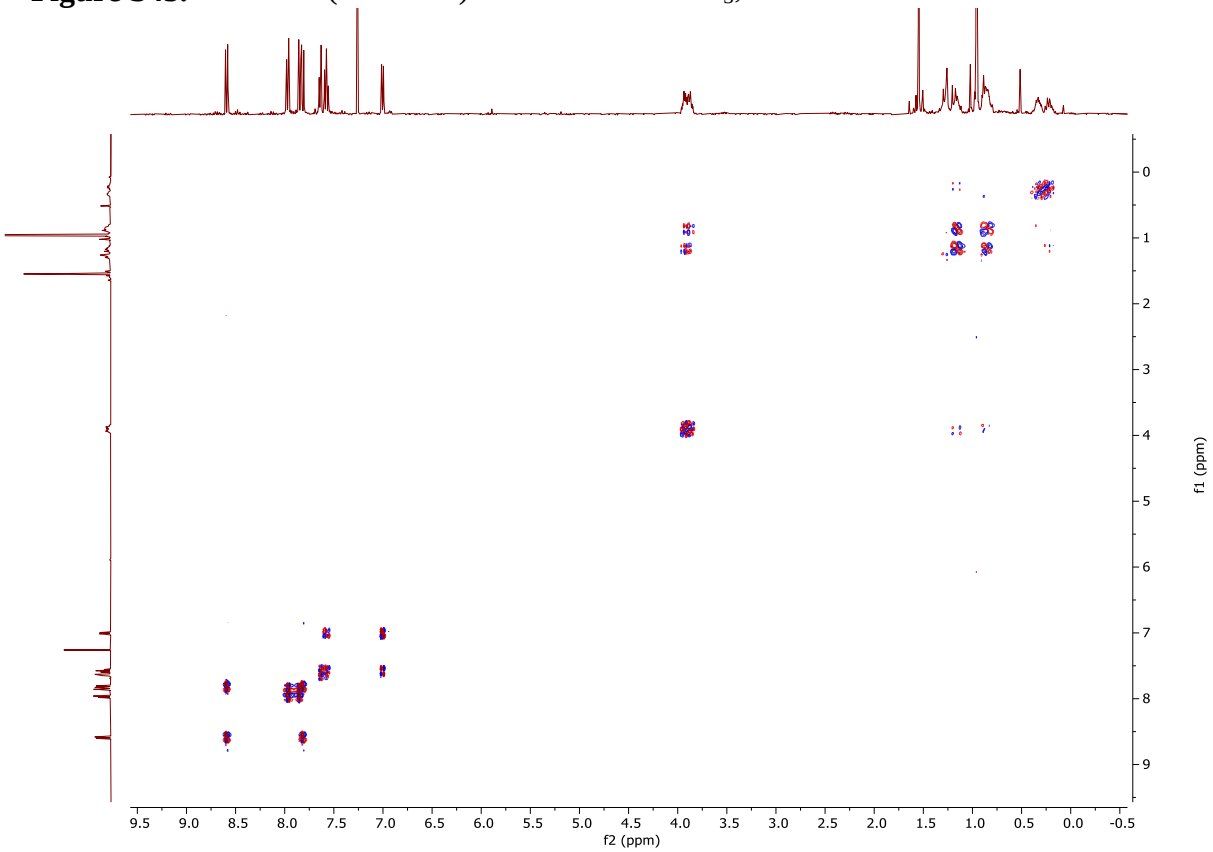

Figure S46. COSY NMR (400 MHz) of **DH-C6** in $CDCl_3$, measured at 298 K.

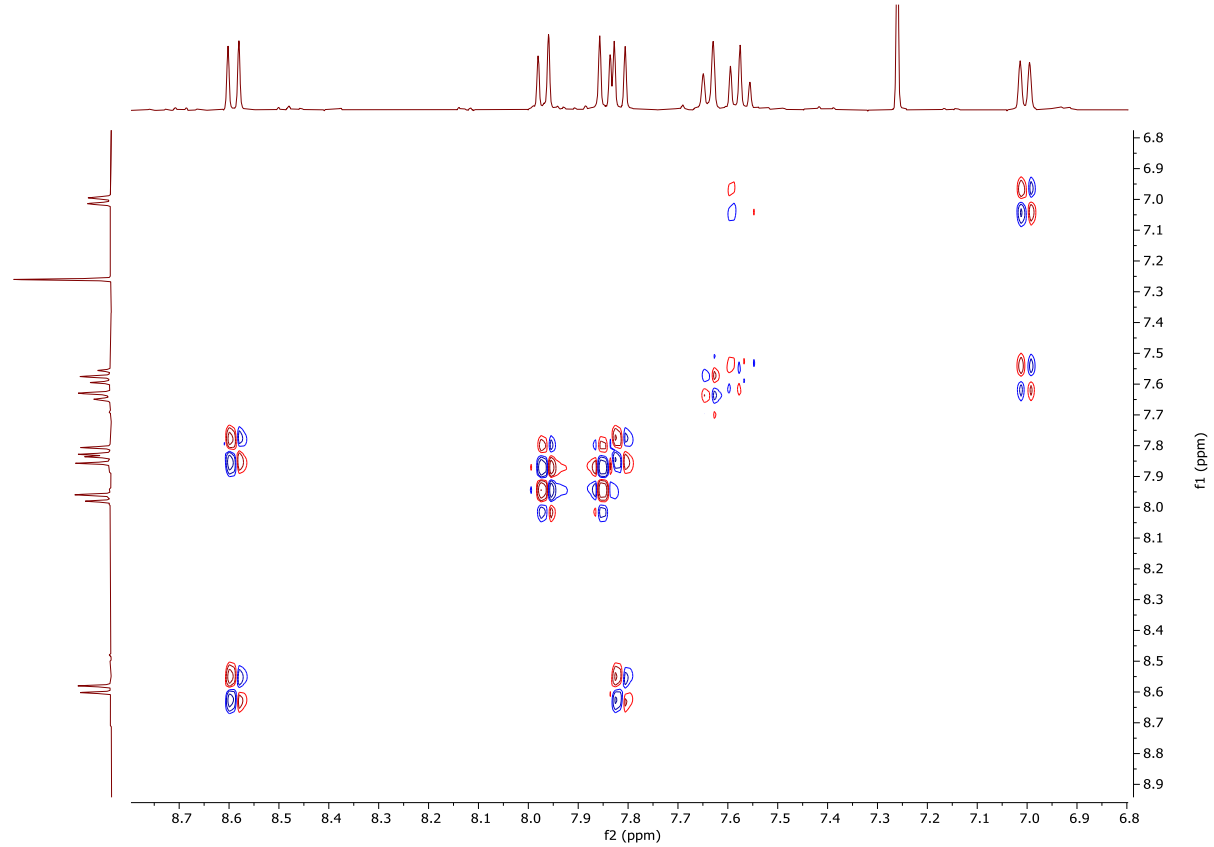

Figure S47. COSY NMR (400 MHz) of **DH-C6** in $CDCl_3$, measured at 298 K (expansion in aromatic region).

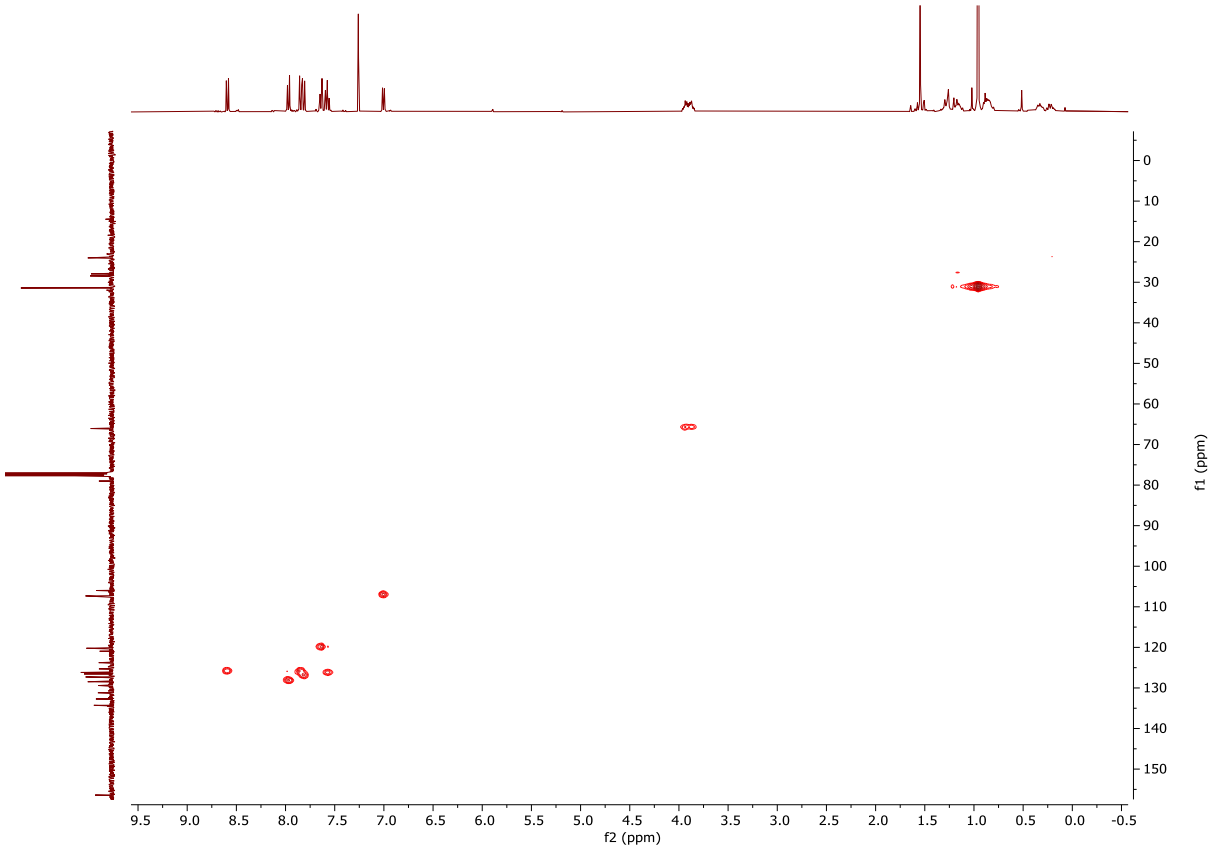

Figure S48. HSQC NMR (400 MHz) of **DH-C6** in $CDCl_3$, measured at 298 K.

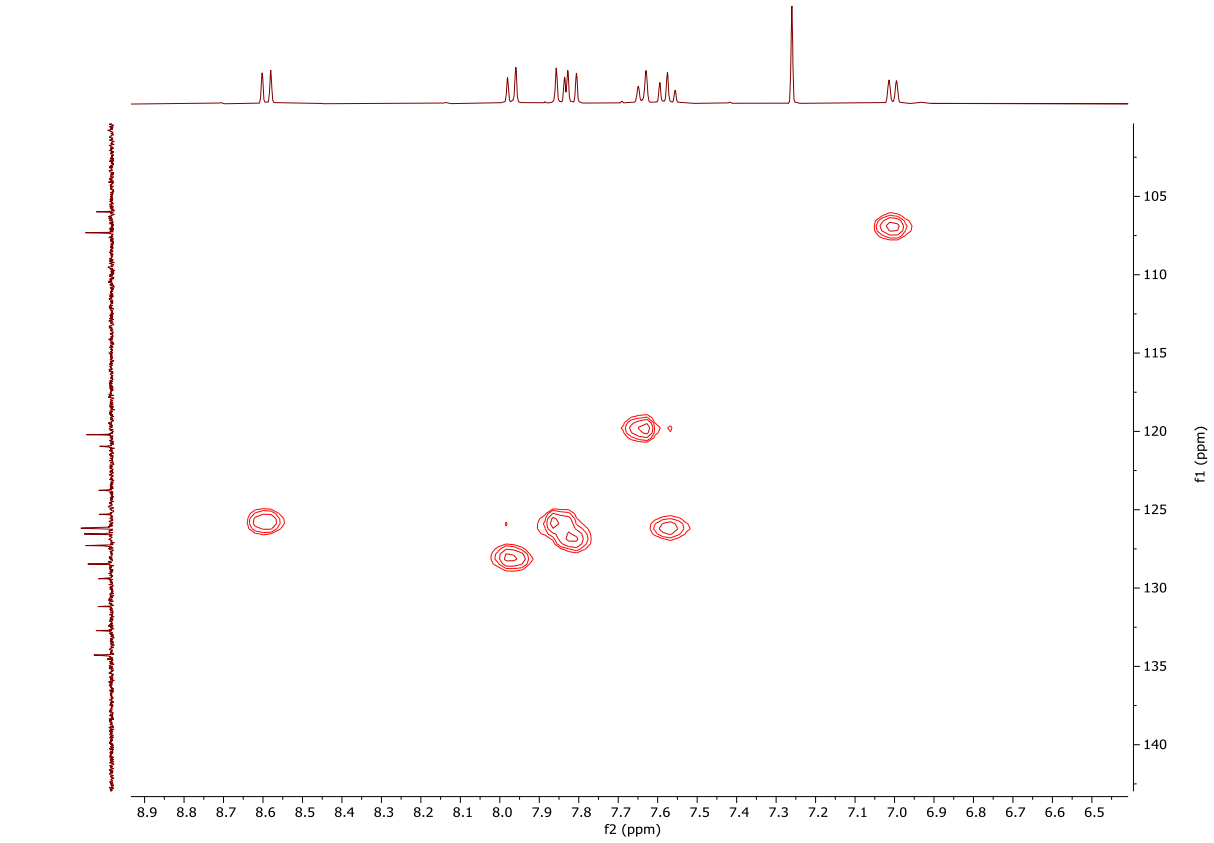

Figure S49. HSQC NMR (400 MHz) of **DH-C6** in $CDCl_3$, measured at 298 K (expansion in aromatic region).

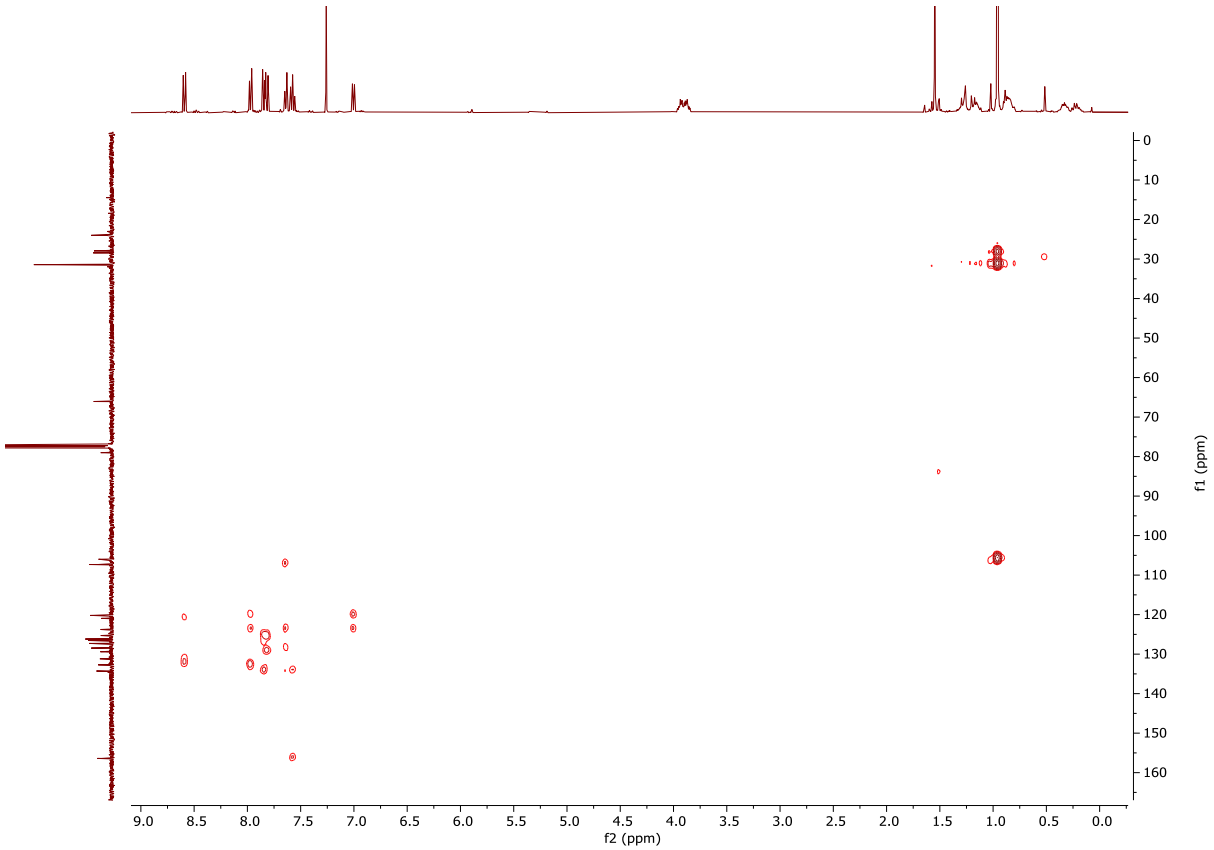

Figure S50. HMBC NMR (400 MHz) of **DH-C6** in $CDCl_3$, measured at 298 K.

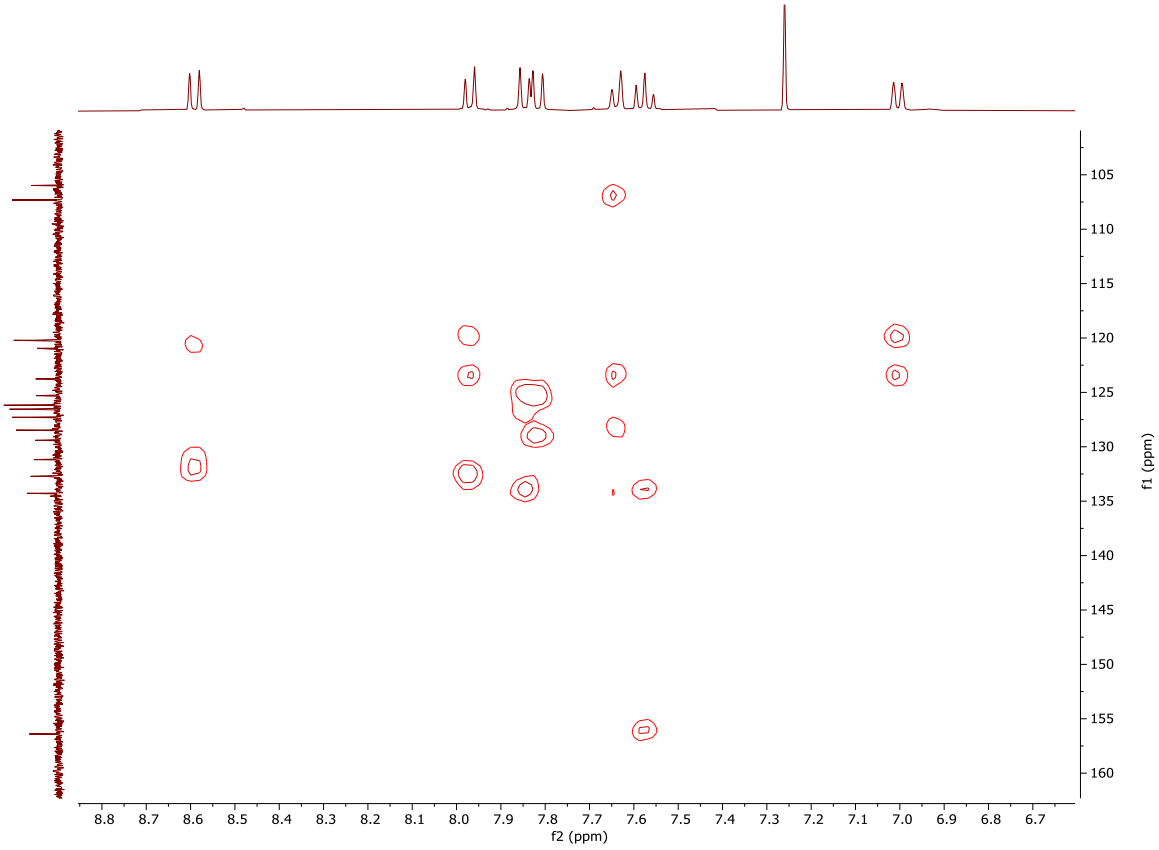

Figure S51. HMBC NMR (400 MHz) of **DH-C6** in $CDCl_3$, measured at 298 K (expansion in aromatic region).

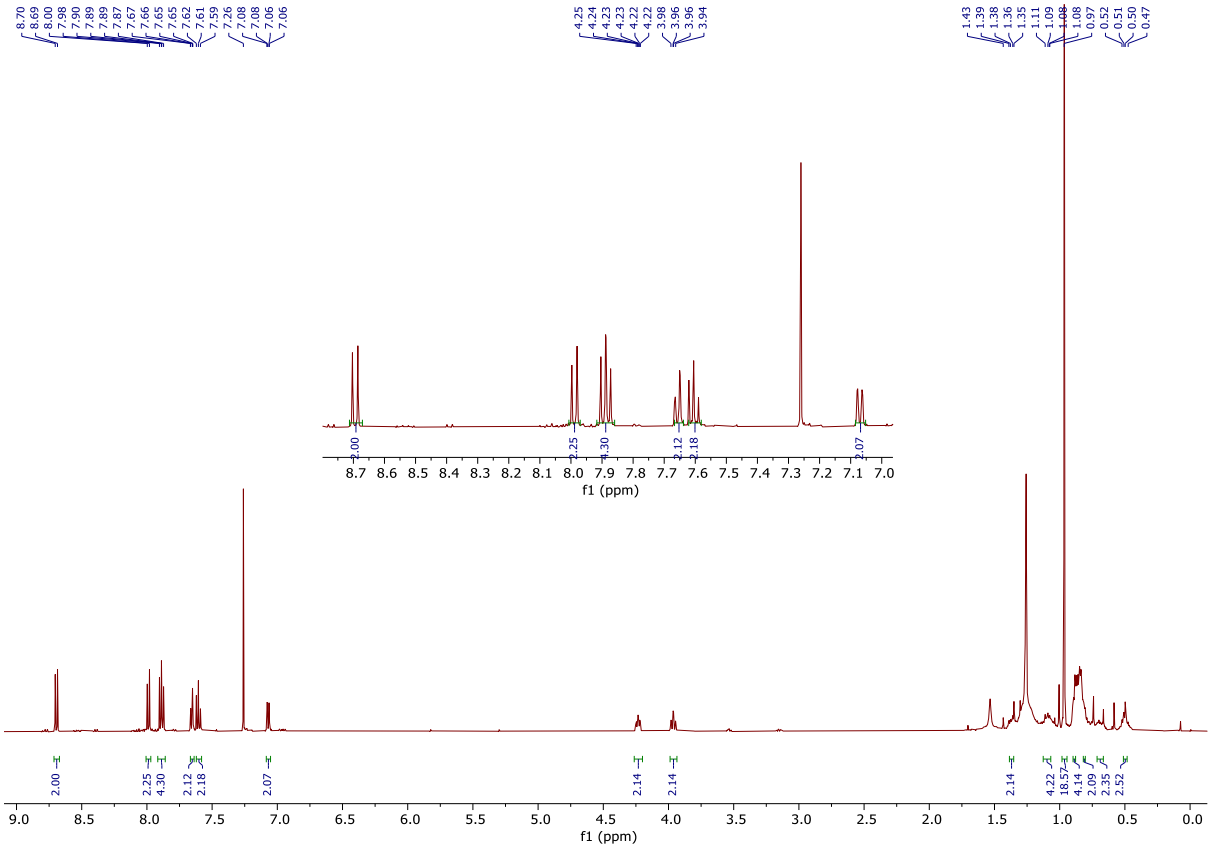

Figure S52. ^{1}H NMR (400 MHz) of **DH-C8** in $CDCl_3$, measured at 298 K.

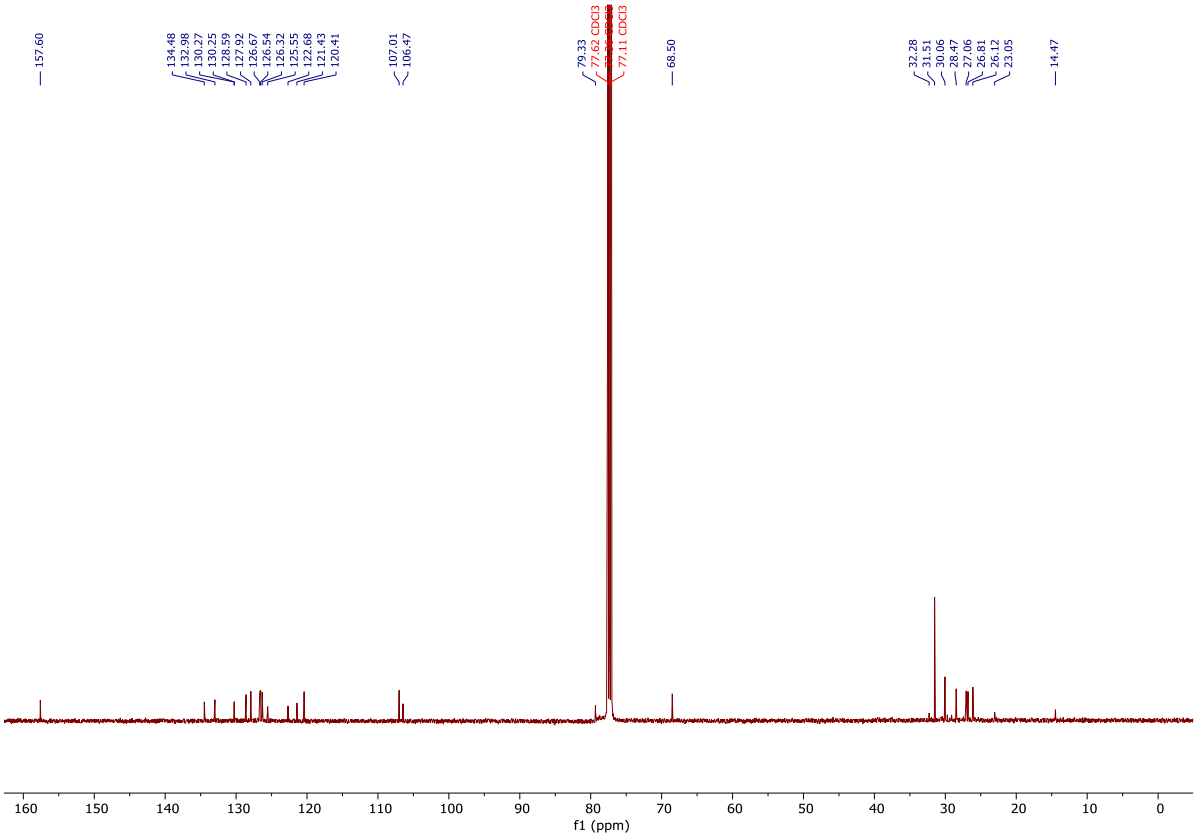

Figure S53. ^{13}C NMR (101 MHz) of **DH-C8** in $CDCl_3$, measured at 298 K.

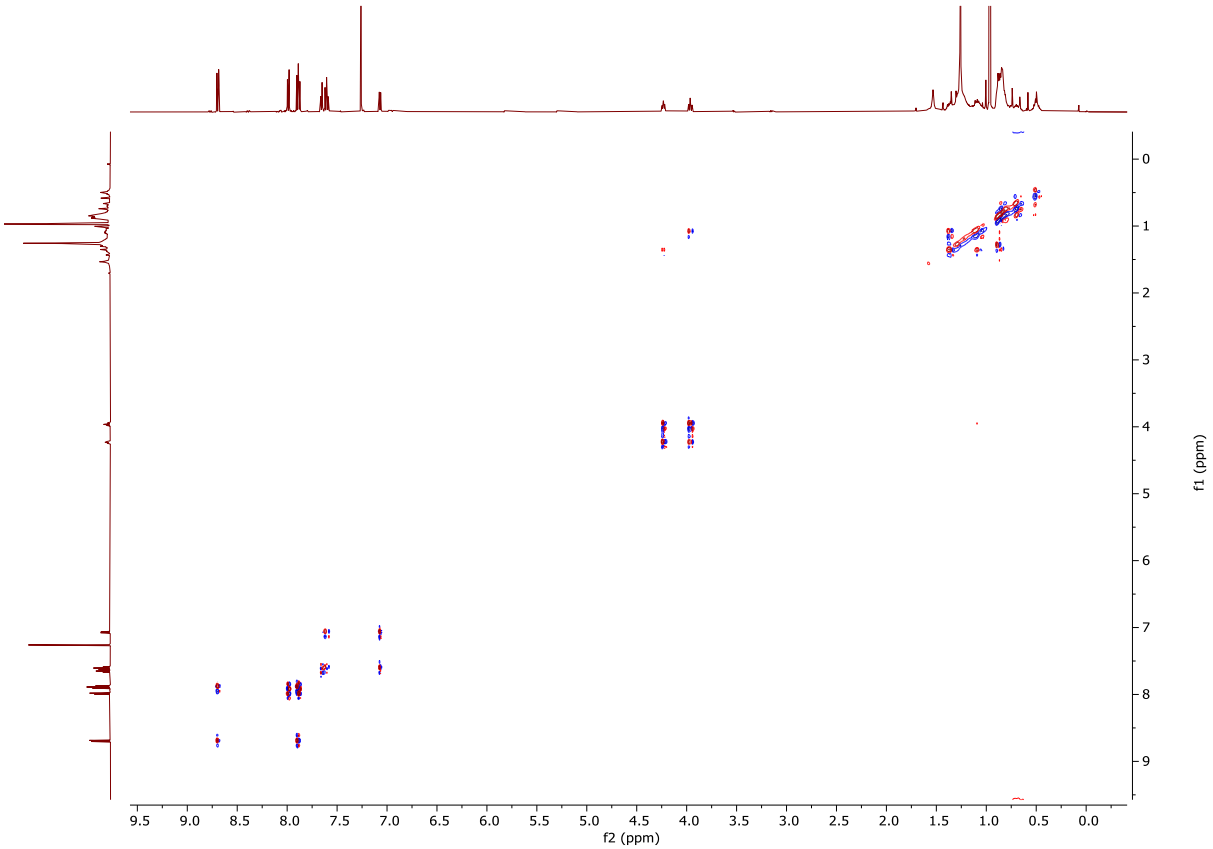

Figure S54. COSY NMR (400 MHz) of **DH-C8** in $CDCl_3$, measured at 298 K.

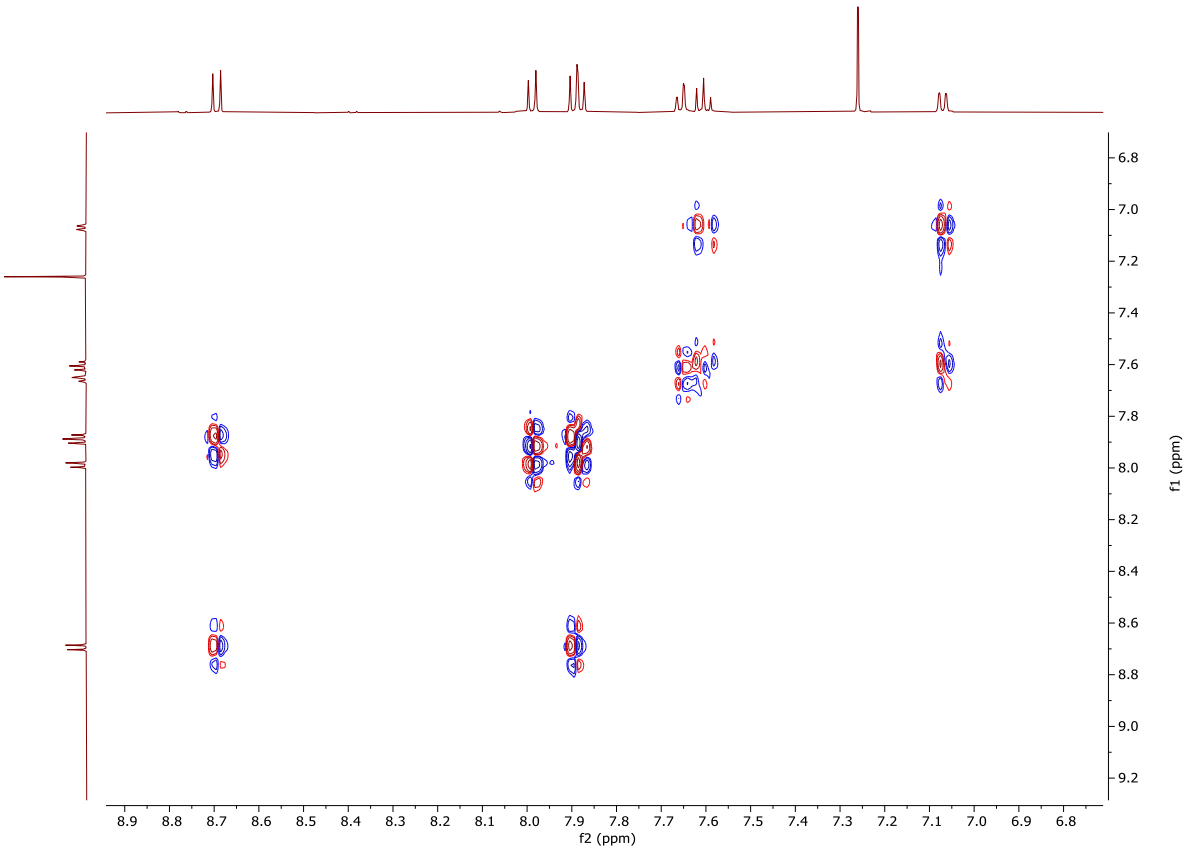

Figure S55. COSY NMR (400 MHz) of **DH-C8** in $CDCl_3$, measured at 298 K (expansion in aromatic region).

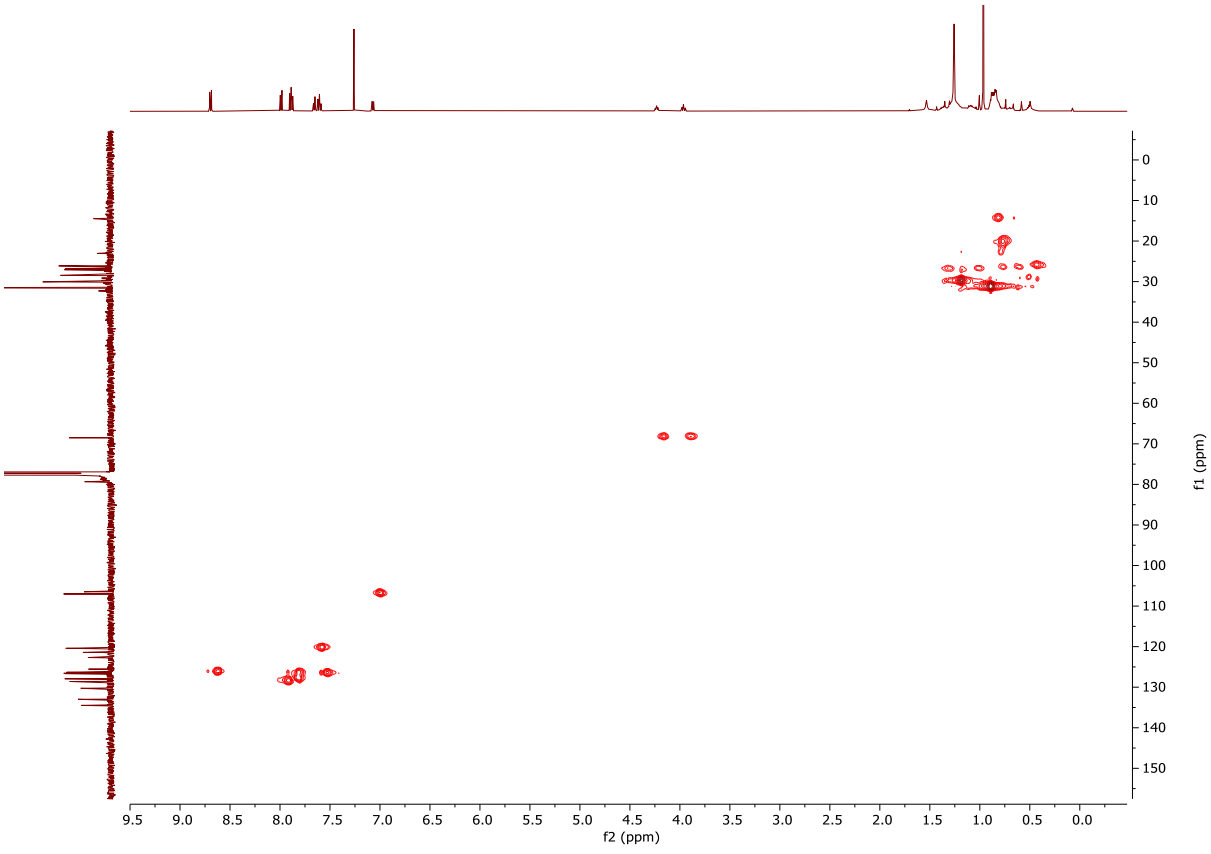

Figure S56. HSQC NMR (400 MHz) of **DH-C8** in $CDCl_3$, measured at 298 K.

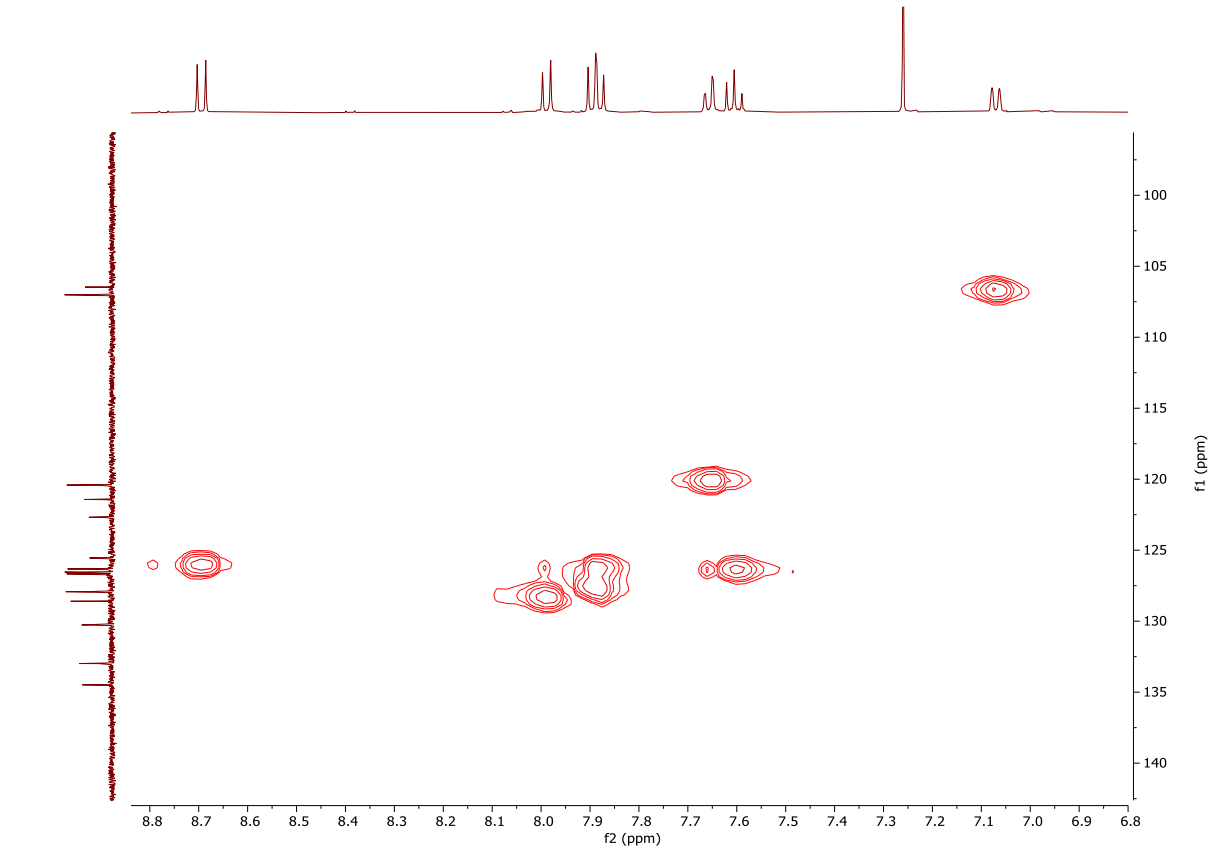

Figure S57. HSQC NMR (500 MHz) of **DH-C8** in $CDCl_3$, measured at 298 K (expansion in aromatic region).

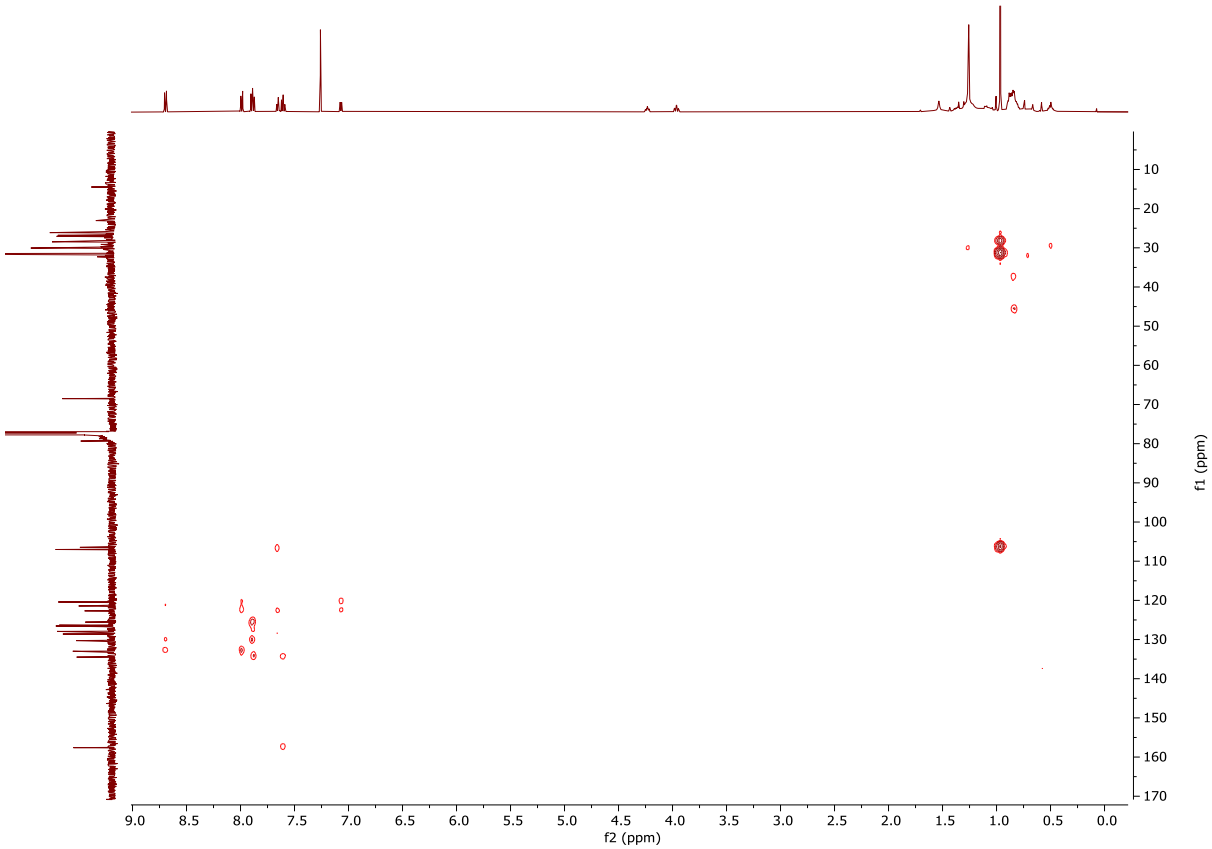

Figure S58. HMBC NMR (400 MHz) of **DH-C8** in $CDCl_3$, measured at 298 K.

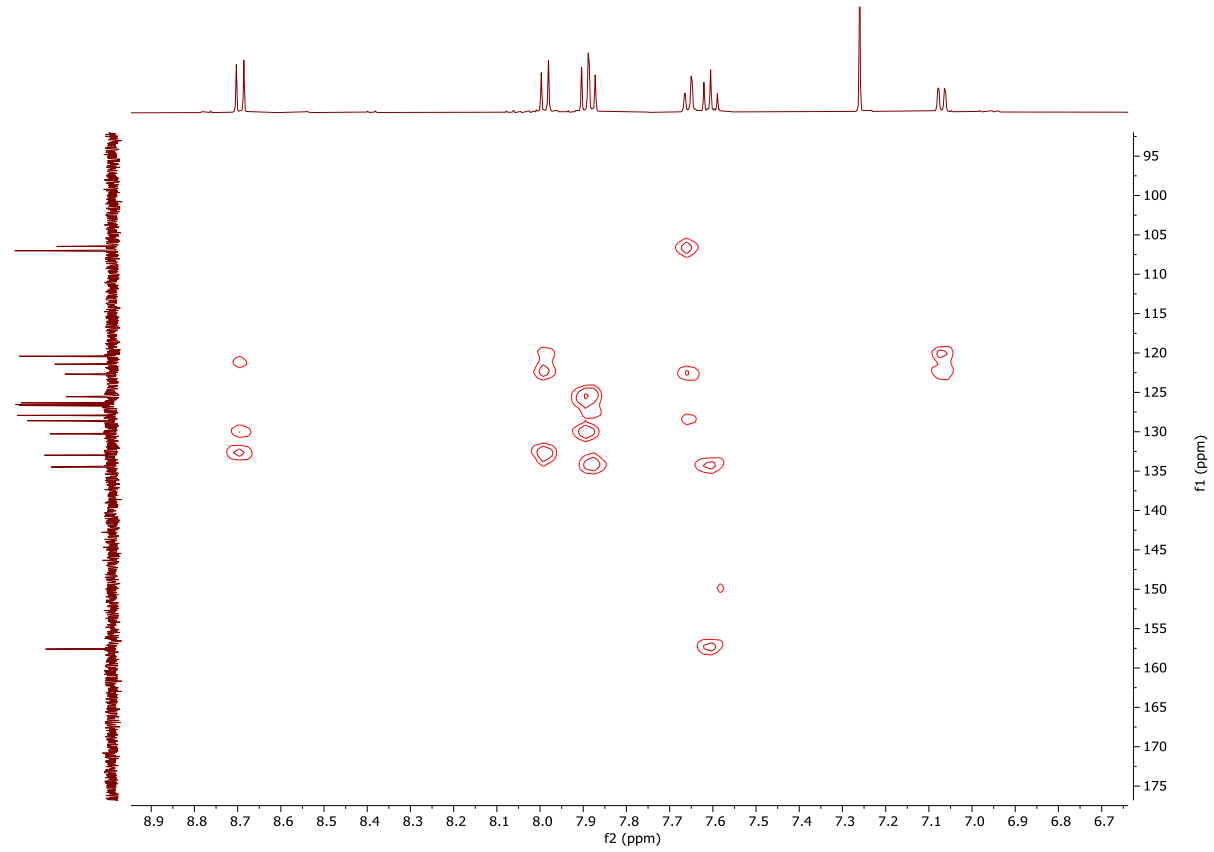

Figure S59. HMBC NMR (400 MHz) of **DH-C8** in $CDCl_3$, measured at 298 K (expansion in aromatic region).

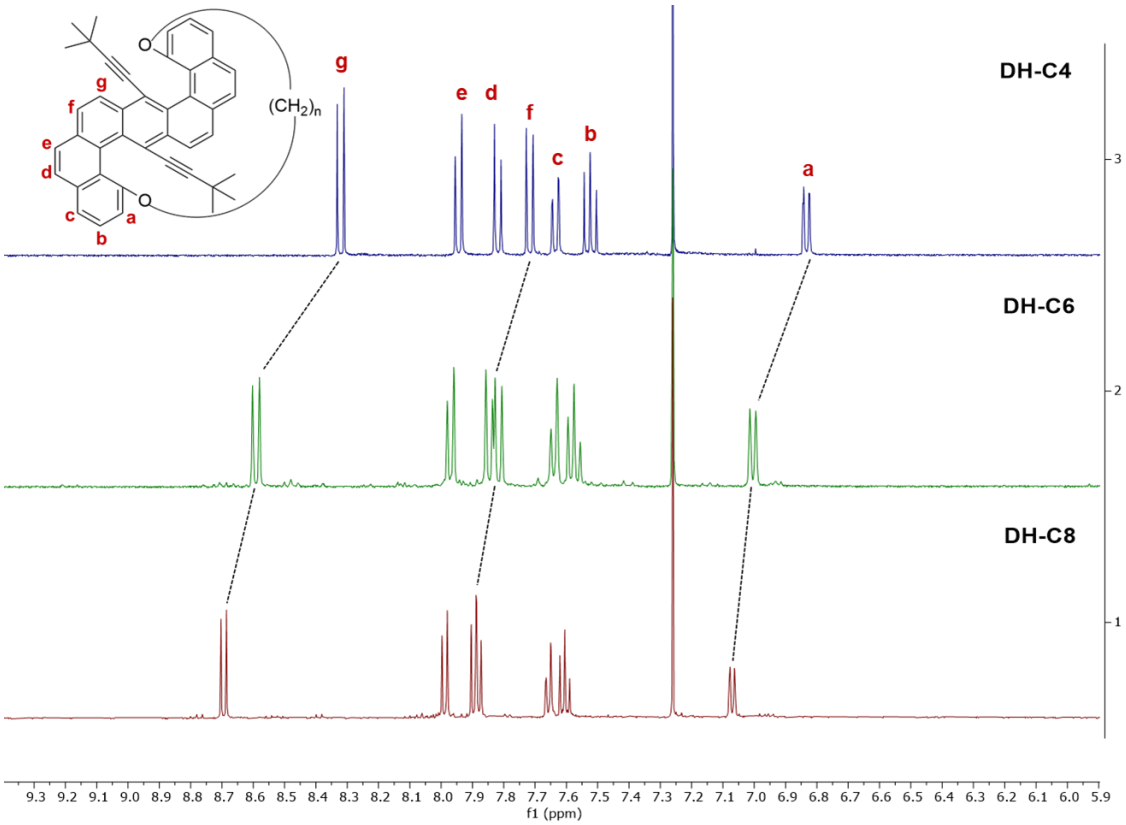

Figure S60. Comparison of ^{1}H NMR in the aromatic region for **DH-C4**, **DH-C6** and **DH-**

C8.

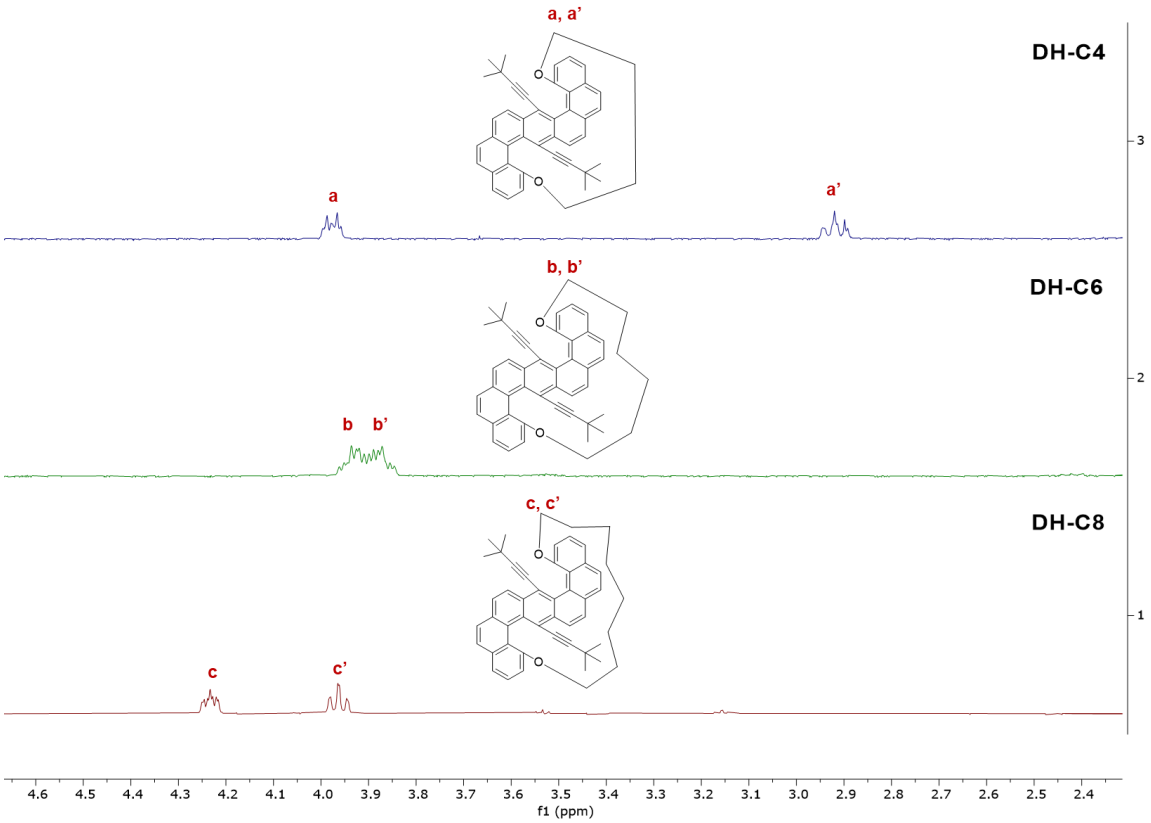

Figure S61. Comparison of O-CH_2 proton for **DH-C4**, **DH-C6** and **DH-C8**.

S5 Photophysical Properties

All photophysical studies were performed with dilute solutions of the compounds keeping the absorbance from the lowest energy band in the range of 0.05 to exclude self-absorption.

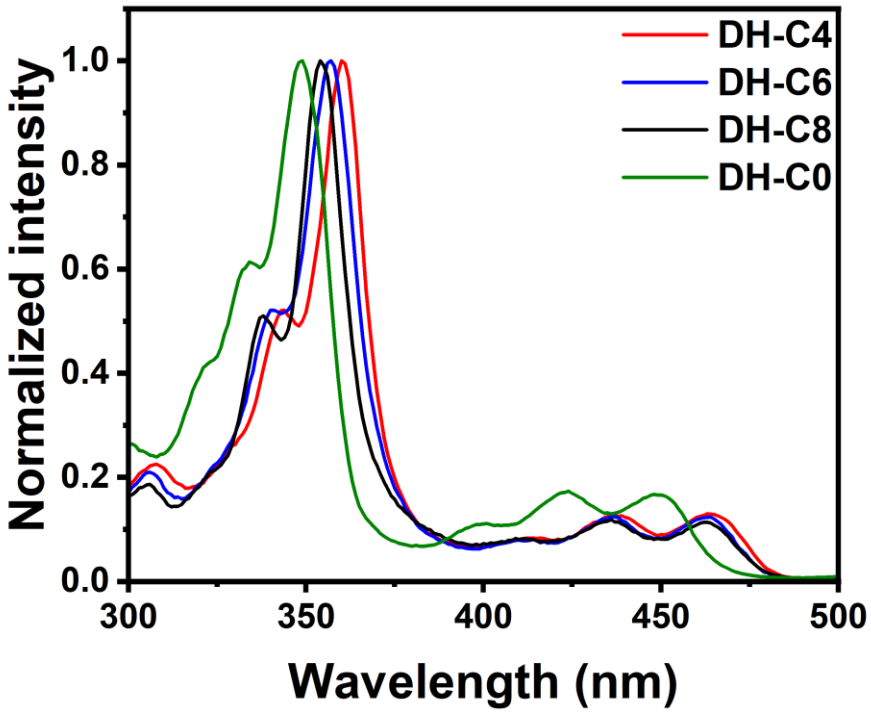

Figure S62. UV-vis absorption spectra of compounds **DH-C4**, **DH-C6**, **DH-C8**, and **DH-C0**

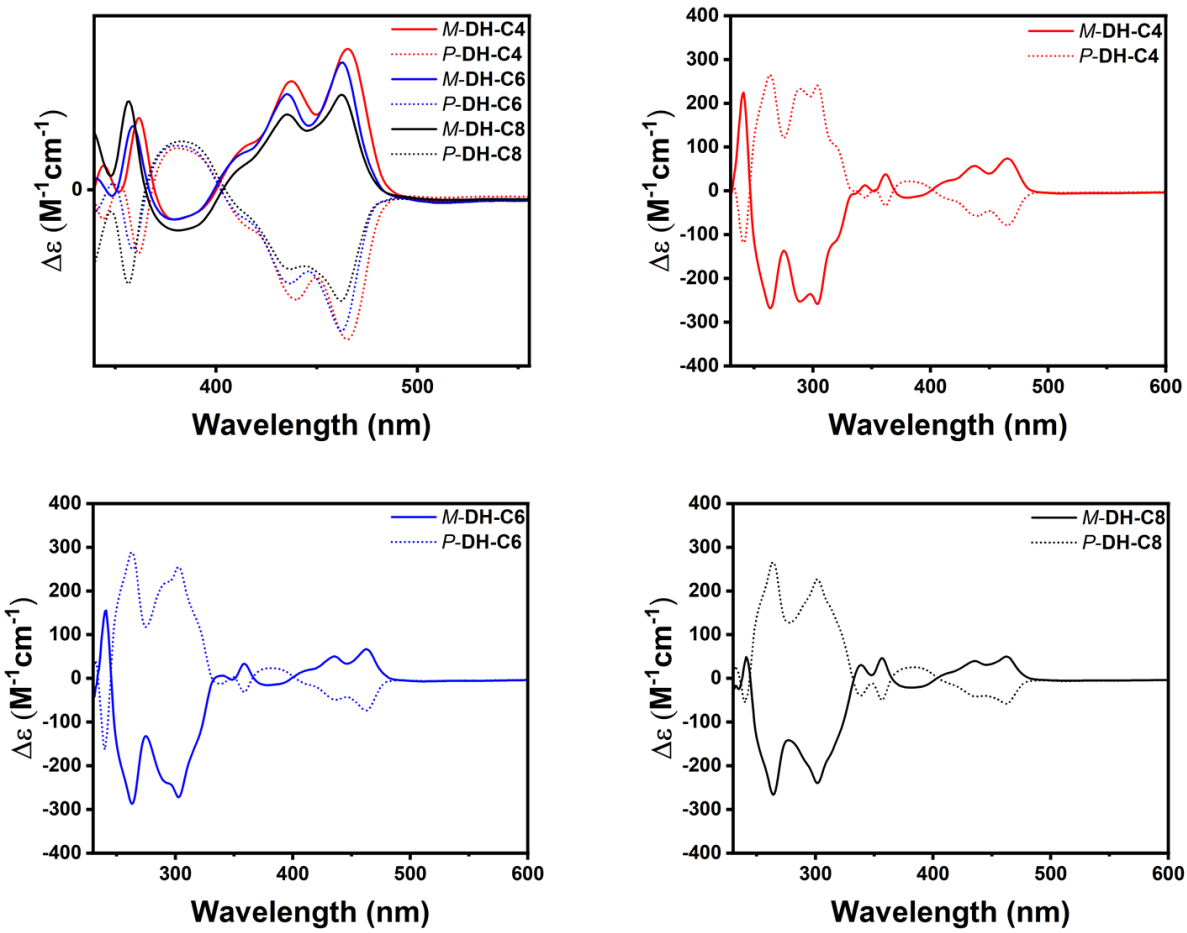

Figure S63. Experimental ECD spectra of the tethered S-shaped double [4] helicene enantiomers **DH-C4**, **DH-C6**, **and DH-C8**.

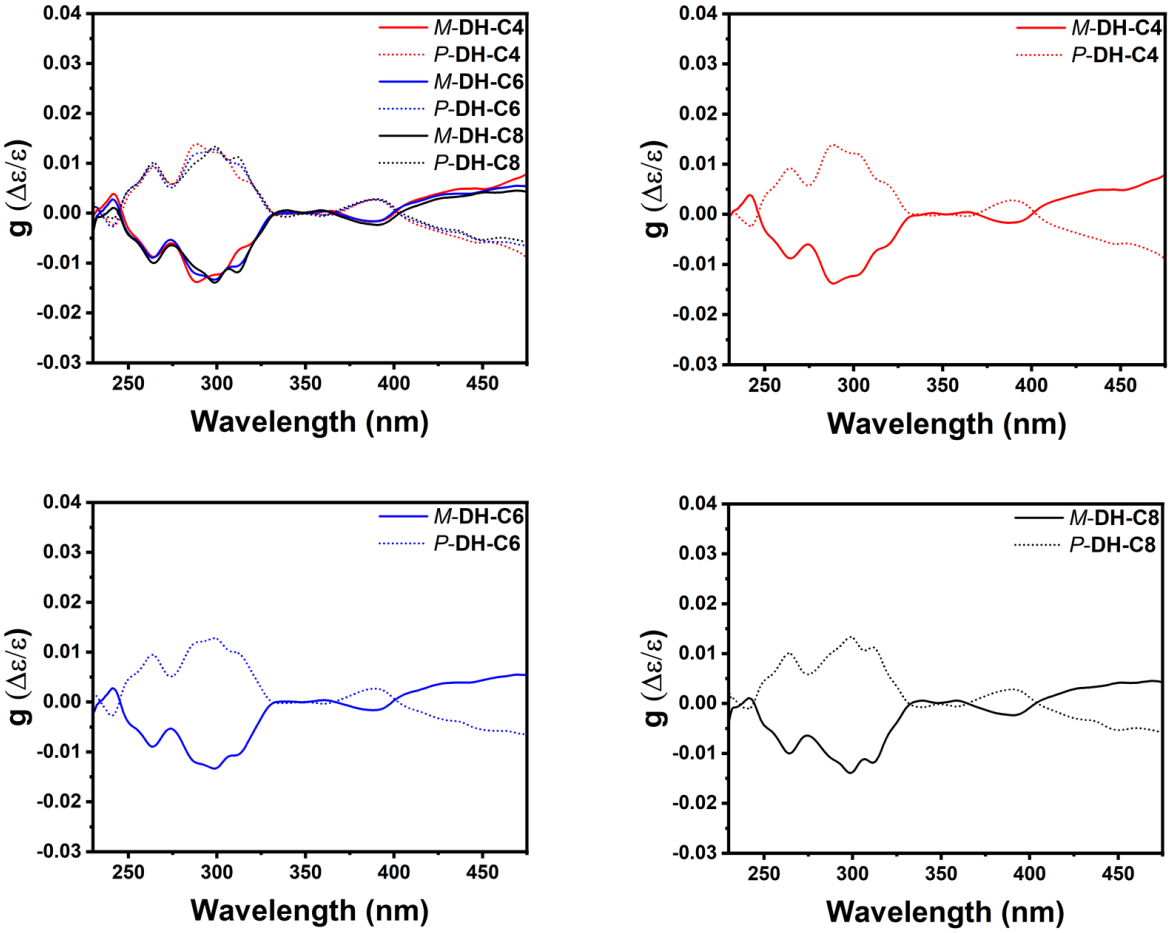

Figure S64. G values of the tethered S-shaped double [4] helicene enantiomers **DH-C4**, **DH-C6**, **and DH-C8**.

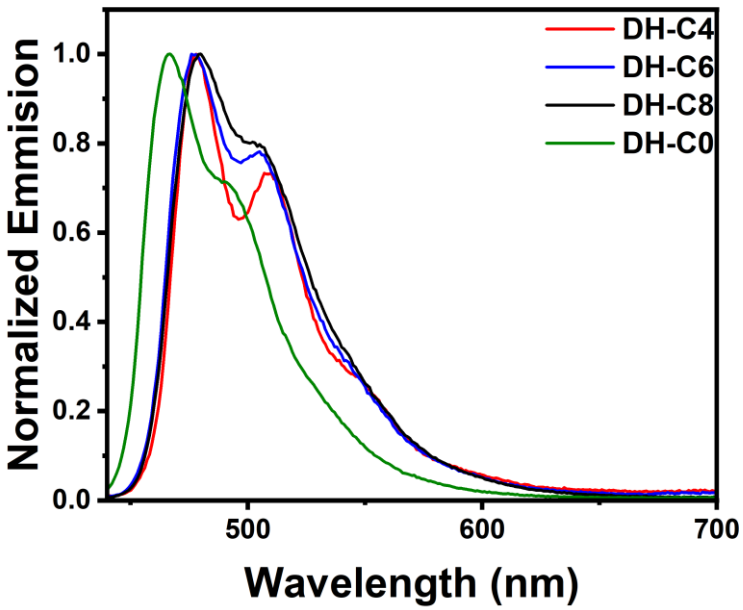

Figure S65. Emission spectra of compounds **DH-C4**, **DH-C6**, **and DH-C8**.

Table 1. Quantum yield, and Fluorescence lifetime of the S-shaped double [4] helicene molecules.

Molecule	Quantum yield %	Life time (ns)
DH-C4	6	1.12
DH-C6	12	1.99
DH-C8	12	2.24
DH-C0	26	3.77

S6 Single crystal X-ray diffraction crystallography (SCXRD)

Single crystals of **DH-C0**, **DH-C4** and **DH-C6** were grown in DCM/hexane, by the slow evaporation method. A single crystal of the tethered S-shaped double [4] helicene was attached to a 400/50 MicroMesh™ with NVH Oil, and transferred to a Bruker SMART APEX CCD X-ray diffractometer equipped with a graphite monochromator. Maintaining the crystals at -150 °C was achieved with a Bruker KRYOFLEX nitrogen cryostat (for the relevant materials). The system was controlled by a Pentium-based PC running the SMART software package. Data were collected at room temperature using Mo-Kα radiation (λ=0.71073 Å). Immediately after collection, the raw data frames were subjected to integration and reduction by the SAINT program package. The structure was solved and refined by the SHELXTL software package.

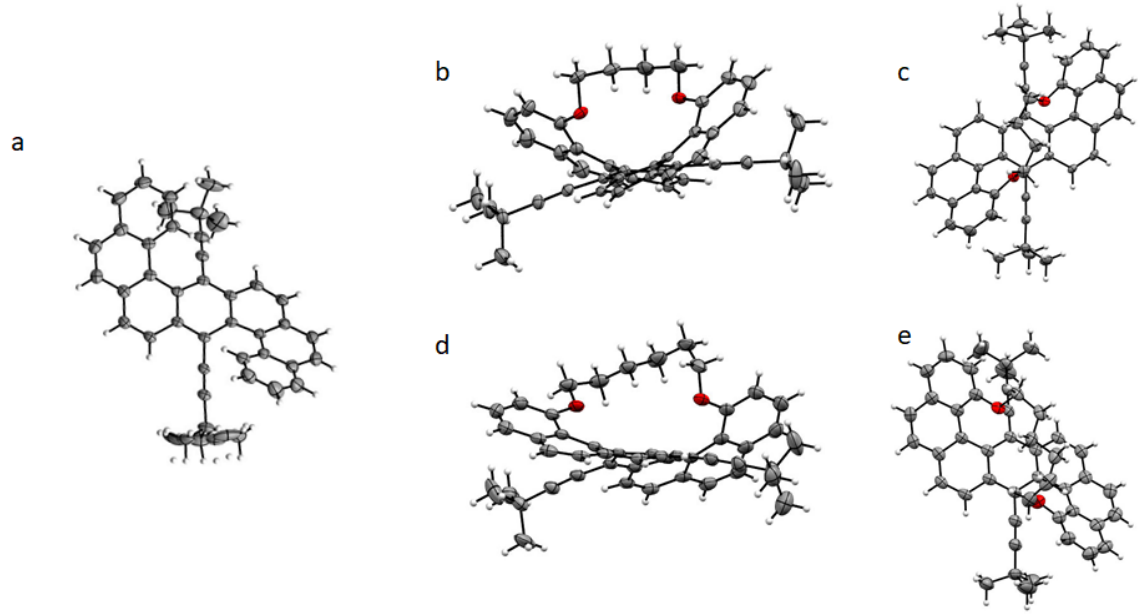

Figure S66. Crystal structures of (a) **DH-C0**, (b–c) **DH-C4** and (d–e) **DH-C6.**

Table 2. Crystallographic refinement parameters

Parameters	**DH-C0**	**DH-C4**	**DH-C6**
Empirical formula	$C_{42}H_{34}$	$C_{46}H_{40}O_2$	$C_{48}H_{44}O_2$
Formula weight	538.69	703.66	662.83
Temperature/K	150.0(1)	150.0(1)	149.99(10)
Crystal system	monoclinic	triclinic	monoclinic
Space group	$P2_1/c$	P-1	$P2_1/n$
a/Å	13.7697(4)	11.2461(3)	17.9449(7)
b/Å	15.4363(5)	11.4386(4)	9.9148(4)
c/Å	14.6704(5)	15.5025(5)	22.8990(9)
α/°	90	92.762(3)	90
β/°	96.138(3)	99.839(3)	103.799(4)
γ/°	90	103.088(3)	90
Volume/Å^3	3100.4(2)	1906.0(1)	3956.6(3)
Z	4	2	4
ρ_{calc}g/cm^3	1.154	1.226	1.113
μ/mm^{-1}	0.065	0.208	0.067
F(000)	1144.0	740.0	1412.0
Crystal size/mm^3	0.25 × 0.16 × 0.11	0.17 × 0.1 × 0.03	0.253 × 0.047 × 0.042
Radiation	Mo Kα (λ = 0.71073)	Mo Kα (λ = 0.71073)	Mo Kα (λ = 0.71073)
2Θ range for data collection/°	4.672 to 64.604	4.602 to 53.998	4.498 to 51.998
Index ranges	-17 ≤ h ≤ 19, -22 ≤ k ≤ 23, -21 ≤ l ≤ 20	-12 ≤ h ≤ 14, -14 ≤ k ≤ 14, -19 ≤ l ≤ 19	-21 ≤ h ≤ 22, -12 ≤ k ≤ 10, -28 ≤ l ≤ 28
Reflections collected	27445	25907	28702
Independent reflections	9200 [R_{int} = 0.0290, R_{sigma} = 0.0369]	8311 [R_{int} = 0.0338, R_{sigma} = 0.0395]	7751 [R_{int} = 0.0699, R_{sigma} = 0.0674]
Data/restraints/parameters	9200/0/415	8311/0/502	7751/0/477
Goodness-of-fit on F^2	1.056	1.052	1.002
Final R indexes [I>=2σ (I)]	R_1 = 0.0630, wR_2 = 0.1677	R_1 = 0.0667, wR_2 = 0.1694	R_1 = 0.0791, wR_2 = 0.2177
Final R indexes [all data]	R_1 = 0.0956, wR_2 = 0.1840	R_1 = 0.0897, wR_2 = 0.1810	R_1 = 0.1273, wR_2 = 0.2474
Largest diff. peak/hole / e Å^{-3}	0.38/-0.22	0.91/-0.46	1.09/-0.31
CCDC deposition number	2296411	2296412	2296413

S7 Computational details

All calculations were carried out using the Gaussian 09 program applying density functional theory (DFT). [2] All molecules were optimized using a hybrid density functional and Becke's three parameter exchange functional combined with the LYP correlation functional (B3LYP) and with the 6-31G(d) basis set (B3LYP/6-31G(d)) with gd3 dispersion correction. All optimized structures were confirmed by frequency calculations and showed no negative frequencies. The UV-vis and CD spectra was calculated using time dependent TD-DFT with CAM-B3LYP basis set (CAM-B3LYP/6-31G(d)).

S7.1 Calculated structures of the tethered S-shaped double [4] helicene

Table 3. Optimized (DFT-B3LYP-6-31G(d)-GD3) structures of the synthesized molecules

Molecule	Absolute energy (Hartree)
DH-C0	-1620.9911
DH-C4	-1927.4714
DH-C6	-2006.12
DH-C8	-2084.752

S7.2 Calculated UV-vis absorption spectrum and CD spectrum of the S-shaped double [4] helicene molecules

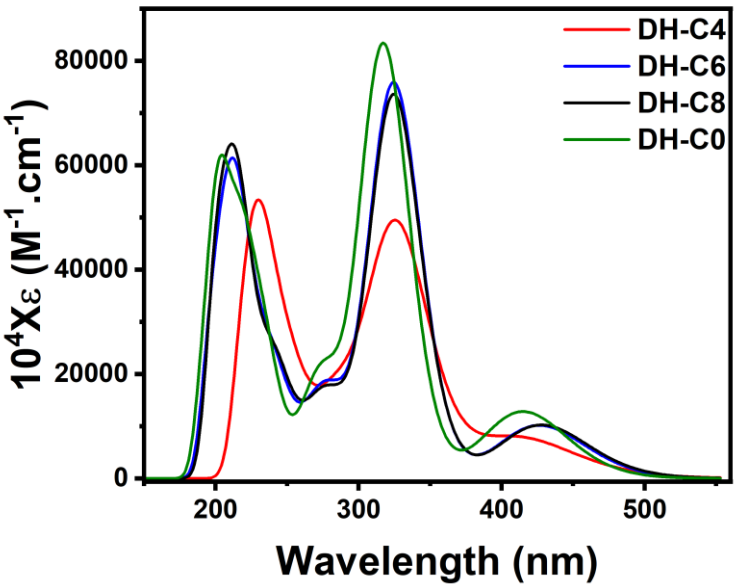

Figure S 67. Calculated (TD-DFT/CAM-B3LYP/6-31G(d)) UV spectra of **DH-Cn**.

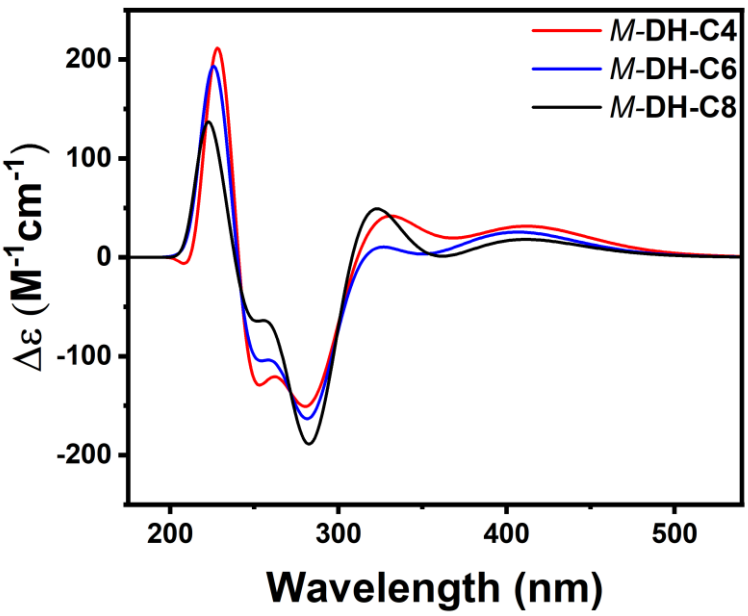

Figure S 68. Calculated (TD-DFT/CAM-B3LYP/6-31G(d)) CD spectra of *M*-**DH-Cn**.

Transition state optimization: all the optimizations of the geometries in the transition state have been also performed in DFT/B3LYP/6-31G(d) with gd3 dispersion correction. We verified that this was indeed the transition state by checking that there was indeed one imaginary frequency and by observing the movement of the imaginary coordinate which shows that indeed it passes between one conformer and another (displacement vectors figure of the imaginary coordinate is add below).

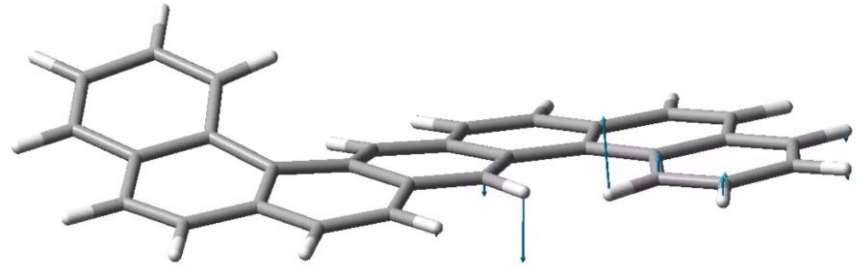

Figure S 69. Transition state geometry for the S-shape double [4]helicene backbone.

S-shaped double [4]helicene displacement vectors of the imaginary coordinate (-213 cm^{-1}). The coordinate mainly contains the movement of hydrogen atoms (since the right side of the molecule is almost planar).

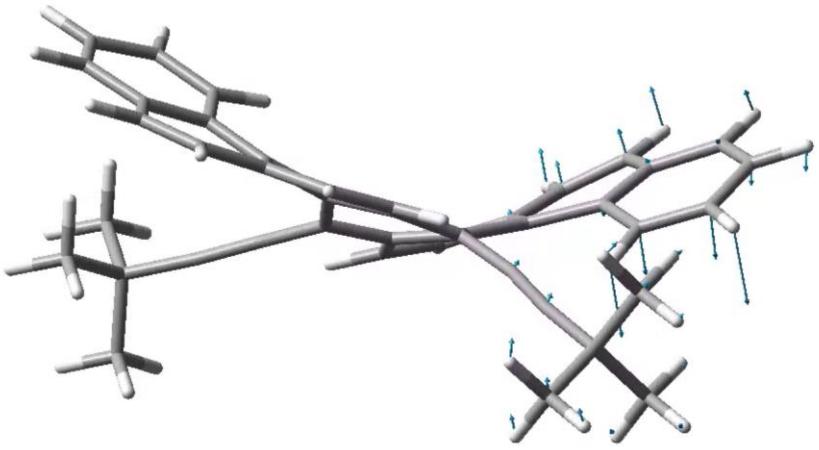

Figure S 70. Transition state geometry for DH-C0.

S-shaped double [4]helicene with tert-butyl-acetylene substituents displacement vectors of the imaginary coordinate (-47.35 cm^{-1}). The coordinate mainly contains the rotation of the tert-butyl group and upward displacement of the aromatic rings that are close to the tertbutyl group. This is the reason why the frequency is very low when the tertbutyl group is present (since the effective mass of the coordinate really increases when the tertbutyl group is present).

S8 References

(1) Bedi, A.; Manor Armon, A.; Diskin-Posner, Y.; Bogosalvsky, B.; Gidron, O. Controlling the Helicity of π-Conjugated Oligomers by Tuning the Aromatic Backbone Twist. *Nat. Commun.* **2022**, *13* (1), 451. https://doi.org/10.1038/s41467-022-28072-7.

(2) Lee, C.; Yang, W.; Parr, R. G. Development of the Colle-Salvetti Correlation-Energy Formula into a Functional of the Electron Density. *Phys. Rev. B* **1988**, *37* (2), 785–789. https://doi.org/10.1103/PhysRevB.37.785.